Dedicated to my grandfather Shri. K. P. N. Singh

...

Optoelectronic Study of Interface and Its Related Effects in Organic Electronic Devices

by

Vipul Singh

A Dissertation submitted to the Faculty of the Biological Functions and Engineering
Graduate School of LSSE, Kyushu Institute of Technology
2-4 Hibikino, Wakamatsu, Japan, 808-0196

Towards the partial fulfillment of the requirements for the degree of

Doctor of Philosophy

Committee in charge:

Prof. Keiichi Kaneto (chair)

(March 11, 2009)

Optoelectronic Study of Interface and Its Related Effects in Organic Electronic Devices

by

Vipul Singh

Optoelectronic Study of Interface and Its Related Effects in Organic Electronic Devices

Vipul Singh

Biological Functions and Engineering
Graduate School of LSSE, Kyushu Institute of Technology
2-4 Hibikino, Wakamatsu, Japan, 808-0196.

Supervisor:*Prof. Keiichi Kaneto*

In the recent past, conjugated polymer based electronic devices viz. Polymeric Solar Cells (PSCs), Polymeric Light Emitting Diodes (PLEDs) and Polymeric Field Effect Transistors (PFETs) have gained special interest due to their transport properties as well as their potential application for the development of cheap and flexible electronic devices. It has been observed that the interface between various polymeric layers and also between polymer and metal is very crucial for development of high performance devices. It is widely accepted that coating a thin layer ($< 2nm$) of LiF below Aluminum (Al) leads to improvement in the charge injection from the cathode into the LUMO of n-type organic semiconductor, and leads to improvement in the efficiency of PLEDs. Similar improvement in the quantum efficiency of thin film bulk heterojunction (P3HT/PCBM) PSCs has also been observed. Although, several models have been proposed to explain these effect. However, still there exists an ambiguity whether LiF dissociates into ions and thus causes doping of the semiconductor layer immediately below it, or does it create a vacuum level offset between the semiconductor and cathode.
In this regard a comparative study was performed between the Al($2nm$)/Poly(3-Hexylth iophene)(P3HT) junction and LiF($2nm$)/P3HT junction. It was demonstrated that LiF does not form a depletion layer with P3HT by a combined study of Photoluminescence (PL) and Photo induced memory devices (PIMDs). This fact was then utilized to cut-off the bulk region in a P3HT based Organic Field Effect Transistors (OFETs) to improve the on/off ratio in these devices. Further, It was observed that metal coating on the conducting polymer led to the increase in high energy peak in the PL emission spectra. It was later attributed to the increase in the intrachain disorder due to $30nm$ thick coating of Al on top of P3HT film.
A unique model to study the depletion layer optoelectronically using bias dependent PL spectra was developed, and later demonstrated experimentally. Using this model the non uniform distribution of charge carriers in the bulk of P3HT was demonstrated. Later this model was used to study the Al/P3HT and Al:LiF/P3HT junctions to further elucidate the effect of LiF in bilayer structures, which is in particular significant for the development of PSCs. It was found that in bilayered structures LiF helps in creating high electric field over a narrow region of its interface and hence leads to better dissociation of excitons near the interface. Which further leads to improved quantum

efficiency of PSCs. Moreover, it was also observed that inclusion of LiF also protects the pristine polymer film from the hot Al atoms during the thermal deposition process. This optoelectronic technique was further successfully applied to various other organic materials to investigate the role of morphology in the field assisted dissociation of excitons. In order to change the morphology a series of Poly (3-Alkylthiophene) PAT films were studied. These PAT films differed in their regioregularity as well as the length of their alkyl chain substituent. It was found that better film morphology ensures easy diffusion of excitons formed in the bulk of semiconductor, to the interface and hence leads to better field assisted dissociation of excitons. Thus our technique can also be used to probe different materials for their possible photovoltaic applications.
In the end the bias dependent PL spectra under the forward bias regime for ITO/P3HT/Al Schottky cell was studied, and clearly gave the evidence of PL quenching caused by injected charge carrier in the P3HT film. It was observed that the space charge built up in the bulk of P3HT causes change in morphology of the film and thus leads to the observed PL quenching.

Acknowledgements

First and foremost I would like to thank Prof. Keiichi Kaneto for providing me with an opportunity to work under his able guidance. I would also like to thank him for his valuable comments during the course of this work. He motivated me and also supported my decision, showed faith in me and called me from India. He gave me an opportunity to explore different areas of organic electronic devices. Furthermore, I would like to thank Assistant Prof. Wataru Takashima for guiding me throughout my work. I am thankful to him for teaching and demonstrating the Laboratory equipments and also for the long hours of discussions he had with me. It is his vision that has provoked my own thought process in many ways. I would further like to thank all the members of the review committee Prof. Shuji Hayase, Prof. Takashi Yasuda and Prof. Ryuichi Shiratsuchi for giving their valuable comments on this work.
I would then like to thank Dr. Anil K. Thakur for teaching me the Photoluminescence spectroscopy. It was from him that I learned the basic philosophy of research. I would also like to thank Dr. S. S. Pandey for his valuable comments and suggestions on my entire work. I am also thankful to him for synthesizing some of the compounds for my research work. I enriched a lot from his knowledge about organic chemistry in general and conducting polymers in particular. Apart from this I am thankful to all the fellow members of the Kaneto Laboratory for providing me a conducive environment to carry out my research work. In particular I am thankful to Dr. Mala Ekanayake, Dr. D. M. G. Preethichandra, Mr. Daisuke Tanimura, Mr. Makoto Yano, Mr. Akitoshi Kawazoe, Mr. Takeomi Morita, Mr. Kozue Tominaga, Mr. Oku Shinya and Mr. Kentaro Yamato. I am grateful to my colleague Mr. Kentaro Yamato for helping me write my progress reports in Japanese.
I would further like to thank SATO International Scholarship Foundation (SISF),Japan Student Service Organisation (JASSO), Heiwa Nakajima Foundation for providing me with scholarships. I would also like to thank Kyushu Institute of Technology for providing me the Research Assistantship during the three years of my Doctoral research work. I am also thankful for the research grant provided by Kyushu Institute of Technology for the purpose of buying equipments and materials as well as sponsoring my travel for attending various conferences.
Finally, I am greatly indebted to my wife Ms. Nivedita Singh for her support and cooperation in all walks of my life, also for her understanding my commitments as a Ph.D.student. She has not only ensured conducive environment for me to study but also motivated me in my bad times. I am also thankful to my little daughter Ms. Vamika Singh that she was my source of inspiration during these three years. I am thankful to my parents Dr. V. P. N. Singh (who happens to be my role model)and Mrs. Pushpa Singh. Both my parents believed in me and supported my decision to do Ph.D. and also to my younger brother Mr. Vineet Singh who has always motivated me to do Ph.D.

Contents

List of Figures

Chapter 1

Introduction

Summary

In this chapter we present the advent, significance and application of organic electronics. We further move on to discuss the range of different materials that fall under the broad category of organic electronics. Furthermore, we see the role of conducting polymers as materials for the development of organic electronic devices. Also, the basic physical principles governing the electrical and optical properties of conducting polymers and conducting polymer based devices have been briefly discussed.

1.1 Organic Electronics

Organic electronics is a highly interdisciplinary field of science, technology and engineering; involving the use of small organic molecules or conjugated polymers as active thin layers. These materials are synthesized by the methods of organic chemistry. Their electronic structure and electronic properties fall within the domain of condensed matter physics. Efficient processing of these materials into useful forms and the fabrication of electronic and optoelectronic devices require input from engineering; i.e. materials science and device physics. Figure 1 shows the energy contribution by different sources of energy.

The basis of organic electronics is predicted on the ability of a class of functional organic molecules[1-5] known as organic semiconductors to actively transport charge, emit light, or to absorb light under appropriate conditions[6-15] . Transistors, light emitting diodes, and photovoltaic cells are some of the examples of devices comprising of these organic materials. From the fabrication point of view these materials can be classified into two categories namely that of solution processable and processable via thermal evaporation. While π-conjugated polymers clearly belong to the solution processable category[16-20]. Small molecule[21-25] based organic compounds can be functionalized to belong to either group. Evaporation technologies have till date dominated the semiconductor industry and thus these technologies are more advanced. However, the potential to print at a high throughput and high resolution from formulated inks offers the greatest commercial opportunity[26-30]. Today a range of organic devices exist starting from Organic Field Effect Transistors (OFETs), Organic Solar Cells (OSCs), Organic Light Emitting Diodes (OLEDs) and Organic Memory Devices (OMDs). OFETs [31-35] require organic semiconductors having highly organized microstructure, with the molecular orbital systems closely packed together. While the active layer in an OSC comprises of a light absorbing semiconductor, which typically is also the hole transport material. In a typical design this component is blended with n type organic semiconductors[36,37]. However, there remains a large number of challenges in optimizing transport

within the layer, absorbing more photons, and separating charge at the semiconductor interfaces. Organic Light Emitting Diodes (OLEDs) presently consist of two different types. While Small molecules based OLEDs (SMOLEDs)[38-40] are becoming increasing complex due to the use of multiple stacked layers. These layers consisting of different materials perform range of functions viz. injection, transport, blocking and emissive. Electroluminescence may be obtained in these by the use of fluorescent or phosphorescent semiconductors. It should be noted that although phosphorescent dopants exhibit excellent efficiencies in both red and green, due to their ability to harvest both singlet and triplet excitons, deep blue emission still remains a problem. The other class of OLEDs consist of Polymeric Light Emitting Diodes (PLEDs)[41,42], consisting of a single polymeric layer of conducting polymer.

Despite being the highly applicative it is only the OLEDs that has shifted from the research and development phase to the scale up phase. In the year 2007 Sony launched an 11- inch television based on OLED technology, whose salient features include a 3-mm thick panel and a 178^o viewing angle. In the display arena OLED technology promises to compete with the existing Liquid Crystal and Plasma technologies. OLEDs unnique attributes including its ultra brilliant colors, low power consumption and wider viewing angle make it a highly desirable technology for future display development. It is the cost constraints that have dictated the research in OFETs. It is now widely accepted that OFETs can never replace Si MOSFETs, which is a fast moving technology and has already reached $45nm$ channel. The last few decades have witnessed a drastic increase in number of circuit elements packed on a single chip, although the chip size and its price have been on a decreasing trend. OFETs are presently having their mobility 3 to 4 orders lower than the MOSFETs. However, they may compete to replace amorphous silicon based technologies. Besides this these OFETs are likely to create their own niche in the form of printable RF ID tags, Electronic paper and smart circuits for clothing and food packaging industry[43-45]. Besides the cost factor another factor that has been of crucial interest worldwide is that of energy. It is believed that human population will reach 9.3 billion from its current 6.6 billion mark by 2050 assuming the population growth rate remains constant at 1.2%. It is the ever growing energy demands

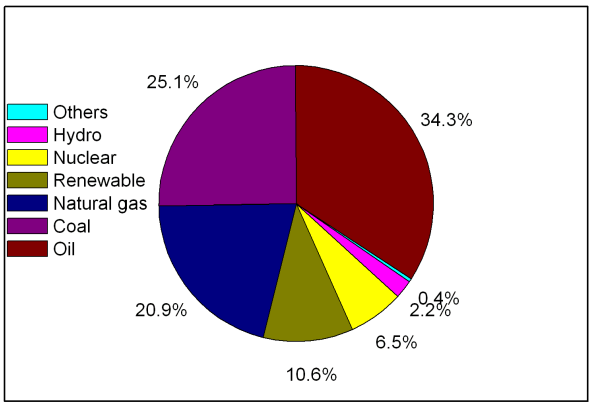

Figure 1.1: Percentage contribution of different energy sources *(courtesy MRS magazine)*

that has fuelled research activities in both OSCs and OLEDs. OSCs on one hand are seen as a possible source of tapping solar energy. OLEDs on the other hand particularly the white light emission from the OLEDs is seen as a possible replacement for Compact Fluorescent Lamps (CFL). Figure 1.1 shows the relative contribution of different sources of energy for the overall energy requirement of the world. It can be seen that nearly one third of energy is supplied by Oil. While Coal and oil together supply more than half of the energy. One fifth of the energy requirement is fulfilled by natural gas. It is worthwhile to note that all these are non renewable sources of energy. While renewable sources of energy together contribute less than 15% of the world's energy requirement. It is believed that the world energy requirement would stand at $30TW$ by the year 2050. However, sun provides us with $120,000TW$ of clean energy. It is this figure that has attracted the attention of scientists worldwide towards developing solar cells as a viable source of energy generation. Although, the efficiency of OSCs are far less than their inorganic counterparts. It is the ease of production at a very low cost that has fuelled research in organic materials as an alternative.

Besides the Photovoltaic devices, applications of OLEDs in the Solid state lighting (SSL) [46-50] holds a tremendous potential for the future. Nearly 20% of the energy produced in the United States is consumed by lighting alone. It is now widely accepted that there is a pressing need to develop viable technologies to conserve 50% of the energy load

by the year 2010. This cannot be achieved only by energy conservation using advanced electronic controls. The main enabler of the energy conservation effort will be new lighting fixtures such as SSL. Development of highly efficient SSLs using organic materials would not only ensure the replacement of existing lighting fixtures but would also at the same time contribute to reduced energy consumption, and reduced level of emission of greenhouse gases. Presently both Inorganic and organic LEDs are competing to be a viable source of white light emission. While Inorganic LEDs have a higher luminous power efficiency, however, its use for SSL is limited by its high cost of production and inability to be used for large area based applications. It is large area applications where organic based SSL offers a huge advantage.

Thus in all we would like to conclude that the new and emerging field of organic electronics helps us gain better insight into material properties at the molecular level. While Displays based on OLEDs have already hit the market and are likely to replace the existing display technologies. A host of other applications involving organic materials as well are catching up fast.

1.2 Conjugated polymers as Semiconductors

Conducting Polymers are the most recent generation of polymers. Polymers have been known in the form of wood, skin and fibers to mankind since prehistoric time. Initial studies on polymers were mostly limited to saturated polymers which were uninteresting from the point of view of electronic materials. In conjugated polymers the electronic configuration is fundamentally different. The chemical bonding leads to one unpaired electron (the π-electron) per Carbon atom as can be seen from Fig. 1.2. Moreover, π bonding, in which the carbon orbitals are in the sp^2p_zconfiguration and in which orbitals of successive carbon atoms along the backbone of the polymer. This electronic delocalization provides the "highway" for charge mobility along the backbone of the polymer chain. Some of the common conducting polymers have been shown in Fig. 1.3.

Range of electrical conductivity that can be obtained by controlling the doping level

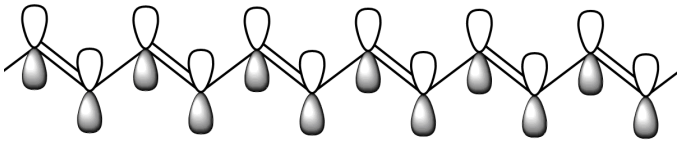

Figure 1.2: π orbitals of various carbon atoms in Polyacetylene

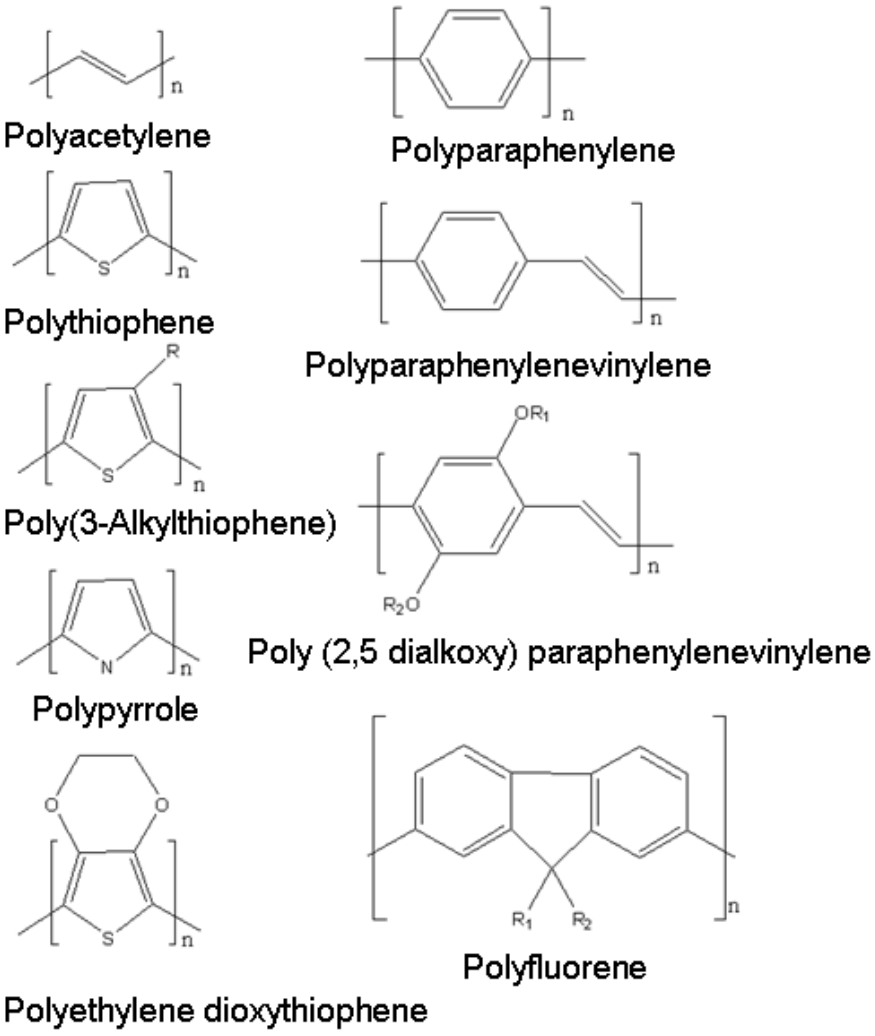

Figure 1.3: Structure of some common conducting polymers

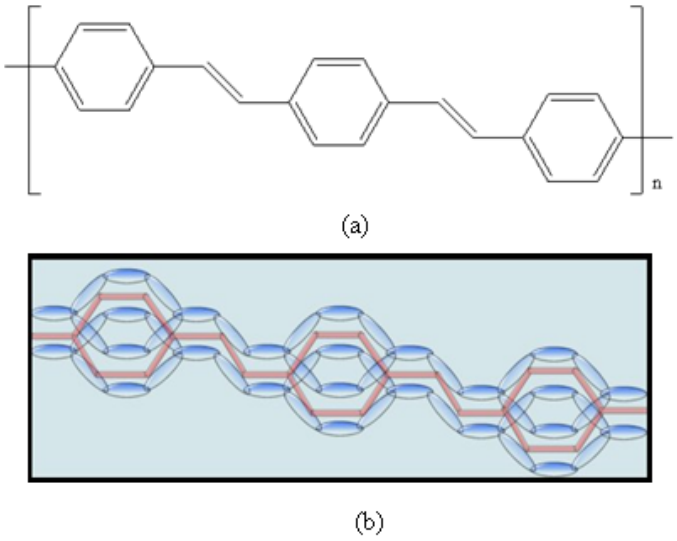

Figure 1.4: (a) Shows the structure of PPV (b) Shows the electron delocalization

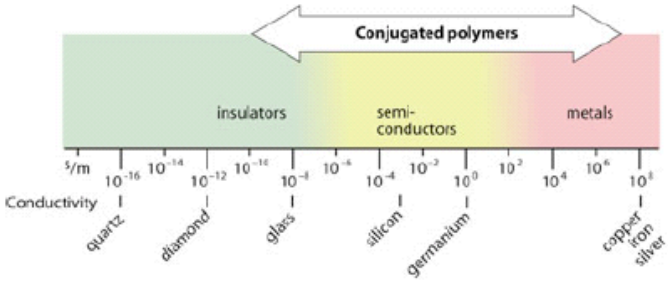

Figure 1.5: Range of electrical conductivity that can be obtained by controlling the doping level

The most Classic example is that of Polyacetylene, $(-CH)_n$, in which each carbon is σ bonded to only two neighboring carbons and one hydrogen atom with one π electron on each carbon. If the carbon-carbon bond lengths were equal, the chemical formula, $(-CH)_n$ with one unpaired electron per formula unit, that implies a metallic state. In real polyacetylene, the structure is dimerized as a result of the Peierl's instability with two carbon atoms in the repeat unit, $(-CH = CH)_n$. Thus the π electron density is divided into π band (filled) and π^* band (empty). The energy difference between the highest occupied state in the π band and the lowest unoccupied state in the π^* band is the $\pi - \pi^*$ energy gap E_g. The bond alternated structure of polyacetylene is characteristic of conjugated polymers, as is shown in Fig 1.4.

Another important property that is known as the reversible "doping" of conducting

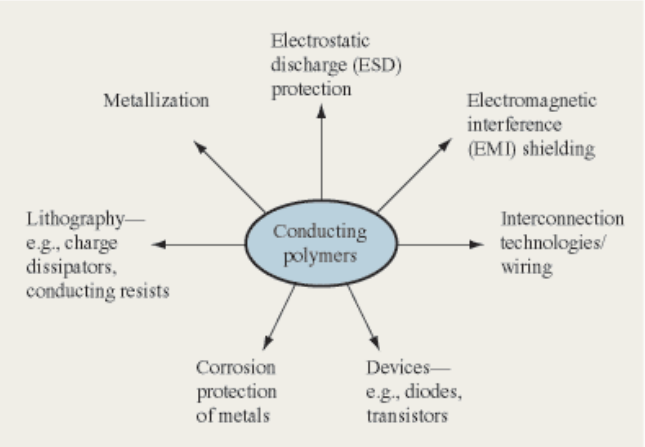

Figure 1.6: Various applications based on Conducting polymers

polymers, with associated control of electrical conductivity over the full range from insulator to metal as can be seen from Fig 1.5, can be accomplished either by chemical doping or by electrochemical doping. Charge neutrality is maintained by the introduction of counter ions. Metallic polymers are, therefore salts. The electrical conductivity results from the existence of charge carriers (through doping) and from the ability of those charge carriers to move along the $\pi-$ bonded "highway". Consequently, doped conjugate polymers are good conductors. Disorder however limits the carrier mobility and in the metallic state, limits the electrical conductivity. Indeed, research directed toward conjugated polymers with improved structural order and hence higher mobility is a focus of current research activity in the field. Besides this electrochemical doping of conducting polymers was discovered by MacDiarmid-Heeger collaboration in 1980 [51-53] and opened the way to research in yet another scientific direction. The electrochemistry of conducting polymers since then developed into a field of its own with applications that range from polymer batteries and electrochromic windows to light emitting cells as is shown by Fig. 1.6.

1.3 Electronic properties of Conjugated polymers

A description of electronic and chemical structure of polymeric and condensed molecular solid systems is an important frontier in the field of organic polymeric and molecular

materials in the modern electronics applications. The investigation of the interaction between conjugated polymer materials and various metals has become an important issue, both for interfacial characteristics as well as for doping induced effects. Studies on the interface characteristics are also of high significance in connection with various device applications.

1.3.1 Junction

Junctions are the elementary building blocks for all electronic devices. These include interfaces between semiconductors of different doping type (homojunctions) or of different composition (heterojunctions), and junctions between a metal and a semiconductor, which can either be rectifying (Schottky junction)[54-60] or ohmic. Because of their primary importance, physics of semiconductor junctions. Metal semiconductor (MS), and, Metal-insulator-semiconductor (MIS) junctions, which are involved in the Organic Field Effect Transistors (OFETs).

Metal Semiconductor junction

The usual way to visualize a junction is to draw an energy diagram that shows the bottom of the conduction band E_c and top of the valence band E_v as function of distance. The band curvature that appears shows the variation in the potential with a distance in the direction perpendicular to the junction surface. Fig. 1.7 shows the MS junction in the case of p-type semiconductor and low work function metal such as Al, Ca, Li and Mg etc. As can be seen from Fig. 1.7 ϕ_m denotes the Fermi level in the metal, χ_s is the conduction band edge of the semiconductor. E_f is the Fermi level of the metal. Connecting the metal and the semiconductor results in the equalization of the Fermi level in both media. This is obtained by a transfer of charge from the semiconductor to the metal. As the energy of electrons outside the surface of the of the two solids is different. An electric field grows in the gap between them, together with a negative charge at the metal surface, exactly balanced by a positive charge in the semiconductor. The charge at the metal surface concentrates within the Thomas-Fermi screening distance ($0.5\mathring{A}$). Since the free carrier concentration in the semiconductor is considerably lower than that

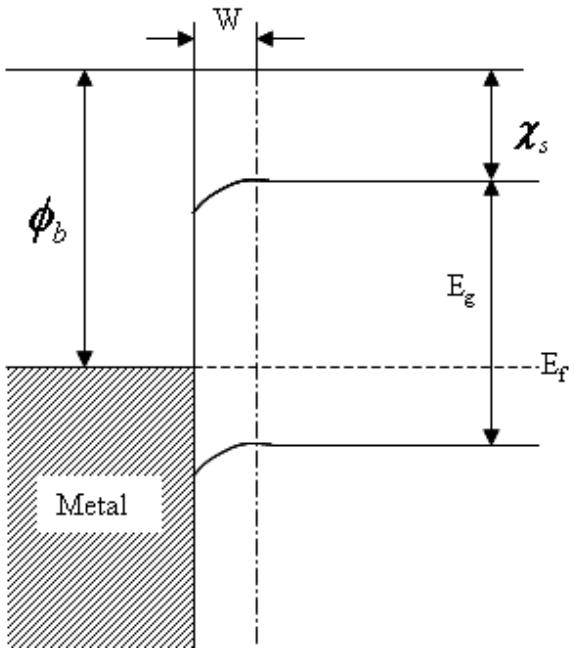

Figure 1.7: Metal Semiconductor junction for low work function metal and a p-type conducting polymer

in the metal, the charge here extends over a region of substantial thickness, called the depletion layer. At the same time an Electric field also develops at the semiconductor surface, which results in the downward bending of the bands. The barrier height ϕ_b is simply given by

$$\phi_b = \chi_s + Eg - \phi_m \tag{1.1}$$

The profile of the electrostatic potential V in an MS junction can be calculated by solving the Poisson's equation

$$\frac{\partial^2 V}{\partial x^2} = -\frac{\rho(x)}{\epsilon_s} \tag{1.2}$$

Integrating the above equation we get,

$$\frac{\partial V}{\partial x} = \frac{-qN_A x}{\epsilon_s} + K_1 \tag{1.3}$$

where K_1 represents the constant of integration. It is known that the Electric field is zero at $x = W$. applying this boundary condition we get,

$$E(x) = \frac{\partial V}{\partial x} = \frac{qN_A(W - x)}{\epsilon_s} \tag{1.4}$$

Further integrating one more time we get,

$$V = \frac{-qN_A(2Wx - x^2)}{2\epsilon_s} + K_2 \tag{1.5}$$

Where K_2 is also constant of integration. Applying the boundary condition at $x = 0$, $V = V_{bi}$. Thus we get,

$$(V - V_{bi}) = \frac{-qN_A W^2}{2\epsilon_s} \tag{1.6}$$

Hence the depletion layer width at any given potential is given by

$$W = \sqrt{\frac{2\epsilon_s(V_{bi} - V)}{qN_A}} \tag{1.7}$$

1.3.2 Carrier transport in organic semiconductors

Charge carrier injection into the organic dielectric media is one of the area that has attracted considerable attention of the researchers worldwide. Till date several models based on Field and Temperature dependence have been proposed. Some of the most general models have been discussed in great detail.

Richardson Schottky model of Thermionic Emission

Thermionic emission in general is the branch of physics which deals with the effect of heat on the interaction between electricity and matter. In 1873 Guthrie showed that a red hot iron ball in air could retain a negative but not a positive charge. In a series of researches that followed Elster and Geitel examined the charge collected on an insulating plate. Later, J. J. Thomson showed that the discharge from incandescent carbon filament in a vacuum tube was carried by negative electrons. However, in 1901 Richardson was able to show that each unit area of a Pt surface emitted a limited number of electrons. He also observed that this number increased very rapidly with the increase of temperature. It was later put forth that it is the Kinetic energy of the charge carriers in a solid that increases with increasing temperature and therefore the probability that a charge carrier passes a given potential barrier also increases. The thermally induced current flow of the charge carriers from a metal contact into a polymer film can be derived from the

Richardson equation, which takes into account the temperature induced emission of hot charge carriers from a metal electrode and is as given below,

$$J_{th} = A^* T^2 \exp\left(\frac{-q\phi}{kT}\right) \tag{1.8}$$

Where ϕ is the potential barrier, q is the charge of the carrier, T is the absolute temperature, and A^* the material dependent effective Richardson constant. This model considers that the emitted carriers are pulled away from the surface by an electric field. On describing a metal/polymer transition using this formula, the back flow of the injected charge carriers into the contact has to be taken into account. In metal polymer metal structures a characteristic temperature dependence of the current versus voltage curves, a characteristic of thermionic emission is observed provided the metal polymer contact have a low barrier height and the applied fields are kept low. It should be noted that in metal insulator polymer structures the potential barrier heights from the metal to insulator are usually very high and the contribution of the thermionic emission process to the current flow in the device is negligible. Taking log of the above equation we get,

$$\ln\left(\frac{J}{T^2}\right) = \ln A^* - \frac{q\phi}{kT} \tag{1.9}$$

Thus the thermionic emission is often confirmed by obtaining a linear plot between $\ln\left(\frac{J}{T^2}\right)$ and $\frac{1}{T}$. The slope of the linear line could yield the information about the barrier height and the intercept would help determine the value of the parameter A^*, which is a material specific constant.

Fowler Nordheim model

Under high electric fields the electrons can surmount a potential barrier even at low temperatures. This process is based on field induced tunneling of the charge carriers across the potential barrier. The probability for the tunneling depends strongly on the height and width of the potential barrier. the Field induced tunneling across a potential barrier is given by the equation

$$J_{FN} = AE^2 \exp\left(\frac{-4\sqrt{2m^*\phi_B^3}}{3\hbar qE}\right) \tag{1.10}$$

where m* is the effective carrier mass, E is the magnitude of the applied electric field, and ($A = q^3/8\pi h\phi_B$) is a rate coefficient that contains a tunneling prefactor and rate of backflow current,15 and it is expressed in A/V^2. When the electric field induced tunneling currents are analyzed on a logarithmic scale, the equation becomes,

$$\ln\left(\frac{J_{FN}}{E^2}\right) = \ln(A) - \frac{-4\sqrt{2m^*\phi_B^3}}{3\hbar qE} \tag{1.11}$$

Thus, a plot between $\ln(J_{FN}/E^2)$ versus $(1/E)$ should be a straight line. The height of the potential barrier ϕ_B can be obtained from the slope of the straight line thus obtained. In metal insulator polymer structures large barrier heights exist at the interface of the metal/insulator. Therefore, the charge carrier injection can be described by field induced tunneling. The current versus electric field characteristics of metal polymer structures can be fitted to a straight line at high applied fields in a Fowler-Nordheim plot, when the barrier heights at the interface are large compared to kT as it has been first described by Parker et al. However, the values for the current, which are obtained using Fowler-Nordheim equation with actual device parameters, are often several orders of magnitude higher than the values for the measured current in real devices[61].

Mott-Gurney Law

Although a significant role is played by the injection mechanisms, however, they are essential but not sufficient to discuss the conduction through the bulk of organic film. Thus, in order to best describe the IV characteristics of organic devices, the charge transport mechanisms in the bulk have to be taken into account. In simplest terms it can be said that the electrical conductivity in the solid state is determined by the product of the carrier concentration and carrier mobility. In π-conjugated polymers both entities are material dependent and, are different for electrons and holes on a conjugated polymer lead to a relaxation of the surrounding lattice, forming the polarons as described in previous section. Therefore the conductivity σ, is the sum of both positive P^+ and negative P^-.

$$\sigma = en_{P^-}\mu_{P^-} + en_{P^+}\mu_{P^+} \tag{1.12}$$

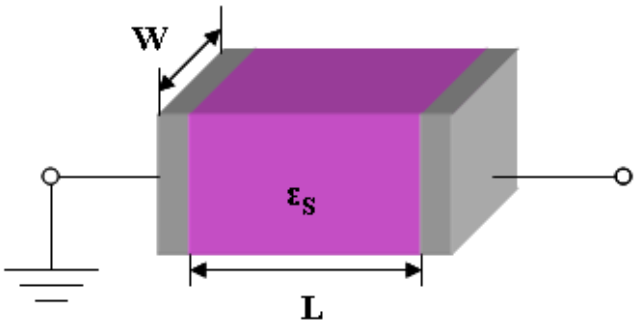

Figure 1.8: A Dielectric slab of lengh l and width W

where n and μ are the concentration and mobility of the respective species P^+ and P^- and e denotes the elementary charge. In contrast to carrier injection, which depends on the properties of the polymer/electrode interfaces, carrier transport is a bulk property of the polymer layer. In an interesting report Blom. et al [62-65] stated that the IV characteristics in various ohmic organic devices are determined by the bulk conductivity and not by the charge carrier injection. They observed that the current flow in these hole only devices depends quadratically on the voltage. Consider the conduction through an intrinsic semiconductor with an applied bias as is shown in Fig. 1.8. The intrinsic carrier concentration in the semiconductor is assumed to be negligible ($i.e. n_i \approx 0$) and the conduction takes place by holes that are injected from one ohmic contact and extracted from the other ohmic contact. Electrons are not injected and the conduction due to electrons is ignored. As a result of hole injection the semiconductor is not charge neutral. The expression describing the displacement of holes is given by

$$J = qpv = qp\mu_p E \tag{1.13}$$

Also from Poisson's equation we have the relation between the gradient of electric field and charge carrier density

$$\frac{dE(x)}{dx} = \frac{qp(x)}{\epsilon} \tag{1.14}$$

combining the above equations we get

$$\frac{dE}{dx} = \frac{J}{\epsilon\mu_p E} \tag{1.15}$$

imposing the boundary condition we get.

$$\int_0^E EdE = \frac{J}{\epsilon\mu_p}\int_0^x dx \tag{1.16}$$

which upon solving gives

$$V = \frac{2}{3}\sqrt{\frac{2J}{\epsilon\mu_p}}L^{3/2} \tag{1.17}$$

Finally we arrive at the *Mott-Gurney law* for space charge limited current in a trap free intrinsic semiconductor as is described by the following equation

$$J = \frac{9\epsilon_0\epsilon_r\mu_p V^2}{8d^3} \tag{1.18}$$

In the conventional semiconductor theory electrons in the conduction band of metals and semiconductors move in delocalized states, and their wavefunction can be approximated to that of a free electron, that is, a plane progressive wave

$$\psi_k(r) = \exp(ikr) \tag{1.19}$$

In these delocalized bands, the charge transport is limited by scattering of the carriers by lattice vibrations (phonons). Therefore, an increase in the temperature, which induces an increase in the density of phonons, leads to an decrease in the mobility. However, on the contrary in the case of disordered organic semiconductors, the mobility is so low that it corresponds to a mean free path lower than the distance between the atomic sites, which is physically not pertinent. Anderson et al have shown that the disorder in a solid may result in delocalization of the states, in which case the one-electron wave function takes en exponential form

$$\psi(r) = \exp\left(\frac{-r}{a}\right) \tag{1.20}$$

where a denotes the size of the localized state. Charge transport in that case occurs via tunneling between the localized states. When states are localized, the tunneling of carriers from one site to the next is assisted by phonons. Hence, the mobility is thermally activated, which means that it increases when the temperature increases. This mechanism is often termed as phonon activated hopping. Interestingly, such a mechanism is

not restricted to disordered materials; it can also occur in well ordered crystals, where strong electron phonon interaction results in the formation of self localized states called polarons. As pointed out in the literature, in real solids, the activation energy of the mobility is the sum of two terms, one arising from disorder, and the second one from the change in molecular confirmation upon addition of a charge. The essential difference between hopping and polaron models is related to the relative importance of both contributions. In the hopping model, it is assumed that the coupling between charge and vibration modes is weak, and that most of the temperature dependence is because of the energy disorder of the hopping sites, whereas the polaron model considers disorder to be unimportant w.r.t. electron phonon coupling. Conjugated polymers are intrinsically semiconducting materials. They lack intrinsic mobile charge carriers, but at the same time are capable of transporting charge generated by light, injected by electrodes, or provided by chemical dopants.

Due to the disorder and the localization of charge, the motion of the charge carriers in organic semiconductors are typically by hopping transport, which typically follows phonon assisted tunneling mechanism from site to site. The hopping transport takes place around the Fermi level. Many of the hopping transport models are based on the single phonon jump rate description as proposed by Miller and Abraham [66]. In this model the hopping rate between an occupied site i and an adjacent site j, which are separated in energy by $E_i - E_j$ and in distance by R_{ij}, is described by

$$\nu_{ij} = \nu_0 \exp(-2\gamma R_{ij}) \begin{cases} \exp -\{\left(\frac{E_i - E_j}{k_B T}\right)\}; E_i > E_j \\ 1; E_i < E_j \end{cases} \tag{1.21}$$

Where ν_0 is a prefactor, γ^{-1} quantifies the wavefunction overlap between the sites, and k_B is the Boltzmann constant. The Miller-Abraham model [63] addresses hopping rates at low temperatures between shallow three dimensional impurity states, assuming that the electron lattice coupling is weak. When the Miller-Abraham's model is applied to polymeric semiconductors, it is assumed that the conjugated segments of the polymer play the role of nearly isolated impurity states, and that the above equation is still valid at high temperatures.

Depending on the structural and energetic disorder of the system it can be energetically

favorable to hop over a longer distance with a low activation energy. This extension to the Miller-Abraham's model is called variable range hopping. Monroe et al have also developed a model describing hopping transport around the fermi level in an exponential density of states. He found that this hopping description is very similar to a model in which charge carriers are thermally activated to a transport level. For the description of the temperature and gate voltage dependencies of OFETs Vissenberg and Matters developed percolation model based on variable range hopping in an exponential density of states [67,68].

For Polycrystalline organic semiconductor layers the temperature dependent transport data is often interpreted in terms of a multiple trapping and release model. In this model the organic semiconductor film consists of crystallites, which are separated from each other by amorphous grain boundaries. In the crystallites the charge carriers can move in delocalized bands, whereas in the grain boundaries they become trapped in localized states. The trapping and release of carriers at these localized states result in a thermally activated behavior of the Field effect mobility. The description of trapped, i.e. localized charges which can be thermally activated to a transport level, in this case the band, is very similar to hopping in an exponential density of states as stated in the previous section. As the grain boundary in a polycrystalline system determine DC charge transport and typically an exponential trap distribution is used to model the experimental data, no clear distinction can be made between hopping transport and multiple trapping and release, on the basis of the temperature dependence of the mobility. One should be able to separate a trap limited mobility from hopping mobility if the Hall mobility in a Hall effect experiment could be determined, since in a magnetic field there will be no Lorentz force on trapped charges. Unfortunately due to low charge carrier mobilities in these materials the Hall effect is very difficult to measure experimentally.

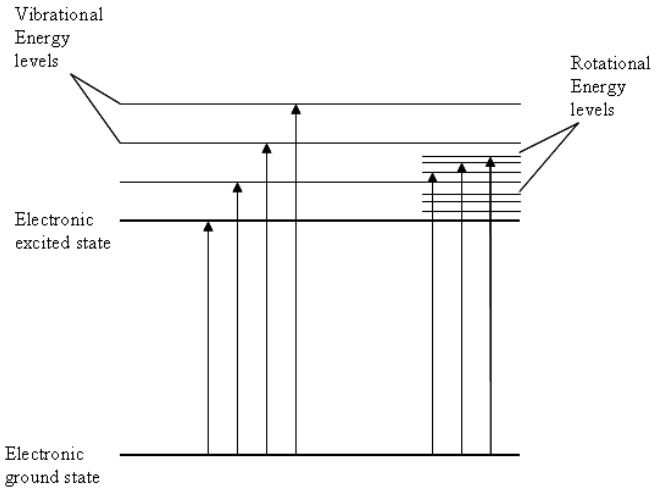

Figure 1.9: A Dielectric slab of lengh l and width W

1.4 Optical properties of Conjugated polymers

1.4.1 Light absorption in Conjugated polymers

When light either in the visible or ultraviolet is absorbed by the valence electrons in organic molecules, and these electrons are then promoted from their normal ground states to the higher energy states. The energies of the orbitals involved in the electronic transitions have fixed values. Because the energy is quantized, it can be safely assumed that the absorption peaks in the UV/Visible spectrum will be sharp peaks. However, this is rarely the case. Instead the commonly observed spectrum of π-conjugated dyes/polymers the spectrum consists of broad peaks[69,70]. This is because there are also vibrational and rotational energy levels available as can be seen in Fig. 1.9. The exact energy differences between the orbitals varies. In organic molecules double bonds which are next to each other can conjugate join together and delocalize the electrons over all of the atoms. This lowers the energy to promote the outer electrons.

The π electrons on the backbone of π-conjugated polymers do not interact with one another and move on a straight line path which extends up to the length of the molecule or a single polymer chain. This means that the potential is constant on this path and infinite off this path. In quantum mechanical terms the behavior is identical to that of a particle in a box. In quantum physics it has already been shown that a particle trapped

in a one dimensional box of length L has quantized energy levels, and the energy of such a particle is given by

$$E_n = \frac{n^2\pi^2\hbar^2}{2m_eL^2} \tag{1.22}$$

Where m_e denotes the mass of the particle and n denotes the quantum number. It is to be noted that particle can only occupy certain discrete energy levels, and that the energy between any two consecutive energy levels is forbidden for the particle. The corresponding wavefunction of such a particle can then be written as

$$\psi_n = \sqrt{\frac{2}{L}} \sin\left(\frac{n\pi x}{L}\right) \tag{1.23}$$

In this simple model light is absorbed if it can induce an electron to jump to higher energy level. So that the change in its energy as given by $\triangle E = E_2 - E_1$ satisfies the basic Planck's relation

$$\lambda = \frac{hc}{\triangle E} \tag{1.24}$$

Since the wavelength is inversely proportional to transition energy, the longest absorption wavelength observed therefore corresponds to the smallest possible transition energy. Although it is possible to predict the absorption wavelengths for an organic molecule, however, the intensities of electronic transitions have always proved extremely difficult to calculate accurately from molecular wavefunctions. The reason for this is that the calculated values are quite sensitive to the exact details of the wave functions, so that approximate wavefunctions tend to give poor agreement with the experimentally observed values. However, different types of transitions observed in molecules have intensities which vary over a range of about eleven orders of magnitude, so that even approximate calculations of intensities can be very valuable in identifying observed spectral bands.

In general the intensity of an electronic transition σ, is related to the integral of the electric dipole moment operator, μ, and the wavefunctions of the two states involved as is given by

$$\sigma \propto \left| \int \psi_G \mu \psi_E d\tau \right|^2 \tag{1.25}$$

Where ψ_G and ψ_E are wavefunctions for the ground and the excited states of the molecule by an orbital approximation and assume that the center of positive charges remains fixed

during the transition. In case of π-conjugated polymers the optical band gap of polymer was estimated by fundamental relation given by

$$\alpha h\nu = B(h\nu - E_g)^n \tag{1.26}$$

Where α is the absorption coefficient, $h\nu$ is the energy of absorbed photon, B is a proportionality constant. In case of allowed transition $n = 1/2$. Therefore the above equation becomes

$$(\alpha h\nu)^2 = B^2(h\nu - E_g) \tag{1.27}$$

Thus the slope of plot of $(\alpha h\nu)^2$ vs. $h\nu$ in its linear region, upon extrapolation can yield the value of bandgap E_g. Immediately after the absorption of light what follows is the generation of electron-hole pairs which may relax to occupy the lowest available energy states, and under such a state may well then become bounded under their mutual force of attraction (Coulomb's force) resulting in the formation of another quasiparticle that we now know as exciton.

1.4.2 Exciton in Conjugated polymers

An exciton [71-73] is a bound state of an electron and a hole in an insulator or semiconductor, and such is also referred to as Coulomb-correlated electron-hole pair. It is an elementary excitation, or a quasiparticle of a solid. The bound electron and hole pairs (excitons) provide a means to transport energy without transporting net charge. A vivid picture of exciton formation is as follows: a photon enters an organic semiconductor, exciting an electron from the HOMO into the LUMO. The missing electron in the HOMO leaves a hole (of opposite electric charge) behind, to which the electron is attracted by the Coulomb force. The exciton results from the binding of the electron with its hole. As a result, the exciton has slightly less energy than the unbound electron and hole.

Depending on the range of their energies the excitons are further divided into two categories. The first one being Mott-Wannier excitons which usually occur in materials with relatively higher dielectric constant (ϵ) reducing the Coulomb interaction between electron and holes. This leads to weakly bound excitons. Mott wannier excitons are

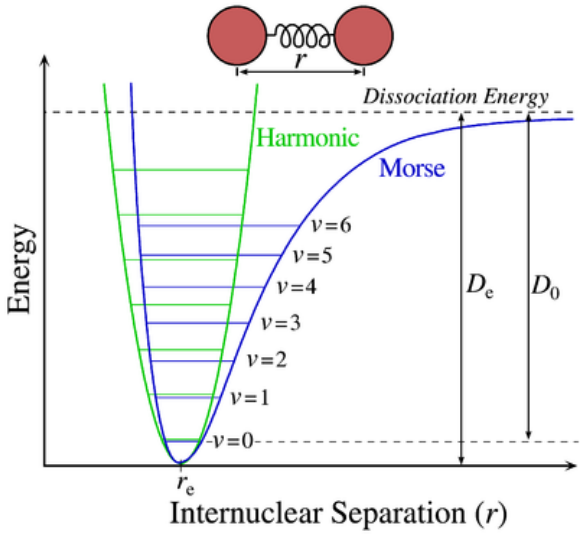

Figure 1.10: Energy level of a diatomic molecule *(courtesy Wikipedia)*

often found in inorganic semiconductors, as they have relatively higher values of ϵ.The binding energies of Wannier excitons are typically of the order of $0.1eV$. The second of the lot are called Frenkel excitons. These are found in semiconductors with relatively low values of ϵ, as is also the case in π conjugated organic semiconductors. Their binding energies are typically of the order of $1eV$.

Often the π conjugated semiconductors are modeled using the diatomic model of molecules. as they are a better approximation for the vibrational structure of the π conjugated system than the quantum harmonic oscillator. It is also shown in Fig 1.1. Morse potential as shown by the blue curve has unevenly space energy levels unlike the harmonic oscillator in which the energy levels are evenly spaced. Morse potential level spacing decreases as the energy approaches the dissociation energy. Also shown in Fig. 1.10 are the Dissociation energy (D_e and r_e denotes the equilibrium bond distance between the constituent atoms of the molecule. The nuclear axis refers to the internuclear separation.

Franck-Condon principle

Franck-Condon principle simply states that electronic transitions are instantaneous with respect to the time scale of nuclear motions. Thus it can also be said that the Franck-Condon principle [74,75] is the approximation that an electronic transition is most likely

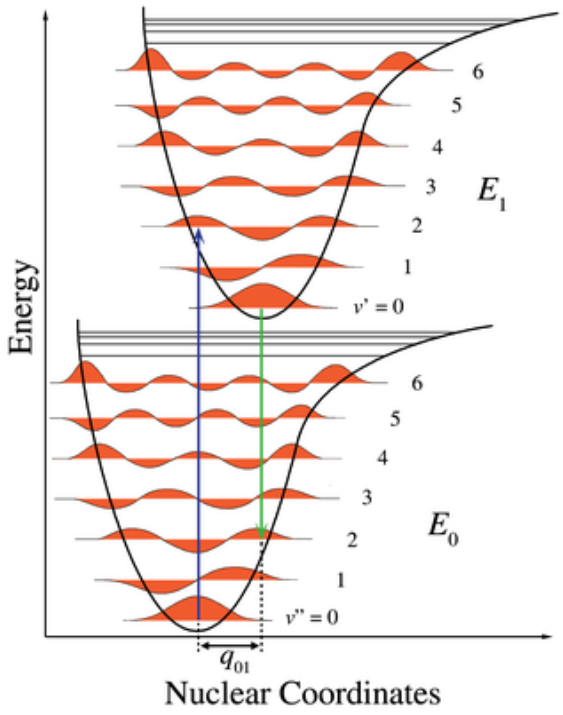

Figure 1.11: Energy level diagram showing Frack-Condon principle *(courtesy Wikipedia)*

to occur without changes in the positions of the nuclei in the molecular entity and its environment. The quantum mechanical formulation of the principle is that the intensity of a vibronic transition is proportional to the overlap integral between the vibrational wave-functions of the two states that are involved in the transition. Figure 1.11 illustrates the Franck-Condon principle for vibronic transitions in a molecule with Morse like potential energy functions in both ground and excited electronic states. The probability that any molecule can end up in a ny particular vibrational level is proportional to the square of the overlap of their vibrational wave-functions of the original and the final state. In the electronic excited state molecules quickly relax to the lowest vibrational level (Kasha's rule), and from there can decay to the lowest electronic state via photon emission. It is also worthwhile to note that the Franck-Condon principle is applicable to both absorption and emission, and together combined with Kasha's rule leads to an approximate mirror symmetry in the absorption and the emission curves as can be seen from Fig 1.12. The vibrational structure of molecules is most clearly visible in a cold sparse gas due to the absence of any inhomogeneous broadening of the individual

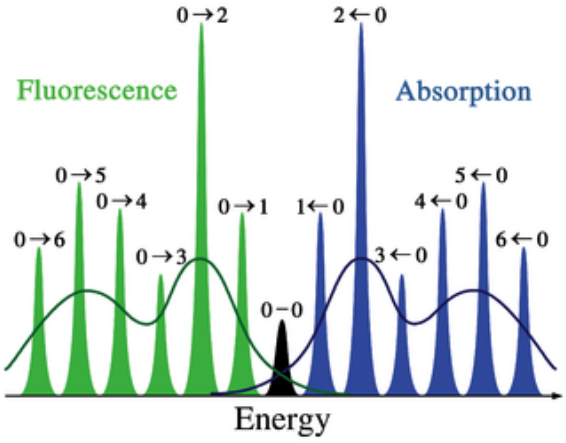

Figure 1.12: Schematic representation of the absorption and the emission spectra *(courtesy Wikipedia)*

transitions. In the case of organic molecules the difference between the absorption and emission maxima is also known as Stoke's shift. It is characteristic of the energy loss by the system. A higher stoke's shift is attributed to higher degree of disorder in the system.

1.4.3 Exciton diffusion in conjugated polymers

While excitons are formed throughout the bulk of material. However, in organic semiconductors the exciton tend to diffuse in regions of low dielectric constant. Besides this, even the population gradient also causes excitons to drift into regions of sparse populations. However, in general the exciton diffusion is limited is characterized by its diffusion length. The diffusion length of excitons itself depends on the morphology of the material.The exciton diffusion lengths in various conjugated polymers reported in the literature show a large variation, ranging from 5 to 14 nm [76-80]. Most of these studies make use of a bilayer model system, comprising an evaporated C60 layer in combination with a conjugated polymer, spin-coated from solution. A direct way to study the exciton diffusion was used by Markov et al in organic bilayer hetero structure based devices. These studies combined with various other reports have laid down the basic framework not only about exciton diffusion but various competing mechanisms of exciton energy transfer from Donor to the acceptor molecules. It is now known that

there are three general mechanisms by which an exciton can transfer its energy from Donor to Acceptor. These are as given below:-

1) Radiative energy transfer.

2) Föster energy transfer.

3) Dexter energy transfer.

In the radiative energy transfer the donor molecules usually undergo deactivation and the energy is reabsorbed by the acceptor molecules. This type of energy transfer is characterized by the following equation.

$$P_{r,t} \propto [A]xJ \tag{1.28}$$

Where $P_{r,t}$ denotes the probability of energy transfer and is directly proportional to the product of $[A]$ the acceptor concentration, x the sample thickness and J the spectral overlap integral between the emission spectra of the donor and the absorption spectra of the acceptor molecules. In the light of PLEDs the former may be termed as the host molecules and the latter may be called as the dopant molecules. Since x is involved in the energy transfer. Thus, this type of energy transfer also depends on the shape and size of the vessel utilized.

The second type of energy transfer is Föster type. This type of energy transfer occurs via resonance mode dipole dipole coupling. A key feature of this type of energy transfer is that Donor acceptor transitions must be allowed. It can occur over a relatively large distance of $(100nm)$. These type of transitions are very fast and occur on the short time scale of $1ns$. The energy transfer rate $K_{D\rightarrow A}$ is given by the following relation.

$$K_{D\rightarrow A} = \frac{K^2 J \times 8.8 \times 10^{-28} mol}{n^4 \omega r^6} \tag{1.29}$$

Where K is the orientation factor. n is the refractive index of the medium, ω is the radiative rate constant of the donor,r is the distance in cm between the donor and acceptor molecules, and J is the spectral overlap integral, as was also defined above. The third type of energy transfer known as Dexter energy transfer occurs via electron exchange excitation transfer. The essential condition for this to occur is the overlap of the donor and acceptor wavefunctions. In common singlet-singlet and triplet-triplet

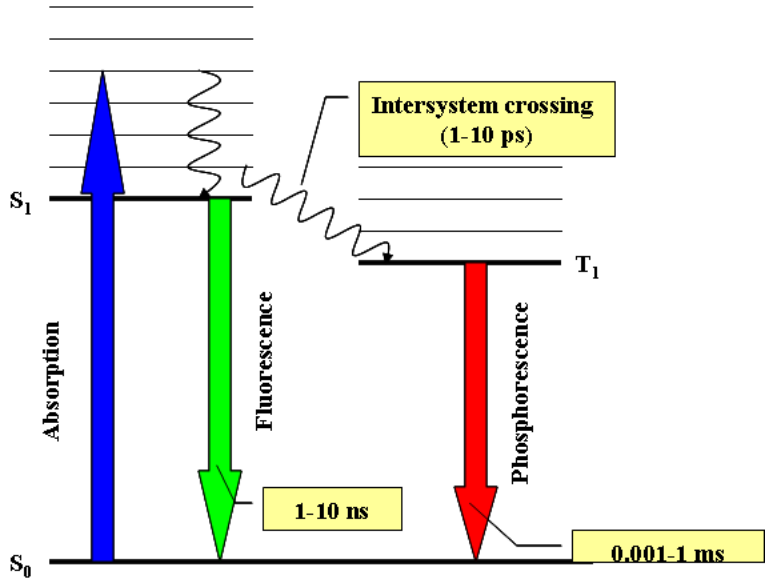

Figure 1.13: Schematic representation of the absorption followed by flourescent or phosphorescent emission in organic semiconductors

energy transfer is allowed. Infact, it is a dominant mechanism in triplet-triplet energy transfer. The rate constant for energy tranfer in this case is given by K_{ET} as mentioned in the following equation,

$$K_{ET} \propto \hbar P^2 J \exp\left(\frac{-2r}{L}\right) \tag{1.30}$$

Where r is the distance between the donor and acceptor molecules. J is the spectral overlap integral as also mentioned in the previous two cases. This mechanism governs the working of Phosphorescent PLEDs. In these devices the energy transfer from host to the dopant (Phosphorescent in this case) is governed by this mechanism. Usually phosphorescent molecules are also employed for tapping the triplet excitons in the case of OLEDs. Figure 1.13 shows the absorption and emission processes occurring in organic semiconductors.

1.4.4 Light emission via exciton recombination in Conjugated polymers

After their creation, followed by their diffusion the excitons either recombine or dissociate. The recombination of excitons can occur either radiatively or non radiatively as is shown in Fig. 1.13. While radiative recombination causes emission of light as in OLEDs.

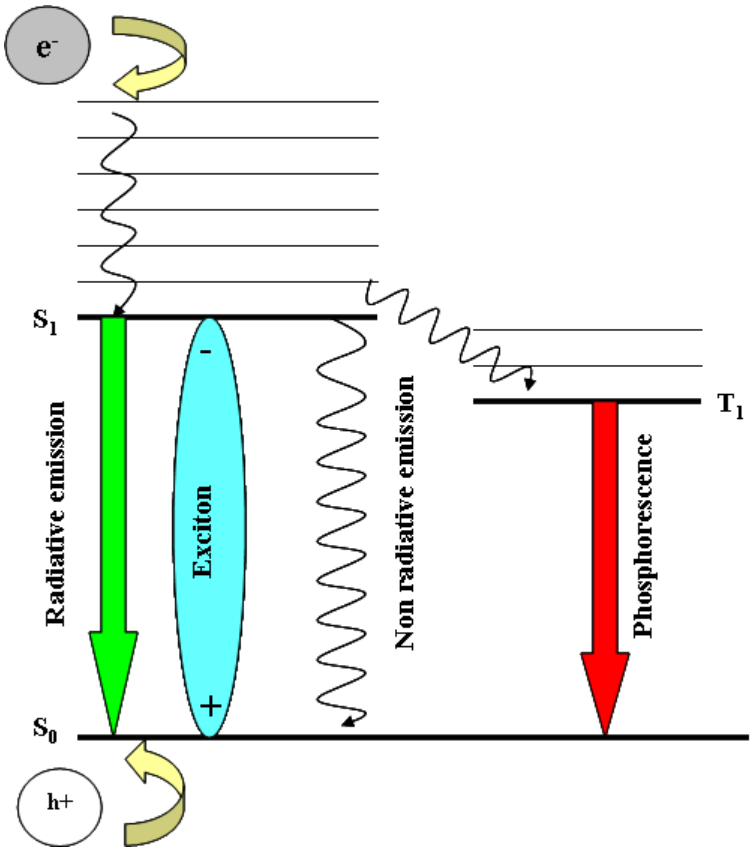

Figure 1.14: Schematic representation of exciton formation in OLEDs, both singlet and triplet states have been shown

Non radiative recombination proceeds via phonon vibrations and does not result in the any radiations. All underlying processes during an OLED operation have been shown in Fig. 1.14. As is also shown in Fig. 1.14 that in the case of OLEDs the excitons are generated due the injection of electrons and holes into the bulk of the respective semiconducting layers. Such a charge injection usually leads to 25% singlet and 75% triplet excitons. Figure 1.5 shows the Excited triplet state as T_1. The inter system crossing results in the formation of triplet excitons. Singlet excitons lead to fluorescence and thus it was thought that the maximum limit of the OLED efficiency is limited to the singlet excitons. However, [81-83] showed that even the triplet states can be utilized in efficient emission of light by the use of suitable phosphorescent molecules. This concept made white light emission possible from a single layer PLED. Exciton dissociation results in electron hole pair generation and thus is utilized in photovoltaic applications like

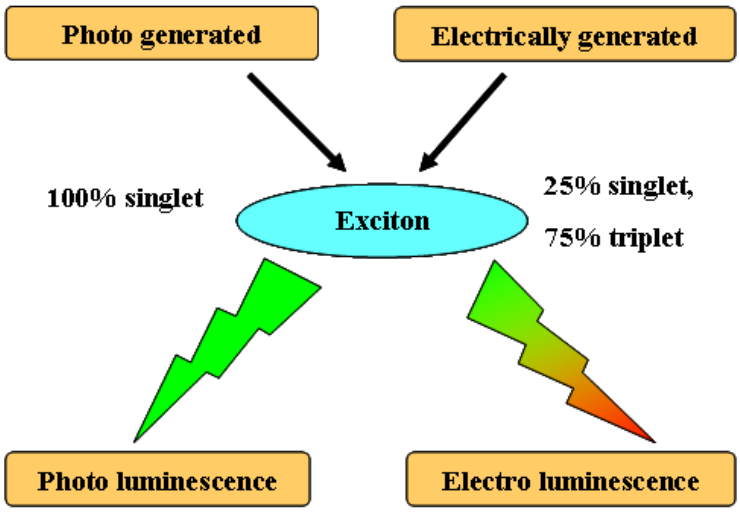

Figure 1.15: Schematic diagram showing the cause of electroluminescence and photoluminescence

OSCs. Several different types of photovoltaic cells have been proposed based on organic materials viz. bilayer organic solar cells, bulk heterojunction thin film solar cells and Dye sensitized solar cells. While the first two belong to the solid state device category the third operates in the liquid state, even though a complete solid state photovoltaic cell is highly desired. While excitons are the basic species involved in the working of both OLEDs and OSCs. It is the nature of their origin that differs in these devices as has been illustrated in the Fig. 1.15. While photo excitations lead to the generation of singlet excitons only. The electrical excitation as in OLEDs lead to the generation of both singlet and triplet excitons, their ratio is governed by the spin conservation rules. The emission due to photo generated excitons is known as Photoluminescence (PL), and that by electrically generated excitons is called electroluminescence (EL). Luminescence in general refers to the emission of light without thermal excitation for a time exceeding the electromagnetic oscillation, and therefore is also called cold emission. Light emitted from hot bodies on the contrary in called incandescent bodies.

1.4.5 Exciton dissociation under electric field

Usually exciton dissociation requires electric field, which may provide the excess energy over the binding energy of exciton, causing its dissociation. This field may be applied

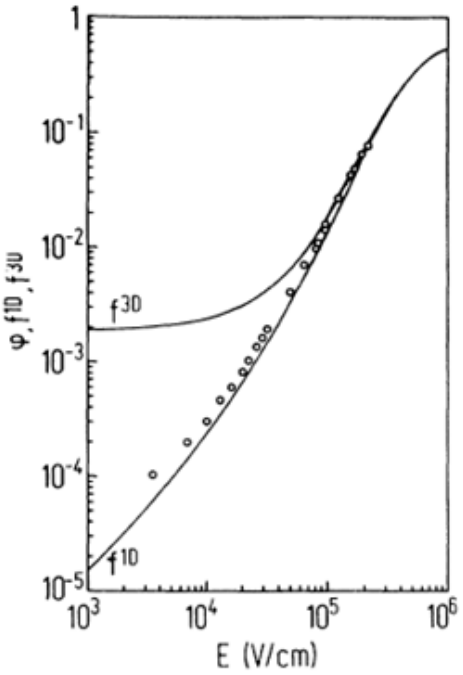

Figure 1.16: Plot of Onsager dissociation yield against applied Electric Field *(Courtesy M. Gailberger et al)*

externally on to the bulk of the organic thin film, or it may be present in the form of built in field near the bilayer heterojunction, in the case of composite thin films, this field is provided by the built in field at every donor acceptor interface throughout the bulk of the composite film.

Onsager Model

The Onsager model [84-86] was originally developed for dissociation of electrolytes into constituent ions.Onsager model emphasizes the importance of the Coulomb interaction in binding the electron hole pair and the role of external field (E) and temperature (T) in processes which dissociate the pair into free carriers. Thus in general the Onsager model predicts a strong dependence of quantum yield ϕ on T and E The Onsager theory states that the dissociation of short lived charge pairs is that photon absorption creates with probability φ_0 a coulombically bound $e-h$ pair with initial pair distance r_0. It can either recombine or dissociate with probability f in the course of a temperature and field assisted diffusion process. The activation energy E_A of the quantum yield,

measured at low fields, is related to r_0 via the relation

$$r_0 = \frac{e^2}{(4\pi\epsilon\epsilon_0 E_A)} \tag{1.31}$$

Gailberger et al found in their case the value of $E_A = 0.165eV$, $r_0 = 25\mathring{A}$. Knowing the value of r_0 allows calculating the pair dissociation probabilities for either one or three dimensional system topology in the limit of the homogeneous medium approximation. The 1D version of Onsager theory predicts

$$f^{1D}(r_0, E) = \frac{\int_0^1 \exp(2\xi t - \eta/t)dt}{\int_0^\infty \exp(-2\xi t - \eta/t)dt} \tag{1.32}$$

where $\xi = \frac{eEr_0}{2kT}$ and $\eta = r_c/r_0$. Figure 1.16 shows the quantum yield φ of the dc photocurrent as a function of electric field ($\lambda_{exc} = 400nm), T = 295K$). Solid curves are Onsager dissociation yields calculated for an initial pair separation of $25\mathring{A}$ assuming $3D$ and $1D$ topology respectively.

1.5 Physics of Organic Electronic Devices

1.5.1 Organic Field Effect Transistors

As Shown in Fig. standard p-channel OFETs are typically built on a Silicon wafer, although there have been reports about all organic OFETs using polymeric gate dielectric materials. High mobility transistors using pentacene utilizing cross-linked Poly(vinylphenol) as a gate dielectric have been demonstrated. However, with conducting polymers it is difficult to fabricate a high performance transistor over a polymeric gate dielectric primarily because of the large leakage currents flowing in these devices. However, the geometrical parameters of the device are the channel length L, defined by the distance between the Source-Drain electrodes. The channel width W, as defined by the width of the Source-Drain electrodes. In order to calculate the current voltage characteristics, the *gradual channel approximation* introduced by William Schokley is used. Under this approximation it is assumed that the charge density induced by the electric field parallel to the channel is much smaller than that induced by the electric field across the channel, i.e. $\mid \partial V_x/\partial x \mid << \mid \partial V_y/\partial y \mid$, where the x and y are the directions parallel and

perpendicular to the channel, respectively. This requires that the channel length L must be much larger than the insulator thickness ($L >> d_i$). Under these circumstances it can be assumed that the charge induced at a given distance x from the source is that is that of a MIS junction where the surface potential V_s would be equal to v. The charge per unit area Q_s induced at the insulator semiconductor interface at a distance x from the source is then

$$Q_s(x) = C_{ins}[V_g - v] \tag{1.33}$$

Where C_{ins} is the Capacitance per unit area, V_g denotes the gate bias voltage. Meanwhile the channel can be thought of as a narrow region just adjacent to the insulator/semiconductor interface. Thus, the drain current I_{ds} can be in terms of channel conductance as

$$g(x) = \frac{W}{L}\int_0^x \sigma(x^{'})dx^{'} = \frac{W\mu \mid Q_s(x) \mid}{L} \tag{1.34}$$

It should be noted that the mobility of charge carriers is assumed to be constant all over the channel region. The elemental resistance dR of an elemental segment dx is given by

$$dR = \frac{dx}{gL} = \frac{dx}{\mu W Q_s(x)} \tag{1.35}$$

and the voltage drop across this elementary segment is given by

$$dV = I_{ds}dR = \frac{I_{ds}dx}{W\mu Q_s(x)} \tag{1.36}$$

Thus upon integrating we get,

$$\int_0^{V_{ds}} W\mu C_{ins}[V_g - v]dv = \int_0^L I_{ds}dx \tag{1.37}$$

which further implies

$$I_{ds} = \frac{W\mu C_{ins}}{L}\left[V_g V_{ds} - \frac{V_{ds}^2}{2}\right] \tag{1.38}$$

Thus in the linear region current in the transistor is given by eq [*]. However in the saturation region the $V_{ds} >> (V_g - V_t)$ then in that case $V_{ds} = (V_g - V_t)$. This further implies

$$I_{ds} = \frac{W\mu C_{ins}}{2L}(V_g - V_t)^2 \tag{1.39}$$

1.5.2 Organic Light Emitting Diodes

OLEDs presently exist under a variety of different geometries and compositions. The simplest of these is a single organic layer sandwiched between two electrodes as is shown in the Fig. The other geometry of these devices is bilayered device. Although multi-layered OLEDs have also been reported and extensively researched over the last few years. However, the addition of each layer increases the cost of the device and the display based on these devices as a whole, simultaneously increasing the complexity of their design. Although limited in their performance by the multilayer OLEDs, the single layer OLEDs are highly desirable because of their ease of processing and their relatively simple structure.

In a single layer device, the organic material must perform all the three functions: hole transport, electron transport and photon emission via electron-hole radiative recombination. In this case the injection rates of holes from the anode into the HOMO and electrons from the cathode into the LUMO must be roughly equal or efficient. Otherwise excess carriers of one sign will just pass through the organic layer without radiative recombination, contributing to the current in the external circuit but not to the emission. During the 1980s Kodak group achieved a major technological breakthrough by the use of two layers of organic materials. In this approach one material (that adjacent to anode) can be selected for good hole injection and transport, while that adjacent to the cathode permits good injection and transport of electrons. Emission may occur from either or both materials. The interface between the two organic layers can have two additional effects on the operation of the bilayer device. First is that the energy level offsets may present a barrier for electrons entering the hole transport layer, and vice versa. This tends to prevent the loss of efficiency caused by the passage of charge from one electrode to the other without recombination. Secondly, because of the high density of carriers on each side of the organic interface , i.e. holes in the hole transport layer (HTL) and electrons in the electron transport layer (ETL), recombination is most likely to occur near the interface and well away from the metallic electrodes. This reduces the probability of exciton quenching by dissociation near the electrode. The exact nature of

recombination and emission depends on the energetics of holes, electrons and excitons in each material.

Besides the bilayered structures the trilayer structures offer additional possibility of selecting the emissive material, independent of its transport properties. Additional layers have also been added to accomplish various other benefits, tailoring the energy profiles and mobilities across the entire organic stack. Splitting the transport layers into two separate layers permits the optimization of injection into the layer nearest to the electrode (sometimes called the injection layer), and the transport in the farther layer. Layers of insulator (Charge confinement layers) have also been used in an attempt to control the motion of the charges and ensure recombination of the desired region. Since the processes of charge injection, transport, and recombination dictate the external quantum efficiency of the OLEDs. For example the external quantum efficiency η_{ext} (fraction of injected electrons that results in the emission of a photon from the device) is given by

$$\eta_{ext} = R_e \gamma \eta_s \phi_f \tag{1.40}$$

Where R_e is the light extraction coefficient, γ is the charge balance ratio, η_s is the fraction of singlet excitons and ϕ_f denotes the quantum efficiency of fluorescence. The light extracted depends upon the number of organic layers encountered in the path of light, as each organic layer acts like a dielectric medium and at the boundary of these dielectric media some of the light is always lost in the form of scattering and reflections or total internal reflections. With the use of minimal layers along with a fine tuning in the the relative dielectric constants of different layers maximum out coupling efficiency has been achieved as pointed out by its theoretical limit. Besides this innovative concepts such as use of a optical grating layer etc could also lead to improvement in the value of R_e. As pointed out by theoretical studies a near to unity value of γ has also been achieved. As has been already discussed the injection of charges leads to two types of excitons, singlet having no over all spin and triplet having an overall spin. The ratio of singlet to triplet states is 1:3. Early researches showed that it was the singlet excitons that lead to light emission from an OLED. This, further made them believe that the overall external quantum efficiency has been limited by singlet excitons. However,

some more recent approaches have been able to tap the energy from the triplet state excitons does leading to a near 100% utilization of the excitons. One such approach is by using suitable phosphorescent dyes. The fluorescence efficiency depends on the relative strengths of excitons undergoing radiative and non radiative recombinations. From an engineering design point of view, a more relevant figure of merit is the power efficiency η_p, defined as the ratio of emitted optical power to the driving electrical power. It is given by

$$\eta_p = \frac{\eta_{ext} h\nu}{eV} \tag{1.41}$$

Where $h\nu$ denotes the energy of the emitted photon, e is the electron charge and V is the externally applied voltage on the OLED. For a high power efficiency, the operating voltage (the voltage at which there is sufficient current flow and light emission) should be as low as possible.

1.5.3 Organic Solar Cells

A tremendous research effort was devoted to the development of photovoltaic cells during the late seventies and early eighties. During this time interest was also developed to the development of organic semiconductors, because they offer the advantages of low cost and facile processing. Organic materials for use in photovoltaic devices require good chemical stability and large optical absorption in the visible range. Efficiencies of the first polymeric solar cells, based on hole conducting conjugated polymers (mainly polyacetylene) were rather discouraging. However, the breakthrough to higher efficiencies was achieved by switching to different classes of electron donor type conjugated polymers (Polythiophenes) and Poly(para phenylene vinylene)(PPV) and their derivatives and by mixing them with suitable electron acceptors. Prototypes on photovoltaic devices based on donor/acceptor networks showed solar energy conversion efficiencies of around 1%[]. In particular the photovoltaic properties and the photo physics of conjugated polymer/fullerene solid composites have been well investigated over the last few years[]. The rectification ratios in the order of 10^4 have been demonstrated, but photovoltaic power conversion efficiencies of these devices were low due to the small charge generating interface. The superior solubility of functionalized fullerenes compared to

C_{60} enabled the fabrication of highly fullerene loaded composite films. Significant improvement in the relatively low collection efficiency of the D/A bilayer has been achieved by control of the morphology of the D/A components in a composite film to obtain an interpenetrating network. It is this interpenetrating network or the percolated structure of the composite film that makes a bulk heterojunction solar cells highly efficient. The mechanism of this type of solar cell is that light is absorbed by the conjugated polymer system and excitons are formed, throughout the bulk of the polymer matrix, these excitons later migrate to polymer C_{60} interface, or the D/A interface. It is these D/A interface distributed randomly throughout the film that make these cells more efficient ones compared to their bilayered counterpart. Near the interface due to the built in field owing to the dissimilar work functions of the materials the excitons undergo dissociation. It should be noted that the underlying principle for both photovoltaic devices and the OLEDs is governed by manipulation of excitons. However, OLEDs on one hand are work on radiative recombination of excitons while on the other hand the photovoltaic devices work on the dissociation of excitons to generate pair of opposite charge carriers. In general three parameters govern the overall performance of a organic solar cell are the following:-

1) Power conversion efficiency η_e as given by the relation

$$\eta_e = \frac{V_{OC}.I_{SC}[inA/cm^2].FF}{P_{in}[W/cm^2]} \tag{1.42}$$

where V_{OC}, I_{SC}, FF and P_{in} are the open circuit potential, short circuit current, fill factor and incident light power, respectively. Where the fill factor was determined by calculation of maximum power rectangular area under the IV curve in the 4^{th} quadrant.

2)The fill factor is calculated using the equation

$$FF = \frac{V_P.I_P}{V_{OC}.I_{SC}} \tag{1.43}$$

Where V_P and I_P denote the intersection of the IV curve with the maximum power rectangle.

3) The spectrally resolved incident photon to conversion efficiency (IPCE) is defined as follows,

$$\eta_C[\%] = \frac{1240.I_{SC}[\mu A/cm^2]}{\lambda[nm]I[W/cm^2]} \tag{1.44}$$

In some of the recent studies Philips group modeled the IV behavior of single layer MDMO-PPV diodes. They found that at higher voltages the electron and hole currents in PPV based devices with low contact barriers are determined by the bulk conduction properties of the polymer and not by the injection properties of the contacts. The conduction of holes is governed by by the space charge effects and the field dependent mobility, while the electron transport is limited by trap density.

1.6 Thesis outline

After giving a brief introduction about the various concepts involved in this thesis, we would like to finally give a brief introduction about the thesis work itself. The research work presented in this thesis was mainly focussed around three main aspects related to organic electronic device fabrication, which are the following:-

1. Role of interface.

2. Exciton quenching mechanism.

3. Role of film morphology in exciton quenching.

In particular this thesis focusses on the interface near the low work function metal viz. Al and that of P3HT, or the so called Schottky junction. One of the pioneering work in this regard was done by Takshi et al [87], who tried to study the Schottky junction using MESFET device. They observed the inherent non uniform charge distribution in the polymer based semiconductors. The results discussed by Takshi et al [87] are of critical significance to understand the nature of Schottky junction in polymeric materials. Although this approach was based on electrical characterization, however, our approach to study the depletion layer was based on an optoelectronic model. Our optoelectronic model was developed by combining the phenomena of absorption and emission occurring during the PL measurement of a Schottky cell. The bias dependent PL have previously been used to study the exciton dissociation processes [88-92]. However, most of these reports have pointed out to the exciton dissociation and thus the PL quenching occurring due to field assisted dissociation. In our optoelectronic approach presented here shows

that the increase in depletion layer width is more dominant factor and largely responsible for Photoluminescence quenching under reverse bias conditions, contrary to the popular belief that photoluminescence quenching observed under increasing reverse bias condition is due to the increase in electric field assisted dissociation of excitons. Although some of the research groups have previously focussed their attention on bias dependent PL quenching in Schottky cell, but they have mainly attributed the PL quenching under reverse bias condition to the field assisted dissociation of excitons. Here we would like to argue that the applied field under reverse bias condition entirely drops across the depletion layer. Thus the applied field is mainly concentrated near the interface. However, with the increasing reverse bias the increase in interfacial field is insignificant. Thus, it was assumed that the PL quenching observed with increasing reverse bias is caused by increasing depletion layer width or decrease of the bulk active region of the P3HT film. Later this model was further extended to study the role of LiF in the efficiency improvement in bulk heterojunction organic solar cells. Although a lot of work to ascertain the role of LiF has already been done. It is important to note that mainly all the work has been targeted to study the interface of LiF with n-type semiconductor. It is to be noted that LiF is usually included below the Al electrode, and gives rise to improved efficiency of OLEDs. It has been established that the lowered band bending near the interface of Al and the LUMO of n-type semiconductor is mainly responsible for improved injection of electrons causing higher observed efficiencies. However, little was known about the interface of LiF with a p-type semiconductor viz. P3HT. Using the optoelectronic model the nature of interface of LiF/P3HT was could be clearly ascertained. Moreover, the studies presented in this thesis explained the observed improvement in the efficiency of OSCs using thin layer of LiF. Besides, it was also discovered that LiF does not form a depletion layer with P3HT. This fact was also then utilized to improve the IV characteristics of P3HT based OFETs. Another successful application of our optoelectronic model was towards the understanding of the role played by the film morphology in the quenching of excitons. It was found that improved film morphology leads to easy diffusion of excitons near the interface. Besides this, the relative contribution of interchain and intrachain excitons in the overall PL spectrum of organic thin film was also studied.

It was observed that metal coating on the polymer thin film led to the increase in the intrachain disorder in these films, which further caused increase in the relative intensity of the high energy peak in these materials.

Finally at last, a signature of exciton-polaron interaction was observed and reported. Although, little or no work has been done in this regard previously. Also, the results presented in this regard are still in their primafacie, a more detailed investigation in this direction could give us some new directions to solve some of the existing problems in the optoelectronic devices based on organic materials. The exciton polaron interaction is a relatively new concept on the physical grounds. The exact nature of such an interaction is also not well established.

Bibliography

[1] A. Iida, K. Nagura and S. Yamaguchi: Chemistry-An Asian Journal. 3 (2008) 1456.

[2] Y. Zhu, A. P. Kulkarni, P. T. Wu and S. A. Jenekhe: Chem. Mat. 20 (2008) 4200.

[3] E. M. J. Johansson, M. Odelius, P. G. Karlsson, H. Siegbahn, A. Sandell and H. Rensmo: J. Chem. Phys. 128 (2008) 184709.

[4] R. Davis, N. S. S. Kumar, S. Abraham, C. H. Suresh, N. P. Rath, N. Tamaoki and S. Das: J. Phys. Chem. C 112 (2008) 2137.

[5] Y. P. Yi, L. Y. Zhu and Z. G. Shuai: Macromolecular Theory and Simulations. 17 (2008) 12.

[6] J. C. Sancho-Garcia and A. J. Perez-Jimenez: J. Phys. Chem. A 112 (2008) 10325.

[7] E. C. P. Smits, S. G. J. Mathijssen, P. A. van Hal, S. Satyesh, T. C. T. Geunus, K. A. H. A. Mutsaers, E. Cantatore, H. J. Wondergem, O. Werzer,

R. Resel, M. Kemerink, S. Kirchmeyer, A. M. Murafarov, S. A. Ponomarenko, B. de Boer, P. W. M. Blom and D. M. de Leeuw: Nature. 455 (2008) 956-959.

[8] H. Z. Gao, C. S. Qin, H. Y. Zhang, S. X. Wu, Z. M. Su and Y. Wang: J. Phys. Chem. A 112 (2008) 9097.

[9] C. Risko, C. D. Zangmeister, Y. Yao, T. J. Marks, J. M. Tour, M. A. Ratner and R. D. van Zee: J. Phys. Chem. C 112 (2008) 13215.

[10] S. Kilina, E. R. Batista, P. Yang, S. Tretiak, A. Saxena, R. L. Martin and D. L. Smith: ACS Nano. 2 (2008) 1381.

[11] T. Y. Kim, T. H. Lee, J. E. Kim, R. M. Kasi, C. S. P. Sung and K. S. Suh: J. Poly. Sci. Part A 46 (2008) 6872.

[12] S Millefilorini, E Kozma, M Catellani and S Luzzati: Thin Solid Films 516 (2008) 7205.

[13] H. Yoon, S. Ko and J. Jang: J. Phys. Chem. B 112 (2008) 9992.

[14] M. C. Tanese, F. Marinelli and L. Torsi: Act. Chi. 320 (2008) 98.

[15] V. N. Prigodin, F. C. Hsu, J. H. Park, O. Waldmann and A. J. Epstein: Phys. Rev. B. 78 (2008) 035203.

[16] P. H. Wobkenber, J. Ball, F. B. Kooistra, J. C. Hummelen, D. M. de Leeuw, D. D. C. Bradley and T. D. Anthopoulos: Appl. Phys. Lett. 93 (2008)

013303.

[17] P. H. Wobkenberg, D. D. C. Bradley, D. Kronholm, J. C. Hummelen, D. M. de Leeuw, M. Colle and T. D. Anthopoulos: Synth. Met. 158 (2008) 468.

[18] H. Usta, A. Facchetti and T. J. Marks: J. Am. Chem. Soc. 130 (2008) 8580.

[19] S. Allard, M. Forster, B. Souharce, H. Thiem and U. Scherf: Angewandte Chemie-International Edition 47 (2008) 4070.

[20] B. S. Ong, Y. L. Wu, Y. N. Li, P. Liu and H. L. Pan: Chemistry-A Eur J 14 (2008) 4766.

[21] H. Fukai, T. Hamaoka, M. Yamada, J. Matsushita and Y. Nishioka: Molecular crystals and liquid crystals 492 (2008) 77.

[22] N. S. Cho, S. K. Lee, J. H. Seo, M. Elbing, J. D. Azoulay, J. Park, S. Cho, A. J. Heeger and G. C. Bazan: J. Mat. Chem. 18 (2008) 4909.

[23] M. Hultell and S. Stafstrom: J. Lum. 128 (2008) 2019.

[24] M. Kawasaki, S. Imazeki, M. E-Oh and M. Ando: Jpn. J. Appl. Phys. 47 (2008) 6247.

[25] K. Ihm, S. M. Chung, T. H. Kang and S. W. Cheong: Appl. Phys. Lett. 93 (2008) 141906.

[26] D. R. Hines, A. Southard and M. S. Fuhrer: J. Appl. Phys. 104 (2008) 024510.

[27] F. C. Krebs: Sol. Energy. Mat. Sol. Cells. 92 (2008) 715.

[28] K. Schroeter: Sensor. Rev. 28 (2008) 6.

[29] A. C .Arias, J. Daniel, B. Krusor, S. Ready, V. Sholin and R. Street: J. Soc. Info. Disp. 15 (2007) 485.

[30] T. Sekitani, M. Takamiya, Y. Noguchi, S. Nakano, Y. Kato, T. Sakurai and T. Someya: Nat. Mat. 6 (2007) 413.

[31] H. Moon, W. S. Jahng, M. D. Curtis: J. Mat. Chem. 18 (2008) 4856.

[32] E. Lim, T. Manaka and M. Iwamoto: J. Appl. Phys. 104 (2008) 054511.

[33] S. H. Kim, D. Choi, D. S. Chung, C. Yang, J. Jang, C. E. Park and S. H. K. Park: Appl. Phys. Lett. 93 (2008) 113306.

[34] F. Maddalena, M. Spijkman, J. J. Brondijk, P. Fonteijn, F. Brouwer, J. C. Hummelen, D. M. de Leeuw, P. W. M. Blom and B. de Boer: Organic

Electronics 9 (2008) 839.

[35] F. Y. Yang, K. J. Chang, M. Y. Hsu and C. C. Liu: Organic Electronics 9 (2008) 925.

[36] F. Matsumoto, K. Moriwaki, Y. Takao and T. Ohno: Beilstein. J. Org. Chem. 4 (2008) 33.

[37] C. L. Liu, J. H. Tsai, W. Y. Lee, W. C. Chen and S. A. Jenekhe: Macromolecules 41 (2008) 6952.

[38] A. K. Bansal, A .Penzkofer: Chem. Phys. 352 (2008) 48.

[39] Y. T. Tao, Q. Wang, C. L. Yang, K. Zhang, Q. Wang, T. T. Zou, J. G. Qin and D. G. Ma: J. Mat. Chem. 18 (2008) 4091.

[40] K. Watanabe, D. Kumaki, T. Tsuzuki, E. Tokunaga and S. Tokito: J. Photopolymer Sci. and Tech. 20 (2007) 39.

[41] C. C. Hua, C. Y. Kuo, S. A. Chen: Appl. Phys. Lett. 93 (2008) 123303.

[42] J. Chung, K. H. Kim, J. C. Lee, M. K Kim and H. J. Shin: Organic Electronics 9 (2008) 869.

[43] K. D. Kim, D. S. Kim, C. K. Kim and C. K. Song: Jpn. J. Appl. Phys. 47 (2008) 6496.

[44] P. Stakhira, V. Cherpak, O. Aksimentyeva, B. Tsizh, D. Volynyuk and I. Bordun: J. Non-crystalline Solids 354 (2008) 4491.

[45] H. J. Jiang, X. Y. Deng, W. Huang: Progress in Chem. 20 (2008) 1361.

[46] D. H. Lee, J. S. Choi, H. Chae, C. H. Chung and S. M. Cho: Curr. Appl. Phys. 9 (2009) 161.

[47] H. Scheiber, M. Graf, H. Plank, E. Zojer, C. Slugovc, S. Kappaun, F. Gabrecht, U. Scherf and E. J. W. List: Adv. Func. Mat. 18 (2008) 2480.

[48] L. Li, J. S. Yu, X. Q. Tang, T. Wang, W. Li and Y. D. Jiang: J. Lum. 128 (2008) 1783.

[49] A. R. Duagal, C. M. Heller, J. J. Shiang, J. Liu and L. N. Lewis: J. Disp. Tech. 3 (2007) 184.

[50] B. C. Krummacher, M. Mathai, F. So, S. Choulis and V. E. Choong: J. Disp. Tech. 3 (2007) 200.

[51] Y. Jin, G. C. Bazan, A. J. Heeger, J. Y. Kim and K. Lee: Appl. Phys. Lett. 93 (2008) 123304.

[52] C. Yang, J. Y. Kim, S. Cho, J. K. Lee, A. J. Heeger and F. Wudl: J. Amer. Chem. Soc 130 (2008) 6444.

[53] P. C. Wang, R. E. Lakis, A. G. MacDiarmid: Thin Solid Films. 516 (2008) 2341.

[54] N. J. Pinto, R. Gonzalez, A. T. Johnson and A. G. MacDiarmid: Appl. Phys. Lett. 89 (2006) 033505.

[55] M. Boussoualem, R. C. Y. King, J. M. Buisine and F. Roussel: Appl. Phys. A Mat. Sci. and Pro. 81 (2005) 773.

[56] W. C. Chen, T. C. Wen, A. Gopalan: J. Eelectrochem. Soc. 151 (2004) F242.

[57] M. Wada, K. Tada, M. Onoda: IEICE Trans. on Elec. E87C (2004) 152.

[58] M. C. Lonergan: Science 278 (1997) 2103.

[59] S. A. CHEN, Y. FANG: Angewandte Makromolekulare Chemie 208 (1993) 79.

[60] S. KARG, W. RIESS, M. MEIER and M. Schwoerer: Synth. Met. 57 (1993) 4186.

[61] A. K. Thakur, A. K. Mukherjee, D. M. G. Preethichandra, W. Takashima and K. Kaneto: J. Appl. Phys. 101 (2007) 104508.

[62] N. I. Craciun, J. J. Brondijk, P. W. M. Blom: Phys. Rev. B 77 (2008) 035206.

[63] M. M. Mandoc, W. Veurman, L. J. A. Koster, M. M. Koeste, J. Sweelssen, B. de Boer and P. W. M. Blom: J. Appl. Phys. 101 (2007) 104512.

[64] P. W. M. Blom, C. Tanase, D. M. de Leeuw and R. Coehoorn: Appl. Phys. Lett. 86 (2005) 092105.

[65] V. D. Mihailetchi, J. K. J. van Duren, P. W. M. Blom, J. C. Hummelen, R. A. J. Janssen, J. M. Kroon, M. T. Rispense, W. J. H. Verhees, M. M.

Wienk: Adv. Func. Mat. 13 (2003) 43.

[66] R. Schmechel: J. Appl. Phys. 93 (2003) 4653.

[67] M. C. J. M. Vissenberg, M. Matters: Phys. Rev. B 57 (1998) 12964.

[68] M. Matters, D. M. de Leeuw and M. C. J. M. Vissenberg: Opt. Mat. 12 (1999) 189.

[69] Y. Jin, S. Song, S. H. Park, J. A. Park, J. Kim, H. Y. Woo, K. Lee and H. Suh: Polymer 49 (2008) 4559.

[70] D. H. Park, H. S. Kim, M. Y. Jeong, Y. B. Lee, H. J. Kim, D. C. Kim, J. Kim and J. Joo: Adv. Func. Mat. 18 (2008) 2526.

[71] J. R. Garcia, M. H. Gehlen, H. P. M. de Oliveira, F. C. Nart: J. Braz. Chem. Soc. 19 (2008) 1306.

[72] M. Yunus, P. P. Ruden and D. L. Smith: Appl. Phys. Lett. 93 (2008) 123312.

[73] D. Varsano, A. Marini and A. Rubio: Phys. Rev. Lett. 101 (2008) 133002.

[74] K. Kanemoto, T. Sudo, I. Akai, H. Hashimoto, T. Karasawa, Y. Aso and T. Otsubo: Phys. Rev. B 73 (2006) 235203.

[75] T. Bakos, S. N. Rashkeev, S. T. Pantelides: Phys. Rev. Lett. 91 (2003) 226402.

[76] P. E. Shaw, A. Ruseckas, I. D. W. Samuel: Adv. Mat. 20 (2008) 3516.

[77] A. Huijser, T. J. Savenije, S. C. J. Meskers, M. J. W. Vermeulen and L. D. A. Siebbeles: J. Am. Chem. Soc. 130 (2008) 12496.

[78] O. V. Mikhnenko, F. Cordella, A. B. Sieval, J. C. Hummelen, P. W. M. Blom and M. A. Loi: J. Phys. Chem. 112 (2008) 11601.

[79] S. Athanasopoulos, E. Hennebicq, D. Beljonne and A. B. Walker: J. Phys. Chem. C 112 (2008) 11532.

[80] S. Westenhoff, I. A. Howard and R. H. Friend: Phys. Rev. Lett. 101 (2008) 016102.

[81] S. Tokito, T. Tsuzuki, F. Sato and T. Iijima: Curr. Appl. Phys. 5 (2005) 331.

[82] S. Tokito: J. Photopoly Sci. and Tech. 17 (2004) 307.

[83] S. Tokito, T. Iijima, Y. Suzuri and F. Sato: Appl. Phys. Lett. 83 (2003) 569.

[84] S. K. Sharma, C. Bothra, G. D. Sharma: Ind. J. Pure and Appl. Phys. 46 (2008) 588.

[85] J. A. OSAHENI, S. A. JENEKHE, J. PERLSTEIN: J. Phys. Chem. 98 (1994) 12727.

[86] S. NESPUREK, V. CIMROVA, J. PFLEGER: Coll. and Poly. Sci. 269 (1991) 556.

[87] A. Takshi, A. Dimopoulos and J. D. Madden: Appl. Phys. Lett. 91 (2007) 083513.

[88] M. Segal, M. A. Baldo, R. J. Holmes, S. R. Forrest and Z. G. Soos: Phys. Rev. B. 68 (2003) 075211.

[89] S. Tasch, G. Kranzelbinder, G Leising, U. Scherf: Phys. Rev. B 55, No.8 (1997) 5079.

[90] M. A. Stevens, C. Silva, D. M. Russel and R. H. Friend: Phys. Rev. B. 63 (2001) 165213.

[91] M. C. J. M. Vissenberg and M. J. M. de Jong: Phys. Rev. Lett. 77 (1996) 4820.

[92] M. Ichikawa, R. Naitou, T. Koyama and Y. Taniguchi: Jpn. J. Appl. Phys. 40 (2001) L1068.

Chapter 2

Experimental Methods

summary

This chapter presents the various experimental methods used for the fabrication as well as characterization of both optical and electrical properties of organic thin film based electronic devices. The discussion here mainly involves the fabrication procedures for diode, Photo induced memory devices (PIMDs) and Organic Field Effect Transistors (OFETs). A brief account of various general steps involved in the fabrication of organic electronic devices has been given in the form of a flow diagram in the beginning of this chapter. Apart from the description of various methods, the principle behind those methods has also been discussed, from the point of view of the theoretical background provided by the previous chapter.

Conventional electronic devices are made of Silicon wafers. The fabrication of a Silicon MOSFET starts with diffusion (or implantantion) of the source and drain, followed by thermally grown Silicon oxide, and ends with the deposition of metal electrodes. However, both Thin Film Transistors (TFTs) using amorphous Si and thin film Organic field effect transistors (OFETs) the semiconductor is not a bulk material, but a thin film. Thus, thin film organic devices are having an inverted architecture. It is usually built on an appropriate substrate and the semiconductor deposition constitutes the last step of the fabrication process. Thin film organic devices are mainly divided into two categories, the first is that of planar type devices and the second is that of sandwich type. While Planar type device geometry has long been preferred for the fabrication of OFETs. While a sandwich type geometry is more suited for the fabrication of Organic light emitting diodes (OLEDs) and Organic Solar Cells (OSCs).
In this work we have mainly focussed on three type of thin film organic devices, namely, OFETs, organic diodes and Photo induced memory devices (PIMDs). While highly doped silicon wafers covered with a thermally grown Silicon dioxide layer were used as substrates for the fabrication of OFETs. The highly doped substrate acts as the gate electrode, and the source drain electrodes are deposited on the insulating layer of SiO_2 layer by the conventional micro lithographic techniques. Other than OFETs, organic diodes and PIMDs were both fabricated on glass substrates. Besides these devices various other samples for the optical characterization of materials were also fabricated using glass substrates. In general the fabrication of organic electronic devices involves several main steps as is also shown in the flow diagram in Fig. 2.1.

2.1 Substrate preparation

Usually the substrate preparation can be further subdivided into four steps as given beow:-

1. Cutting the substrate
2. Cleaning the substrate
3. Etching

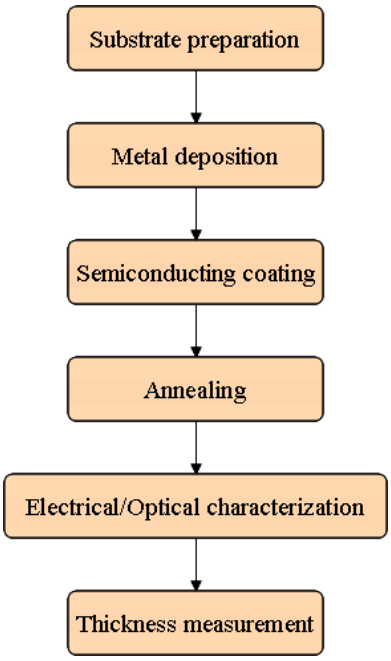

Figure 2.1: Flow diagram of various steps involved in the fabrication of organic electronic device

4. Surface modification of the substrate

2.1.1 Cutting

The substrates glass/Si wafer are cut according to the required dimensions using a diamond cutter. Usually the area of the substrates varied from 1 $3cm^2$, which mainly depends on the type of device and the type of measurement involved. This step is highly critical, as while cutting the Si wafer as abrasive Silicon atoms can make large pinholes in the oxide layer of the dielectric, which might lead to breakdown of OFETs.

2.1.2 Cleaning

The next stage involves cleaning the substrates. The substrates were cleaned for inorganic impurities clinging to the surface of these substrates by using the ultrasonic bath. Substrates were subsequently cleaned in Iso-propanol and Acetone solutions for 10 mins each.

2.1.3 Etching

Etching was only done in case of ITO coated glass substrates. The substrates were covered with Scotch tape, and it is the region defined by the scotch tape that decided the dimensions of the ITO electrode later. It must be noted that region of the substrate not covered by Scotch tape is etched away. Etching was done using a dilute HCl solution in a petridish. While Zn turning are gradually added. It is known that Zn and HCl react with each other as

$$Zn + 2HCl \rightarrow ZnCl_2 + 2[H] \tag{2.1}$$

It is the nascent Hydrogen that evolves almost immediately and leads to the etching of ITO electrode, leaving behind the ITO covered with scotch tape. Besides this there exists another method of etching samples using Aquaregia solution. However, this method is more severe and many times leads to damage of the scotch tape itself.

2.1.4 Surface modification

This step is also a characteristic of Organic thin film device fabrication. It is this step that largely determines the degree of smoothness of the organic thin films deposited on glass/Si wafer substrates. As was also reported by Grecu et al[1,2] that surface modification of the $SiO2$ surface using silanizing agents viz. Hexa(1,1,1,3,3,3)methyldisilazane (HMDS), Octadecyltrichlorosilane (OTS), Octlytrichlorosilane (OTS-8), Dichlorodimethylsilane.

Figure 2.2 shows the structure of HMDS and OTS-8. The basic idea of surface treatment by these compounds is to make the surface of the substrate to hydrophobic from its usually hydrophillic surface. This ensures a good adhesion between the organic semiconductor molecules and the substrate. Usually the SiO_2 or the glass substrates are highly hydrophillic in nature. However, the organic semiconductor materials are known to be hydrophobic in nature. Thus, the silanizing agents while have both hydrophobic and hydrophillic ends attached to them, and hence act as a buffer layer. The films coated over silanized substrates have in general superior morphology. It should also be noted that such a treatment is of particular significance for OFETs, where a highly

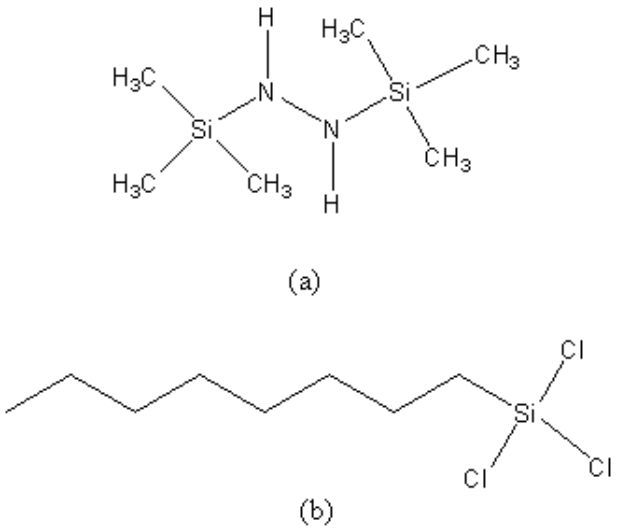

Figure 2.2: Shows the structure of (a) HMDS, (b) OTS-8

smooth interface between the semiconductor and insulator surface are critical for device performance. In this work we have invariably used HMDS for the surface modification of both glass as well as Silicon based substrates.

2.2 Deposition of semiconductor

Since most OFETs reported till date were grown on Silicon wafers, the deposition of semiconductor is the determining step of their fabrication. Depending on the nature of the semiconducting material, polymer or small molecule, various deposition techniques have been used. As mentioned in the previous chapter the polymer based devices in general lag behind the small molecule organic semiconductors viz. Pentacene. While Polymers can only be deposited using solution processing, small molecules can be deposited by both wet or dry processes. However, the highest mobility in OFETs till date has been reported with dry processes such as thermal vapor deposition of the organics. In the case of top contact devices (or staggered device) this step follows the surface modification step. However in bottom contact type devices (Coplanar devices) surface modification step is followed by metal deposition step, and in these type of devices the deposition of semiconductor is the final step of the fabrication process.

2.2.1 Large molecular weight Conducting polymers

Large molecular weight Conducting polymers generally have long alkyl chains attached to the main backbone to make them soluble in common organic solvents viz. $CHCl_3$, CH_3COCH_3, CH_3OH, $CH_3CHOHCH_3$ and $CH3COOC_2H_5$ etc. These solutions can then be used to deposit the organic thin film by a variety of ways. The main lucrative point of Organic devices is their ease of processing. While the solution processing is often referred to as wet processing and the evaporation of organic molecules is referred as dry processing technique.

Spin coating

One of the most elegant ways to realize o good quality organic film is spin coating as shown in Fig 2.3(a). When the technique is well handled, it allows production of very homogenous films with a perfect control of thickness over relatively larger areas. One of the main requirement for this technique is good solubility of the polymer. In case if the conducting polymer is insoluble in organic solvents, an alternative approach using the soluble precursor polymer is used, which is later converted into a conducting polymer by an appropriate chemical or physical treatment.[3-5]. More recently solution deposition has also been used with a short molecule, pentacene [8-10]. However, the main problem with spin coated films is that it results in disordered amorphous films, mainly owing to the high speed rotation of these molecules. This high speed rotation doesn't allow the molecules to attain energetically most favorable position.

Dip coating

Dip coating refers to the immersing of a substrate into a tank containing coating material, removing the piece from the tank, and allowing it to drain as can be seen from Fig. 2.3(b). It is a popular way of coating thin film on substrates along with the spin coating procedure. The dip coating process can be, generally, separated into three stages:-

Immersion: the substrate is immersed in the solution of the coating material at a constant speed preferably judder free.

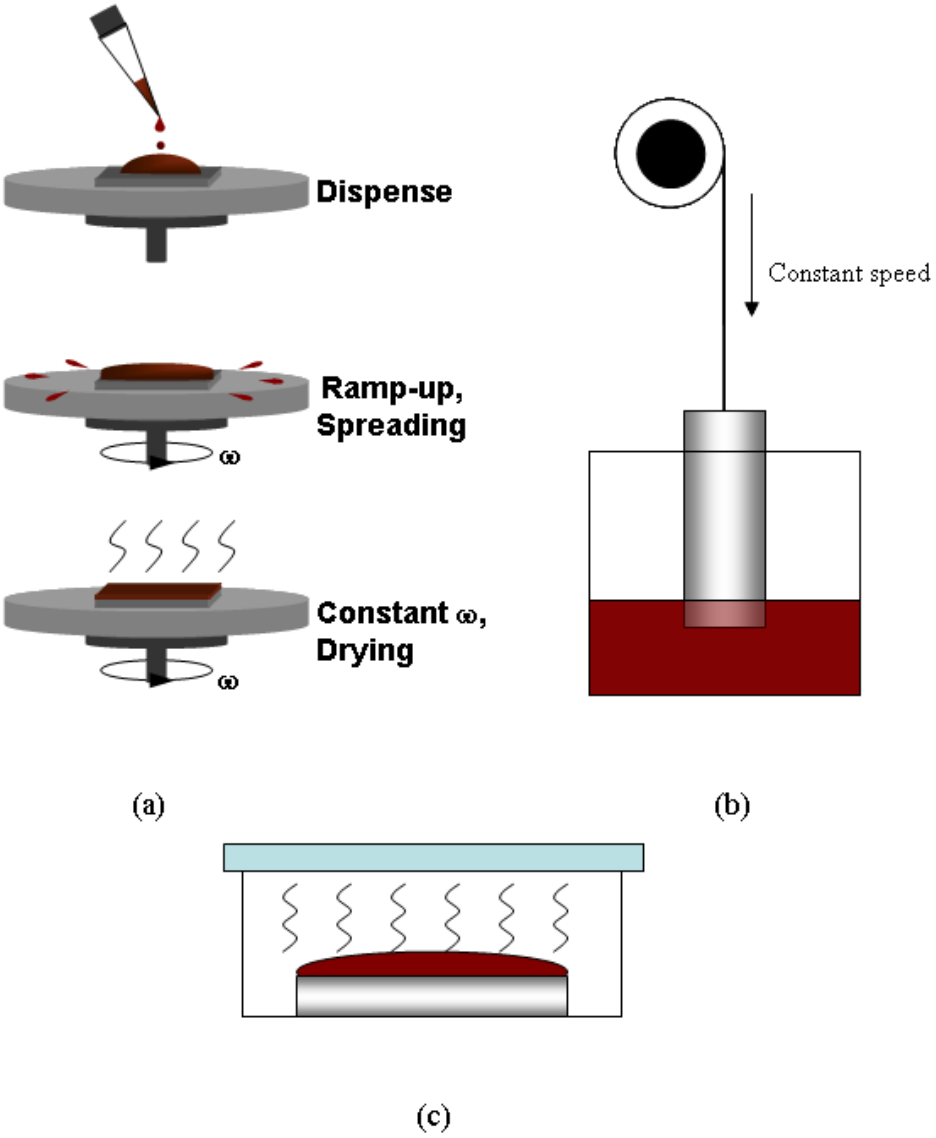

Figure 2.3: Shows (a) Spin coating (b) Dip coating and (c) Casting of polymeric solutions

Dwell time: the substrate remains fully immersed and motionless to allow for the coating material to apply itself to the substrate.
Withdrawal: the substrate is withdrawn, again at a constant speed to avoid any judders. The films formed by dip coating are superior morphologically, which probably results from ordered microcrystalline regions with a lamellar structure formed through self organization of macromolecules as the polymer solution passes from the liquid phase to the solid phase. Dip coated films have resulted in higher mobility of OFETs typically an order of magnitude higher than that obtained from films deposited by spin coating[11-15].

Casting

Casting is a manufacturing process by which a liquid material is (usually) poured into a mold, which contains a hollow cavity of the desired shape, and then allowed to solidify. However, Casting here refers to the film formed when the solution is allowed to slowly evaporate by itself usually at room temperature. This, can be done by pouring the polymer solution on the substrate and let it evaporate in an ambient atmosphere or under controlled saturated vapor pressure environment as demonstrated in Fig. 2.3(c). However, a controlled environment takes long time, due to slow evaporation of the solvent. It also at the same time ensures better stacked structures in these films. Thus, in this way casted films from solution results in a higher degree of crystallinity[11,16]. The main advantage with this method lies with its ease of processing. However, its main disadvantages are that a lot of material is needed as casting requires solution of nearly 10 times in strength as required for spin coating. This causes wastage and also results in few μm thick films. Thus, limits the usage of this technique in the fabrication of OFETs, where only few tens of nm film thickness is all that is required.

Printing

The emergence of high-resolution ink-jet printers and semiconductor inks will enable the some segments electronics industry to undergo transition from an environment in which electronics manufacturing plants are escalating in cost at an exponential rate

to one in which production costs are modest and small, highly customized runs are economically feasible. At the same time the expectations are that low production and material costs and the ability to print [19,20] onto flexible substrates will lead to a new generation of electronics products ranging from throwaway RFID tags to wall coverings with embedded photovoltaic cells or sensors.

Electrochemical deposition

Electrochemical polymerization is one of the leading techniques for the synthesis of conducting polymers, and reports on electrochemically grown OFETs date back to the late eighties[17,18]. The main advantage of this technique is the direct synthesis of the polymer in the form of a thin film. However, its drawbacks are numerous. Firstly, electro polymerization only occurs on conducting substrates. In the case of OFETs this would mean the semiconductor film grows on the source and drain electrodes, its extension over the insulator occurring through lateral expansion of the deposit. This results in a highly disordered film and a poor quality of the insulator semiconductor interface. Secondly the conducting polymer obtained is in its oxidized state, so it must be reduced (generally electrochemically) to become semiconducting. This constitutes an additional source of disorder. Today this technique is no longer used for the fabrication of OFETs.

2.2.2 Small molecular weight Organic molecules

Small molecular weight organic molecules have been widely studied for their potential use as semiconductors in thin film OFETs. They are at present ahead in terms of charge carrier mobility than their counter parts, conducting polymers. Usually wet processing is not applicable to these molecules. although by suitable substitution of long alkyl chains they might become soluble. However, the improvement in solubility comes at the expense of order in the film. Hence, resulting in lower mobilities. Highest charge carrier mobility till date has been reported by using pentacene. Besides pentacene, there are several other potential materials viz. Oligomers of thiophenes, Phinylene-vinylenes and Copper Pthalocyanine (CuPc) etc.

Thermal evaporation

Small molecules based organic semiconductors deposited via thermal evaporation technique[6,7]. In principle, this technique is not applicable for conducting polymers, as they tend to decompose by cracking at high temperatures. The process is conducted in a very high vacuum chamber. The organic material is put in a metal boat, which is heated by joule effects, or sometimes with an electron gun. The substrate is placed few centimeters above the boat. The main merits of the vacuum deposition are easy control of the thickness and purity of the film, and particularly the fact that highly ordered films can be realized by fine tuning the deposition rate and the temperature of the substrate. Its primary demerit lies in the fact that it requires sophisticated instrumentation, which contrasts with the simplicity and low cost of wet processing techniques.

2.3 Metal deposition

Metal Deposition is primarily done to make electrodes for the purpose of contact. Although the choice of metal to be deposited may vary depending upon the type of device functionality required and the HOMO, LUMO levels of the organic semiconductor.

2.3.1 Sputtering

Sputtering [21] is a vacuum evaporation process which physically removes portions of a coating material called the target, and deposits a thin, firmly bonded film onto an adjacent surface called the substrate. The process occurs by bombarding the surface of the sputtering target with gaseous ions under high voltage acceleration as is shown in Fig. 2.4. As these ions collide with the target, atoms or occasionally entire molecules of the target material are ejected and propelled against the substrate, where they form a very tight bond. The resulting coating is held firmly to the surface by mechanical forces, although, in some cases, and alloy or chemical bond may result. Sputtering has proven to be a successful method of coating a variety of substrates with thin films of electrically conductive or non-conductive materials. One of the most striking characteristics of sputtering is its universality. Since the coating material is passed into the

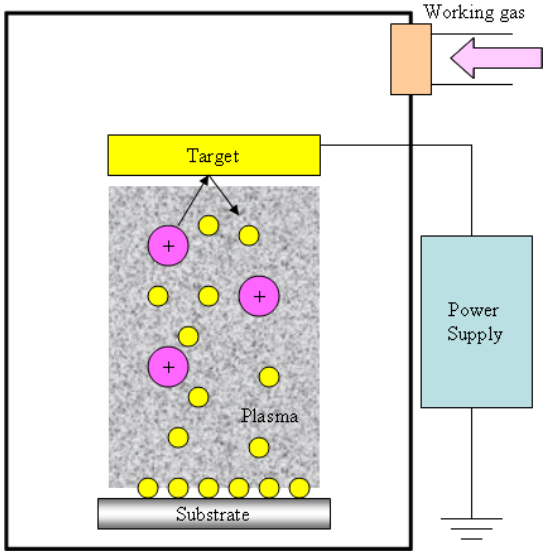

Figure 2.4: Shows the basic mechanism of sputtering

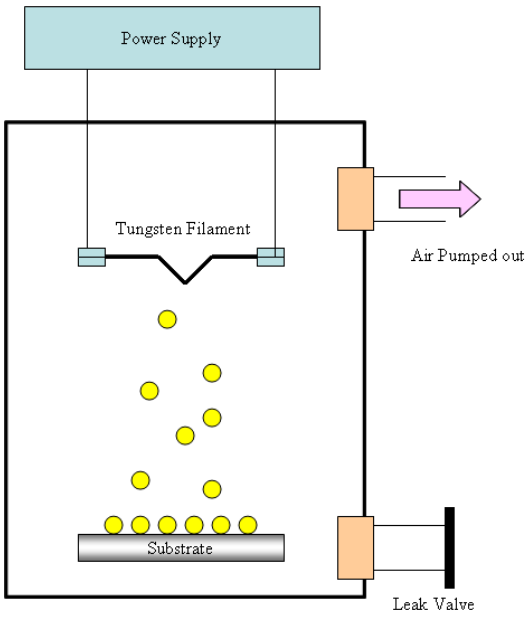

Figure 2.5: Shows the basic mechanism of Physical Vapor Deposition of metals

vapor phase by a mechanical rather than a chemical or thermal process, virtually any material can be deposited. Direct current is used to sputter conductive materials, while radio frequency is used for non-conductive materials. The range of sputtering application include oxide micro circuit insulation layers, amorphous optical films for integrated optics devices, piezoelectric transducers, photo conductors, luminescent films for display devices, optically addressed memory devices, video discs, solid electrolytes and thin film lasers. However, the drawback of sputtered metal electrode is that the boundaries are not well defined this limits its application for OFETs, as well defined channel region by shadow masking is can not be attained.

2.3.2 Physical vapor deposition

Physical Vapor Deposition (PVD) [22-26] is a term used to describe a technique of depositing thin films by the condensation of vaporized form of the material onto various surfaces (e.g. semiconductor wafers) the coating method usually involves purely physical processes such as high temperature vacuum evaporation. Usually the metal to be deposited is heated to a high vapor pressure by electrically resistive heating in

low vacuum. This technique is superior than the Sputtering, as very thin metal films can be deposited. Besides, PVD provides a better control over the deposition of metal. Even the edges are sharply defined thus it is particularly well suited for deposition metal electrodes for various organic electronic devices viz OFETs, OLEDs and PIMDs.

2.4 Electrical characterization

Depending upon the type of desired measurement different type of electrical characterization can be carried out. In our study we were mainly concerned with the IV (Current Voltage) measurement of Organic diodes and transistors, and with the CV (Capacitance Voltage) measurement of Organic diodes. The details of these measurement techniques along with the principle behind their measurement is discussed in the following section.

2.4.1 IV measurement

The IV measurement was mostly done to evaluate the performance of OFETs and organic diodes. Since the materials used in our study are all organic, having high characteristic resistance. Thus, in order to perform IV measurement Keithley 6517 A High resistance electrometer was employed. Figure 2.6 (a) shows the picture of Keithley 6517 A electrometer. It should be noted that Keithley 6517 A can be used to measure resistances upto the order of $10^{16}\Omega$. It has a wide range of current sensitivity from $1fA$ $20mA$. It has a high input impedance of about $200T\omega$, which makes it particularly well suited for high resistivity materials. It offers unmatched accuracy and sensitivity specifications that simplify the measurement of high resistivity samples. It is these features that make it highly suitable for applications related to material science, Impedance measurements in electrochemistry and antistatic material based applications.
In most cases organic material based devices particularly OFETs are characterized by low level currents, thus Keithley 6517 was employed in the measurement of various OFETs and PIMDs. Figure 2.6 (b) shows the effective circuit diagram for the electrometer connected to a load resistance R. while the low terminals of both the current meter and the voltage source are connected with each other. While their respective high terminals are connected across the load resistance. Another important parameter

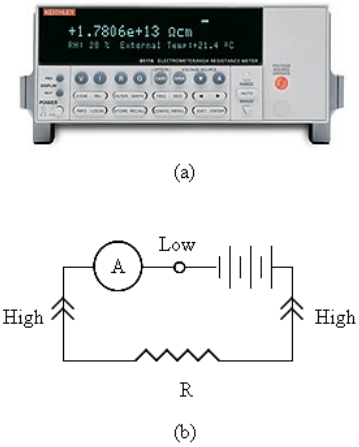

Figure 2.6: Shows (a) Keithley 6517A electrometer (b) the effective circuit diagram of 6517 A electrometer connected across a load

is the voltage burden. A voltage burden is defined as the voltage drop across the current meter. Ideally an ammeter should have zero voltage drop across it. However, in practice this is not the case. Thus, the voltage burden has to be properly taken into consideration to avoid measurement of erroneous readings.

Figure 2.7 shows the type of waveform generated by the Keithley 6517 A electrometer. It is to be noted that for the purpose of OFET measurement two Keithley 6517 A source meters were used. While one was used as a voltage source to supply an increasing step input type Voltage bias to the gate terminal of an OFET. However, the source drain electrodes were given a ramp triangular type waveform. It must be noted here that the time interval of the gate bias at an fixed voltage was identical to the time period of the triangular waveform generated for source drain input. Another important point to note is that while two electro meters are required for the measurement of OFETs. However, only a single electrometer could suffice for the measurement of diode characteristics. Since a diode is a two terminal device. It should also be noted that for both diode and photo induced memory device the IV measurement was done by applying a triangular signal as is shown in Fig. 2.7(b).

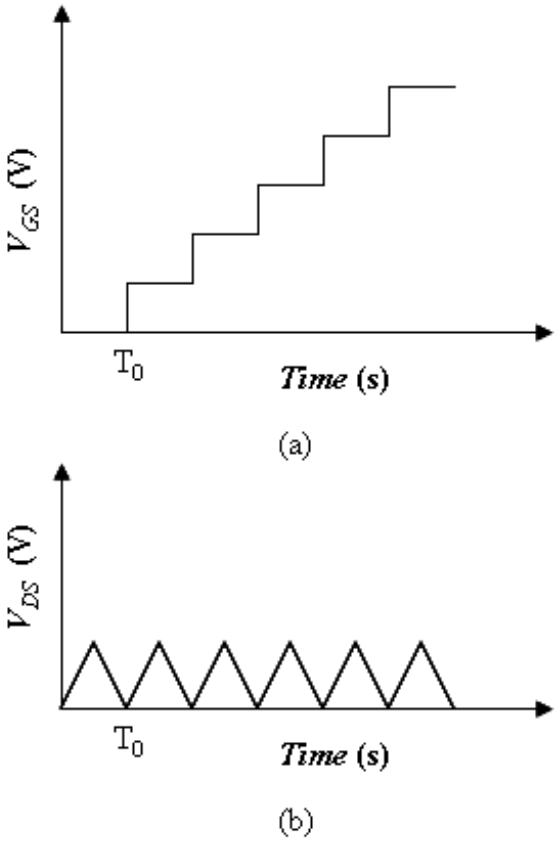

Figure 2.7: Shows (a) The input signal for gate bias V_{gs} of the transistor against time (b) and the input signal for the source drain bias V_{ds} against time

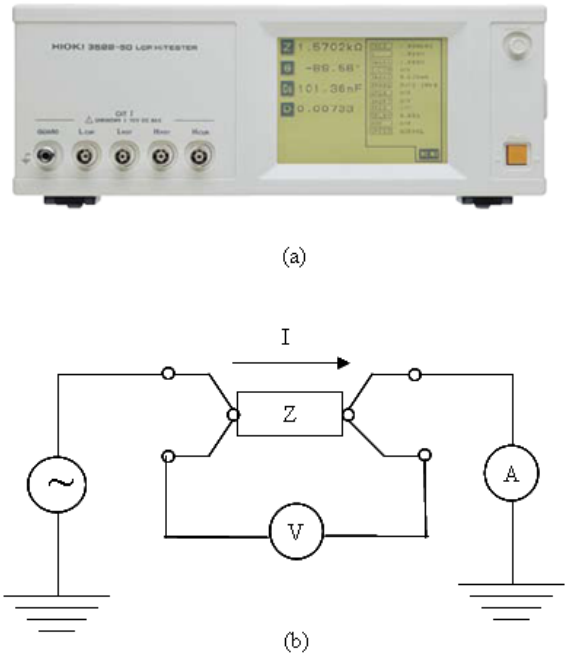

Figure 2.8: Shows (a) Hioki 3522-50 LCR Hi tester (b) the principle of impedance measurement using IV method

2.4.2 Impedance measurement

Hioki 3522-50 LCR Hi tester was used for the purpose of impedance measurements. 3522-50 offers an impedance measurement over a wide range of frequencies from $1mHz$ to $100KHz$, and the 3532-50 covers a range from $42Hz$ to $5MHz$. These LCR meters can measure with a high degree of accuracy and are used for a variety of applications ranging from research, characterization to production line and quality control. These meters can often be employed to measure 14 different circuit parameters. The low frequency measurement from 1 mHz, enables us to measure low frequency electrochemical impedance measurement, which is of utmost interest is basic chemical research. Another important feature of this meter is that it can be used to perform current/voltage dependent measurement besides the usual open loop signal generation. For this purpose an additional module 9268 DC bias unit, needs to be cascaded. The maximum applied bias is $\pm 40V$ DC, but can change depending upon the measurement conditions. Figure 2.8(a) shows the picture of Hioki 3522-50 LCR meter. Figure 2.8(b) on the other hand shows the principle behind the impedance measurement using the IV method. It is to

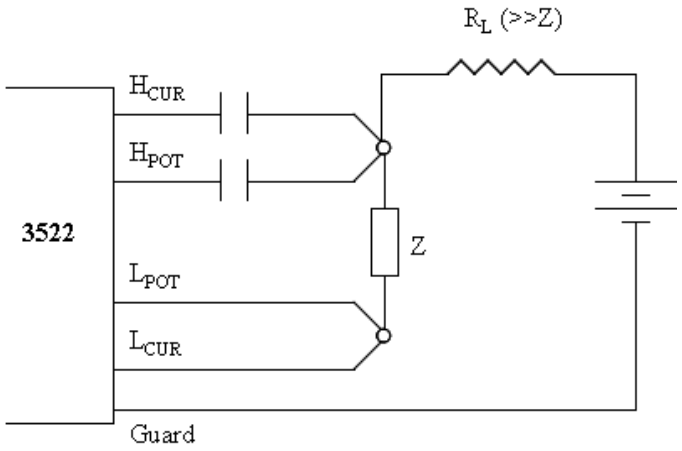

Figure 2.9: shows the principle of voltage dependent capacitance measurement

be noted that many methods can be employed in principle for the impedance measurement. However, here the IV method of impedance measurement is discussed primarily because this is the methodology of measurement of 3522-50. A typical AC source is used to bias the impedance. The current flowing through the impedance is measured using an Ammeter, the Voltage dropped across the impedance is measured with the help of a Voltmeter as is also shown in Fig. 2.8(b). The impedance is finally measured as the ratio of V and I.

Figure 2.9 shows the principle of voltage dependent capacitance measurement. It should be noted that while the connection of the terminals to the 3522-50 remains identical. The external bias is applied using a separate voltage source unit cascaded to the 3522-50 LCR unit via 9268 DC bias unit. An important consideration that must be kept in mind while carrying the voltage dependent measurement is that the series load resistance R_l should be much higher than the impedance to be measured.

2.5 Spectroscopy

Spectroscopy usually means experimental charting of the energy level structure of physical systems. It is often used for the analysis of various types of radiation, electromagnetic or particle emission. Spectroscopic investigations can be of fundamental or an applied nature. Most fundamental spectroscopic techniques can be used to determine energy

levels, transition probabilities etc, experimentally. Spectroscopic methods are also employed for understanding of the studied systems using adequate theory and models. Usually, certain primary quantities viz. wavelength, intensities, etc. are measured in spectroscopic investigations.

The spectroscopic information can be used for various kinds of analysis for instance, optical absorption and emission spectroscopy is used for both qualitative and quantitative chemical analysis. It can also be used to determine the electronic arrangement of various materials. Thus, spectroscopic techniques are one of the most powerful tools for a great variety of molecular structure studies. It should be noted that while absorption and emission spectra can be used to study the electronic properties of different materials. Infrared (IR) and Raman spectroscopy may be used to study the rotational and vibrational energy of the molecules. In addition Nuclear Magnetic Resonance Spectroscopy the effect of the magnetic field on the orientation of certain nuclei in certain directions with respect to the direction of the field. These different orientations correspond to different energies and radiation of a suitable frequency can then be used to study the energy level separations. Similarly in Electron Spin Resonance Spectroscopy the spin of an electron of the sample molecule is oriented one way or the other with respect to the field and again the resulting energy level separation of these two orientations is studied by radiation of suitable frequency.

2.5.1 Absorption Spectroscopy

The nature of excited state and the processes of absorption and emission of light are central ideas in the modern spectroscopy. Absorption spectroscopy refers to the interaction (absorption) of electromagnetic radiation ($\lambda = 160 - 780nm$) by matter. In common cases most chemical species molecules or compounds are made up of electrons. The electrons in turn located in different orbitals which are associated with different energies. When light of sufficient energy falls on an electron in the ground state, the electron absorbs some of the energy and gets excited to the higher energy level. As described in Chapter 1 these energy levels are typically known as HOMO and LUMO respectively.

The principle of operation of a typical UV-Vis Spectrophotometer is shown in Fig. 2.6. The radiation source in a UV-Vis spectrophotometer consists of two different sources. A Deuterium lamp is used for the UV $(190 - 400nm)$. The second source, which can be used upto $1500nm$, is a tungsten-halogen arc lamp. The change of lamp is automatic. A polychromatic light first undergoes wavelength dispersion, and then it is separated into bands which are made as monochromatic as possible. In practice the dispersion elements in most commercially available Spectrophotometers consists of a holographic concave grating, prisms are no longer used. These bands then cross the sample one after other and the transmission is recorded for each band. The bands are selected by the exit slit to fall on to the sample. The entrance slits, dispersion prism and the exit slits combined together make a monochromator. This monochromatic light is later splitted using a beam splitter. Finally two identical beams are made to fall on the sample and the reference cell. The light detected by the detectors is then recorded. In the near UV and the visible region, the detector element always consists of an electron photomultiplier or of a photodiode. However, In the near IR range, the apparatus uses PbS detectors, cooled with Peltier effect.The global results of these recordings forms the absorption spectrum of the sample. For the purpose of our experiments we used the $JASCO570$ for measurement of absorption spectra of thin films.

Beer-Lambert law

Consider a monochromatic light of intensity I_0 impinging on the dielectric media of thickness d as shown in Fig. 2.7. The dielectric can be a solution in a cuvette or a thin film coated on glass. Let I_t be the intensity of the transmitted light through the sample. Let us now consider the condition over a small interval $\triangle x$ in the sample. Before the considered space interval the intensity has been reduced to I, and it will further be reduced by $\triangle I$ in the interval $\triangle x$. The *Beer-Lambert* law then states that the fractional attenuation $\triangle I/I$ is proportional to the number of absorbers, $\triangle n$, in the small interval $\triangle x$ as given by the equation below

$$\frac{\triangle I}{I} \propto -\triangle n \tag{2.2}$$

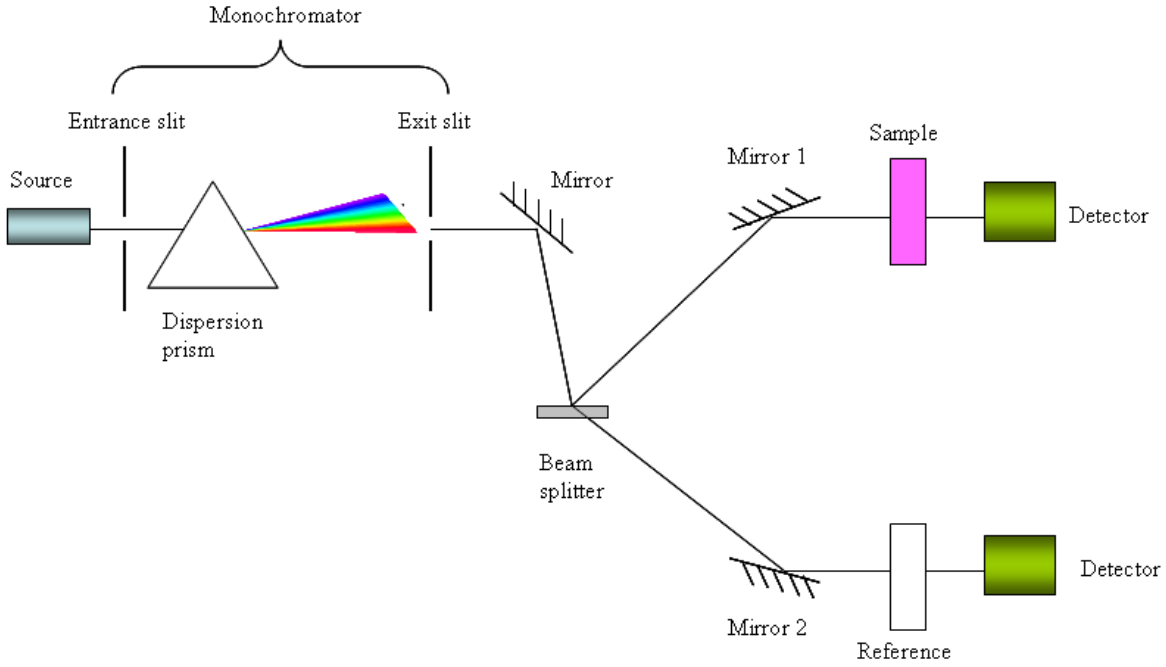

Figure 2.10: Diagram showing the principle of absorption spectrophotometer

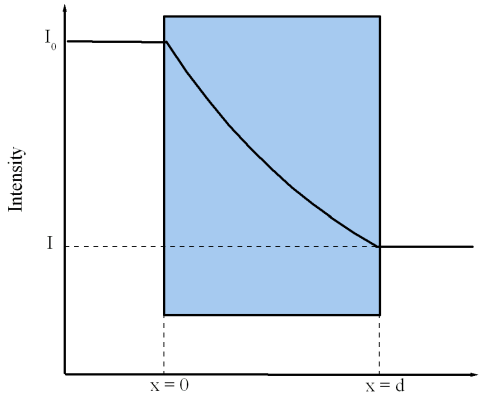

Figure 2.11: Shows the phenomenon of light absorption in a dielectric media

which further implies

$$\frac{\triangle I}{I} = -k\triangle n \tag{2.3}$$

this can further simplified as

$$\frac{\triangle I}{I} = -k_1 c\triangle x \tag{2.4}$$

where k and k_1 are constants, and c denotes the concentration of the sample assumed uniform throughout. Upon integrating we get

$$\int_{I_0}^{I_t} \frac{dI}{I} = -\int_0^N kdn = -\int_0^d k_1 cdx \tag{2.5}$$

Absorbance is now defined as A given by

$$A = \ln \frac{I_0}{I_t} \tag{2.6}$$

Thus A can also be written as $A = k_1 cd$ or so to say $A = k_2 c$, where $k_2 = k_1 d$. This is *Beer-Lambert law*, stating that the absorbance is proportional to the concentration of the absorbers in the sample. Another important parameter often used to describe light interaction with matter is the transmittance T. It is defined as the ratio of I_t to I_0. Thus absorbance A can also be defined as

$$A = \ln \frac{1}{T} \tag{2.7}$$

2.5.2 Photoluminescence Spectroscopy

Photoluminescence (PL) is the spontaneous emission of light from materials under optical excitation. The typical experimental set-up for PL measurement has been shown in Fig. 2.12. The excitation energy and intensity are chosen to probe different regions and excitation concentrations in the sample. PL based investigations can be used to characterize a variety of material parameters [27-30]. PL spectroscopy is a selective and extremely sensitive probe of discrete electronic states. Various Features of PL emission spectrum can be used to identify surface, interface, and impurity levels and can also be used as a tool to gauge alloy disorder and interface roughness. The intensity of PL signal provides valuable information on the quality on surfaces and interfaces [31]. The Excitation can itself be pulsed instead of continuous wave. Under this type of excitation

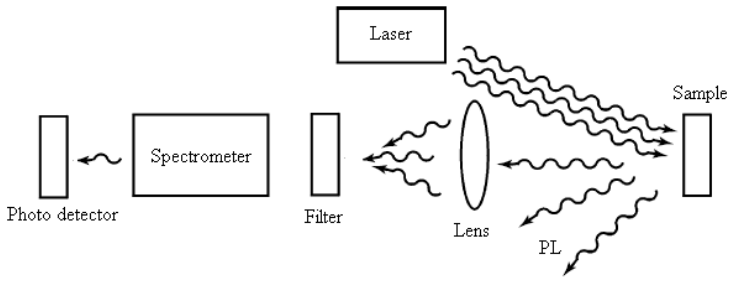

Figure 2.12: Typical experimental set-up for PL measurements

various transient phenomenon may be studied, hence the name transient PL [32,33]is given to it. A transient PL intensity is a direct indication of lifetime of non equilibrium interface and bulk states. Variation of PL intensity under an applied bias can be used to map electric field at the surface of a sample [34,35]. In addition, thermally activated processes cause changes in PL intensity with temperature. The main advantages of PL are the following:-

1. It is a nondestructive technique that requires minimal sample manipulation. item Since the technique is based on optical excitation, highly resistive materials pose no practical difficulty.

2. Besides this, a time resolved PL can be very fast, making it useful for characterizing the most rapid processes in a material.

Despite these advantages there is a fundamental limitation of PL analysis and that is its high reliance on radiative events. Materials with poor radiative efficiency, such as low quality indirect band gap semiconductors are difficult to study via ordinary PL. As we discussed in the previous chapter multilayer material systems are increasingly important in the development of smaller, faster, and more efficient electronic and optoelectronic devices. One of the primary motivation for using multilayered structures is to change the potential energy of electrons and holes at the material interfaces. It has been observed that the phenomena at the surfaces and interfaces dominate the behavior of excitations in these heterostructures, it is due to this reason that the microelectronic devices are

limited by the nature of hetrojunctions.

When a light of sufficient energy is incident on a material, photons are absorbed and electronic excitations are created. These excitations or quasiparticles are bound state of an electron and its quasiparticle hole, usually occurring in an insulator or semiconductor. Since, they are bounded coulombically therefore their energy is less than that of free electron hole pairs. These excitons provide a means to transport energy without transporting net charge. Eventually these excitons relax to the ground state. If the relaxation (recombination) is radiative, it results in PL emission. This emitted light can be collected and analyzed to yield a wealth of information about photoexcited material. PL spectrum is indicative of transition energies, which in turn determine the electronic energy levels. The PL intensity gives a measure of the relative rates of radiative and nonradiative recombination. PL intensity can be varied with external parameters like temperature and applied voltage, which can further be used to study underlying electronic states and bands. The excitation energy selects the initial photoexcited state and it also simultaneously governs the penetration depth of the incident light. When the type or quality of the material under investigation varies spatially, PL signal changes with the excitation position. In addition to this pulsed optical excitation provides a powerful means for studying transient phenomena. More than often PL originates from the surface of the material and hence is an important tool for the characterization of surfaces. The unique sensitivity of PL towards the the discrete electronic states lying near the interface makes this technique useful for probing the energy distribution and density of interface. In particular the presence of surface adsorbates alters the intensity of PL signal. When the states serve as long lived traps, the depth of these traps can be determined by observing the thermal activation in the temperature dependent PL. It should be noted that Continuous wave PL intensity and spectrum is quick and straightforward. On the other hand transient PL is more challenging, particularly when the recombination processes are fast. Even he instrumentation for time resolved detection can be expensive and complex. Compared with other optical methods of characterization PL is less stringent about beam alignment, surface flatness and sample thickness. Besides this, exhaustive analysis of excitation intensity dependence of PL intensity can

be utilized for measuring the density on interface and impurity states. The excitation intensity controls the density of photoexcited electrons and holes, which governs the behavior of these materials.

The choice of excitation energy is critical in any PL experiment and it can have profound effects on the PL signal. Thus, the excitation conditions must be considered carefully. The strength of PL relies heavily on flexibility that these adjustable parameters provide. Also as discussed in the previous section the penetration depth of incident light will depend on the excitation wavelength. Hence, different excitation energies probe different regions of the sample. As lasers are monochromatic, intense and readily focussed, they are best suited for Photoluminescence excitation. More than often these lasers must satisfy the basic requirement of light energy exceeding the bandgap energy. It should also be noted that in the case of direct-bandgap semiconductors, above-bandgap excitation has a penetration depth of the order of $1\mu m$. The diffusion of the photoexcited carriers can widely vary between $1-10\mu m$. Hence, PL with above gap excitation is very sensitive to surface effects. In indirect bandgap semiconductors, absorption is weaker and the light penetrates deeper into the sample. Hence PL is dominated by bulk recombination.

The intensity of the incident light can also be used to control the density of photoexcited electrons and holes. It is to be noted that when the carrier density is low, the measurements are dominated by discrete defect and impurity sites as the interfaces and within the bulk of the semiconductor material. Recombination at these energetically favored sites is frequently referred to as Schockley Read Hall (SRH) recombination. The SRH rate is proportional to the dominant carrier density n. Under intermediate excitation, the discrete states are filled and the bulk radiative recombination plays a greater role, in this case the radiative rate varies as n^2. One important point to note here is that low temperature or quantum confinement can make coulomb binding of electron hole pairs energetically favorable, leading to the formation of excitons which recombine radiatively at a rate that is proportional to n. In systems with high interface to volume ratios and active layers that are thin relative to the carrier diffusion length, interface effects dominate SRH recombination. Evaluating absolute PL intensity requires an es-

timate of what fraction of the emitted light is collected by the detector. However, the PL emission profile is a complicated function of sample geometry, refraction, internal reflection and reabsorption. Hence, large uncertainties in this estimate are inevitable.
Besides PL intensity the optical transitions also provide a direct access to energy level structure of the system. Although, Absorption spectroscopy is a good probe of the overall band structure of a system because bands have a relatively high density of states. PL emissions on the other hand, tend to favor sparse low lying states because photoexcited carriers thermalize through bands and closely spaced states to within kT of the lowest available levels. Apart from identifying discrete states, PL peak positions can be used to evaluate the composition of semiconductor alloys. PL is very sensitive to the interface roughness because fluctuations as small as one atomic monolayer can alter the carrier confinement energy considerably. It is commonly observed that variation of quantum wall thickness in the sampled region causes a general broadening of the PL spectrum. In samples with higher quality interface, variation in the QW thickness is limited, and recombination in different regions of such a sample yields sharp, well resolved peaks in the PL. While a graded interface is likely to shift transition energies, interface roughness tends to produce line broadening and splitting in QWs. Quantum well PL peaks are almost always broader than bulk PL. The line broadening is attributed to unintentional variation in the confinement energy in different regions of the well.
The accumulation of charge in low energy states near the surface leads to curvature of the conduction and the valence bands as is also shown in Fig. 2.13. If the surface states trap electrons, negative charge collects at the surface and the bands bend upward. If the surface states tend to lose electrons (trap holes), then positive charge accumulates, curving the bands downward. The electric field associated with the space charge region sweeps electrons and holes in the opposite directions, forming a depletion free region free of electrons and holes. It should be noted that because electrons and holes are spatially separated and cannot recombine, the depletion layer is often referred to as a dead layer. Thus in a way the PL intensity depends on the thickness of dead layer, which in turn relies on the magnitude of band bending. Increased curvature often extends the recombination free region deeper into the material, quenching the PL signal. The

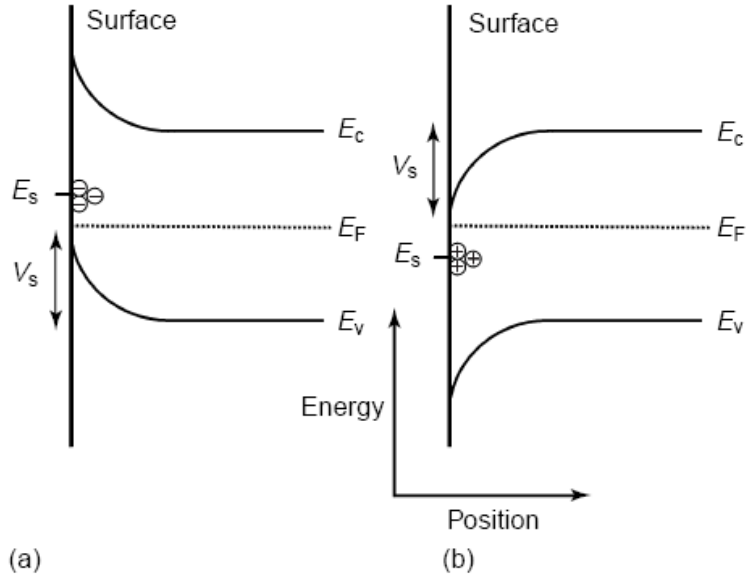

Figure 2.13: (a) When electrons accumulate in surface levels (denoted by E_s) the conduction and valence bands bend upward near the surface. (b) Accumulation of holes bends the bands downward. The magnitude of the effect is characterized by surface potential V_s *Courtesy Gfroerer et al encyclopedia of Analytical Chemistry*

magnitude of band curvature is characterized by the surface potential V_s as indicated in Fig. 2.13. One can compensate for or accentuate the surface potential V_s by applying an external bias to the surface. The resulting change in the depletion thickness can be evaluated by monitoring the PL intensity. It is to be noted here that for high quality surface having a low density of surface states, the dead layer model alone can explain the dependence of PL intensity on the applied bias. In contrast, when the surface state density is large, PL quenching is dominated by surface recombination and the dead layer model does not suffice. Chang et al [34] have observed both of these scenarios in their study about the relative role of the two mechanisms in PL extinction. In such a case where surface state density is large, the difference between the bias dependent PL quenching and the dead layer fit can be used to make a quantitative estimate of the intrinsic surface recombination velocity.

Bibliography

[1] S. Grecu, M. R. Buck, A. Opitz and W. Brutting: Org. Elec. 7 (2006) 276.

[2] T. P. I. Saragi, T. F. Lieker and J. Salbeck: Synth. Met. 148 (2005) 267.

[3] D. D. C. Bradley: J. Phys. D. Appl. Phys. 20 (1987) 1389.

[4] J. H. Burroughes, D. D. C. Bradley, A. R. Brown, R. N. Marks, K. M. Kay, R. H. Friend, P. L. Burn and A. B. Holmes: Nature 347 (1990) 539.

[5] P. L. Burn, D. D. C. Bradley, R. H. Friend, D. A. Halliday, A. B. Holmes, R. W. Jackson and A. Kraft: J. Chem Soc. 1 (1992) 3225.

[6] K. Diallo, M. Erouel and J. Tardy: Appl. Phys. Lett. 92 (2008) 183305.

[7] S. J. Mun, J. M. Choi, K. H. Lee, K. Lee and S. Im: Appl. Phys. Lett. 93 (2008) 233301.

[8] T. Minakata and Y. Natsume: Appl. Phys. Lett. 93 (2008) 153306.

[9] A. R. Brown, A. Pomp, C. M. Hart, D. M. De Leeuw, D. B. M. Klaassen, E. E. Havinga, P. Herwig and K. Mullen: J. Appl. Phys. 79 (1996) 2136.

[10] A. R. Brown, A. Pomp, C. M. Hart and D. M. De Leeuw: Science 270 (1995) 972.

[11] Y. Kanemitsu, N. Shimizu, K. Suzuki, Y. Shiraishi and M. Kuroda: Phys. Rev. B. 54 (1996) 2204.

[12] G. Wang, T. Hirasa, D. Moses and A. J. Heeger: Synth. Met. 146 (2004) 127.

[13] G. Derue, D. A. Serban, Ph. Leclere, S. Melnite, P. Damman and R. Lazzaroni: Organic ELectron. 9 (2008) 821.

[14] H. F. Meng, C. C. Liu, C. J. Jiang, Y. L. Yeh, S. F. Horg and C. S. Hsu: Appl. Phys. Lett. 89 (2006) 243503.

[15] J. Ghim, K. J. Baeg, Y. Y. Noh, S. J. Kang, J. Jo and D. Y. Kim: Appl. Phys. Lett. 89 (2006) 202516.

[16] S. S. Pandey, W. Takashima, S. Nagamatsu, T. Endo, M. Rikukawa and K. Kaneto: Jpn. J. Appl. Phys. 39 (2000) L94.

[17] H. Koezuka, A. Tsumura and T. Ando: Synth. Met. 18 (1987) 699.

[18] A. Tsumura, H. Koezuka and T. Ando: Synth. Met. 25 (1988) 11.

[19] S. C. Chang, J. Liu, J. Bharathan, Y. Yang, J. Onohara and J. Kido: Adv. Mater. 11 (1999) 734.

[20] E. Fisslthaler, S. Sax, U. Scherf, G. Mauthner, E. Moderegger, K. Landfester and E. J. W. List: Appl. Phys. Lett. 92 (2008) 183305.

[21] A. K. Thakur, A. K. Mukherjee, D. M. G. Preethichandra, W. Takashima and K. Kaneto: J. Appl. Phys. 101 (2007) 104508.

[22] V. Singh, M. Yano, W. Takashima and K. Kaneto: Jpn. J. Appl. Phys. 45 No. 1B (2006) 534.

[23] V. Singh, A. K. Thakur, S. S. Pandey, W. Takashima and K. Kaneto: Appl. Phys. Exp. 1 (2008) 021801.

[24] V. Singh, A. K. Thakur, S. S. Pandey, W. Takashima and K. Kaneto: Synth. Met. 158 (2008) 283

[25] V. Singh, S. S. Pandey, A. K. Thakur, W. Takashima and K. Kaneto: Organic Electron. 9 (2008) 790.

[26] V. Singh, A. K. Thakur, S. S. Pandey, W. Takashima and K. Kaneto: Jpn. J. Appl. Phys. 47, No. 2 (2008) 1251.

[27] L. M. Woods, P. Silvestre, P. Thiagarajan, G. A. Patrizi, G. Y. Robinson, K. M. Jones and M. Al Jassim: J. Electron. Mater. 23 (1994) 1229.

[28] A. Patane, A. Polimeni, M. Capizzi and F. Martelli: Phys. Rev. B. 52 (1995) 2784.

[29] H. J. Frenck, W. Kulisch and R. Kassing: Proc. SPIE 1144 (1989) 250.

[30] V. Y. Timoshenko, J. Rappich and Th. Dittrich: Appl. surf. Sci. 123 (1998) 111.

[31] H. Wang, K. S. Wong, B. A. Foreman, Z. Y. Yang and G. K. L. Wong: J. Appl. Phys. 83 (1998) 4773.

[32] T. Fukuda, T. Okada, B. Wei, M. Ichikawa and Y. Taniguchi: Appl. Phys. Lett. 90 (2007) 231105.

[33] T. Trupke, R. A. Bardos and M. D. Abbott: Appl. Phys. Lett. 87 (2005) 184102.

[34] R. R. Chang, R. Iyer and D. L. Lile: J. Appl. Phys. 61 (1987) 1995.

[35] J. F. Kauffman, C. S. Liu and M. W. Karl: J. Phys. Chem. B. 102 (1998) 6766.

Chapter 3

Study of LiF/P3HT interface and its application in P3HT based OFETs

Summary

LiF [1]is often used to improve the injection of electrons from the cathode into LUMO of an n-type semiconductor in Organic Light Emitting Diodes (OLEDS). It is also used to improve the quantum efficiency of thin film bulk heterojunction (P3HT/PCBM) Organic Solar Cells (OSCs). Although several models have been proposed to explain these observations. Some of these models quite well explain the injection enhancement in OLEDs. However, little is known about the nature of interface between LiF and P3HT. In order to investigate the nature of interface between LiF and P3HT the PL spectra of P3HT thin films coated with LiF and Al were studied separately. Also the memory currents in Photo induced memory devices (PIMDs) were studied. The results indicate that LiF unlike Al, does not form a depletion layer with P3HT. This fact was then successfully utilized to improve the on/off ratio and the $I - V$ characteristics of OFETs fabricated on top of Si wafer using P3HT thin film.

[1]LiF is an ionic molecule having a dipole moment of about 6.2D, also it is transparent to the vis and IR spectrum of light

3.1 Introduction

Owing to the different requirements of devices viz. Organic Light Emitting Diodes (OLEDs)[8-11], Organic Field Effect Transistors (OFETs)[12,22,23] and Organic Solar Cells (OSCs)[1,2], different types of device structures have been proposed, viz., planar type and the stacked type. While OLEDs and OSCs have been primarily fabricated in stacked geometry, having either single or multilayered structures, OFETs are preferred in the planar geometry, owing to the ease of integration of these devices on a single chip. However, new types of transistors based on stacked structure are becoming popular[3,4]. As more and more stacked structures are coming into play, the role of interface is becoming far more significant. A fundamental understanding of the mechanism of interface formation plays an important role in determining the device performance. The interface property primarily depends on the alignment of energy levels, viz., vacuum level and the Fermi level. Former gives rise to the built-in potential while the latter leads to the formation of interfacial dipole by means of diffusive charge transfer across the metal and organic layer [5,6]. The degree of charge transfer is reflected by the bending of energy band of polymer with respect to the Fermi level of metal[7].

Presently OLEDs use a thin layer of LiF below the cathode metal. It has been observed that inclusion of a thin layer of LiF (0-2 nm) improves the External quantum efficiency of OLEDs[8-11]. Although, LiF/Al electrodes have been widely used for enhancing the external quantum efficiency of OLEDs, the underlying mechanisms[8-11] are still under investigation. Several mechanisms suggested till date include the following:-

(1) Lowering the effective work function of the Aluminum (Al) electrode.

(2) Dissociation of LiF and subsequent chemical reaction (doping) of the organic layer.

(3) Formation of a dipole leading to a vacuum level offset between organic layer and the Al.

(4) Protection of the organic layer from the hot Al atoms during thermal deposition.

Similar results have also been obtained in the case of thin film bulk heterojunction Organic Solar Cells (OSCs) using P3HT/PCBM composite film[11]. Although, several models have been proposed to explain these experimentally observed facts. How-

ever, most of these models are particularly applicable to Alq3(tris-(8-oxyquinolato) aluminum)/LiF/Al interface. Alq3 has been a material of interest for past several decades after it was first reported in a pioneering work at Kodak[30]. Alq3 belongs to class of organo-metallic chelates, and shows a good electron transport behavior with a reasonably efficient emission. Amongst the above proposed mechanisms some are general and may be applicable to nature of interface that LiF forms with a range of other organic materials as well. However, other mechanisms are highly specific to the Alq3/LiF/Al interface. In particular our interest was whether LiF actually dissociates into ions, and hence results in subsequent doping of the organic layer below it. We were also interested to study the LiF/P3HT interface and to verify which one of the above proposed mechanisms is also applicable to LiF/P3HT interface, and hence is more general in approach. PL has long been used to study the nature of interface[13-16]. In this chapter we studied the qualitative difference between the nature of LiF/P3HT and Al/P3HT interfaces using photoluminescence spectroscopy. Al is well known to form a depletion layer[30-35] with P3HT[17-19]. Also the memory currents from the photo induced memory devices[20] were measured and it was found that LiF does not form a depletion with P3HT.

OFETs fabricated using P3HT are presently limited in their performance mainly because of low charge carrier mobility and poor on/off ratio. While the charge carrier mobility is limited by the bulk transport in these materials. The on/off ratio in OFETs limited by the large leakage current occurring through the bulk of the P3HT film. It is now established that the bulk transport comprises of intrachain transport and interchain transport. While the intrachain mobility is very high, it is the interchain mobility that leads to reduced overall bulk transport[36,37]. It should also be noted that high charge carrier mobility in OFETs is a prime requirement for them to be used for high speed applications. However, higher on/off ratio in these OFETs is desired particularly for slow speed applications e.g. barcodes.

3.2 Experimental Procedures

In all three types of devices A, B and C were fabricated on two different substrates viz. glass and silicon wafer. Devices A and B were fabricated on glass substrate. Device C was fabricated on silicon wafer based substrate. While device A was used to study the LiF/P3HT and Al/P3HT interface using Photoluminescence spectroscopy, device B on the other hand was used to fabricate Photo Induced Memory Devices (PIMDs)[20]. Device C was further used to study the characteristics of P3HT based OFETs[12].

The experimental set up of PL along with the schematic diagram of device A is shown in Fig. 3.1. PL measurement was done under ambient condition using Hamamatsu photonic multi channel analyzer (PMA11), Model C7473, kept at a distance $70cm$ from the sample. A $300mW$, Class III B, CW, He-Cd Laser having an excitation wavelength of 442 nm (Kimmon Electric co. Ltd.) was used to illuminate the sample at an inclination of 30^o to the normal of the sample. The device shown in the left of Fig. 3.1 shows P3HT films coated with $2nm$ of Al, and the one shown in the right shows the P3HT films coated with $2nm$ LiF separately. It should be noted that a depletion layer below the Al layer has been shown in Fig. 3.1. However, no such layer has been shown below the LiF layer. This difference will become more clear as we discuss the results in the next section.

Glass substrates having an area of 3 cm^2 and 4 cm^2 were separately taken for the fabrication of device A and B respectively. However, Si wafer substrate having an area of 1 cm^2 were taken for the fabrication of device C. All these substrates were then sonicated in iso-propanol and acetone solutions for a period of 10 mins each. Later these substrates were treated with a mixture of NH_4OH and H_2O_2 for 15 mins, by heating these substrates at 85^oC. This step was mainly done to make the surface more hydrophillic prior to doing to the hydrophobic treatment of the substrate. Making the surface more hydrophillic prior to hydrophobic treatment is usually done to ensure better attachment of Silanizing molecules on to the surface of the substrate. Following this, these substrates were sonicated in distilled water subsequently followed by drying. In the next step surface of these substrates were made hydrophobic by treating them with

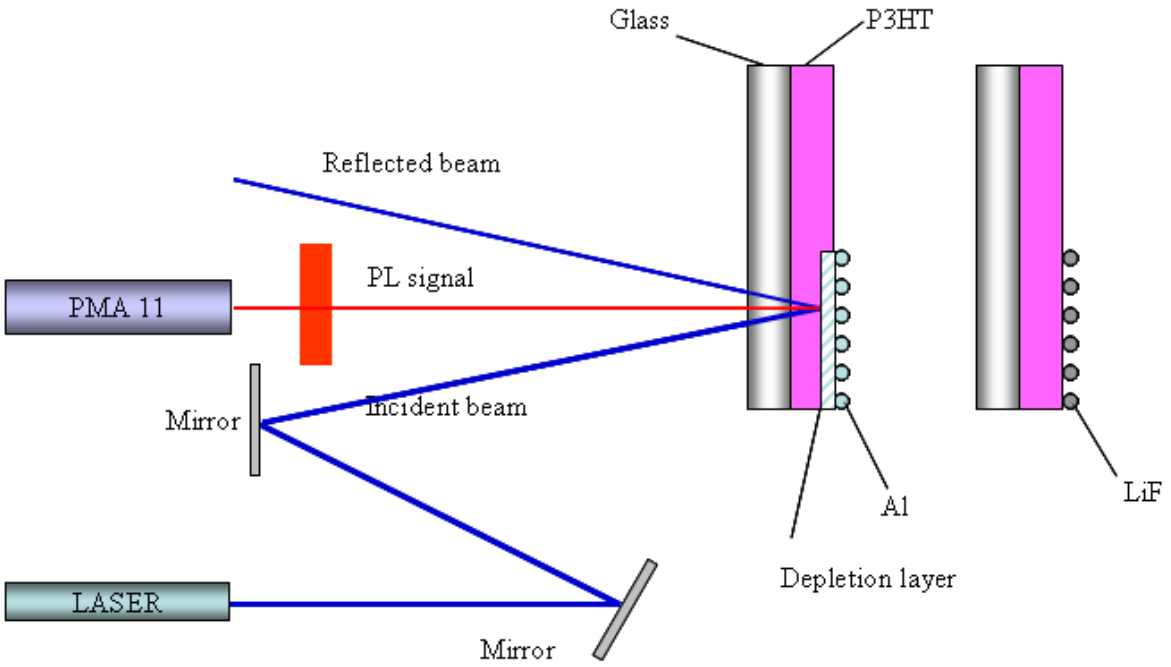

Figure 3.1: Schematic diagram showing the Photoluminescence set-up

HMDS (Hexa-1,1,1,3,3,3-methyldisilazane) for about 90 mins. Later, these samples were washed in $CHCl_3$ solution. Thus a highly hydrophobic surface of these samples were obtained.

In the case of device A on top of these samples, a Chloroform solution of P3HT was spin coated @ $[1500, 3000]r.p.m.$ for $[30, 10]s$ respectively. Variation in the film thickness was done by changing the strength of chloroform solution of P3HT. Samples were annealed at 90 ^oC for $60mins$ inside vacuum oven[24-25]. Finally these samples were divided into three lots. While the first two lots were coated with Al $(2nm)$ and $(20nm)$ separately, the third lot was coated with $20nm$ thick LiF. This was done mainly to study the effect on the emission spectra of pristine P3HT films due to the deposition of Al and LiF thin overlayers separately. It should also be noted that both LiF and Al were coated using physical vapor deposition technique, at a pressure of $(4.0X10^{-6}torr)$.

Si wafer substrates were taken in order to fabricate the OFETs. Figure 3.2(a) shows the schematic diagram of typical OFETs fabricated using P3HT, while Fig. 3.2(b) shows the schematic diagram of an OFET coated with ($10nm$) LiF. Fig 3.2(c&d) demonstrate the effect of film thickness variation in OFETs. The IV characteristics of the OFETs were

measured using Keithley 6517 A electrometer. Figure 3.3(a) shows the typical biasing arrangement of these OFETs. Schematic diagram of PIMDs along with its biasing

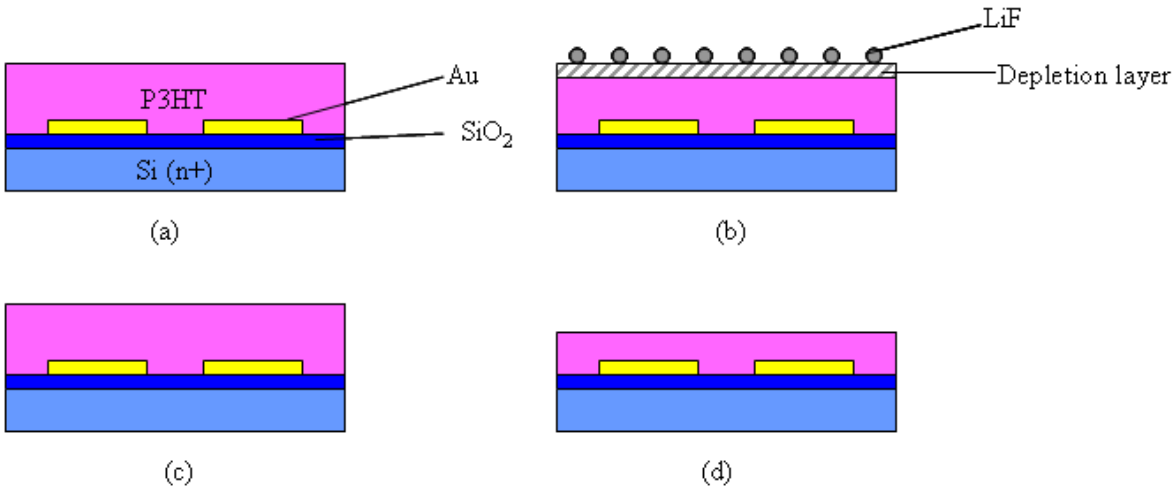

Figure 3.2: (a) Shows the schematic diagram of P3HT based OFET fabricated on top of Si wafer, (b) shows an OFET coated with $5nm$ LiF layer, (c) shows an OFET having thick P3HT layer and (d) shows an OFET having thin P3HT film

arrangement has been shown in Fig. 3.3 (b). Fabrication of PIMDs and OFETs was done under almost identical conditions as mentioned above, the only difference being that the PIMDs were two terminal devices and OFETs were three terminal. Thick gold (Au) source drain electrodes having thickness upto $30nm$ were evaporated using physical vapor deposition technique, leading to a typical bottom contact type device structures. In the case of both PIMDs and OFETs the channel region was defined by shadow masking technique, a schematic diagram of which is shown in the Fig. 3.3(a and b). The channel length and width in both these devices were found to be $l = 50\mu m$ and $w = 2mm$ respectively. Subsequently P3HT was spin coated and annealed under exactly identical conditions as for sample A. Finally sample B were divided into two lots. While one lot was coated with Al ($2nm$) the other was coated with LiF ($2nm$). In the case of Samples C were coated with ($10nm$) thick LiF on top of P3HT films.

IV characteristics of OFETs and PIMDs were measured using Keithley 6517 A electrometer. It must be noted that in the case of both these devices the IV measurements were performed after coating respective overlayers without breaking the vacuum. Also, the film thickness of the P3HT in PIMDs as well as in OFETs were varied by varying

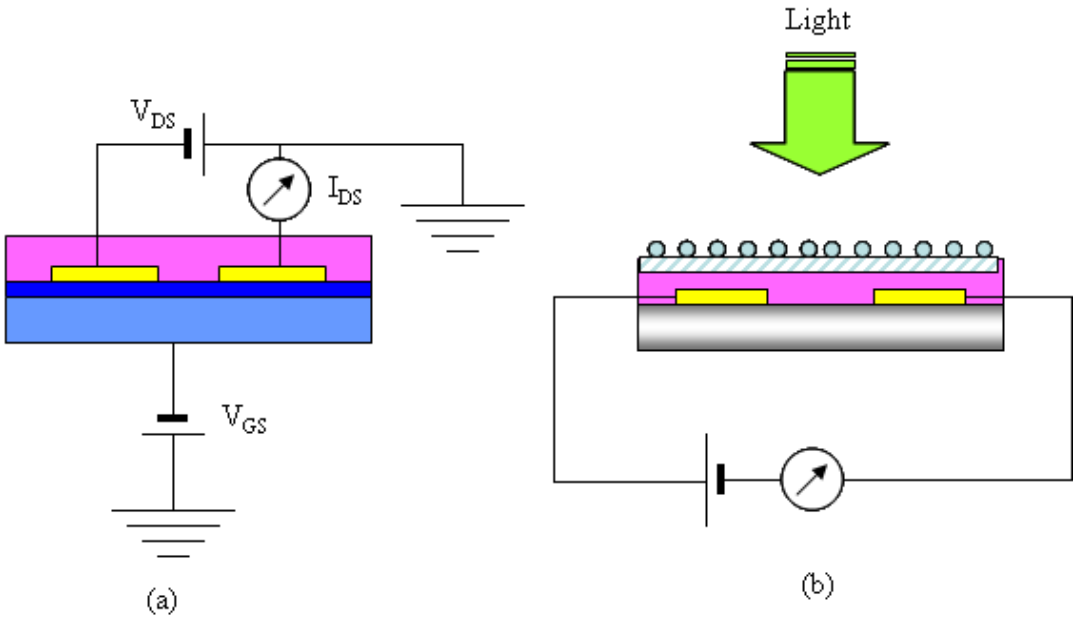

Figure 3.3: (a) Shows the typical biasing arrangement in OFETs, (b) shows the Schematic diagram of PIMDs and its biasing arrangement

the strength of $CHCl_3$ solution of P3HT. The respective film thicknesses were later measured using Dektak 6M surface profiler.

3.3 LiF/P3HT interface

Photoluminescence can be used to characterize the nature of interface both qualitatively and quantitatively, as has also been mentioned in detail in Chapter 1. On one hand a change in band energy level results in shift of peak position in a PL spectra. A relative decrease in the magnitude of PL intensity on the other hand results in what is called *PL quenching* [13-16]. Usually a PL quenching is caused by the following two reasons:-
1)Increase in the number of non radiative recombination of excitons, mainly occurring due to increased non radiative energy transfer of excitons via additional impurity states. This type of energy transfer of excitons leads to an overall loss of the absorbed energy. Thus a PL quenching occurring via energy transfer through phonon coupling mode implies the increased loss of energy.
2) Increase in the number of excitons undergoing electric field assisted dissociation into pair of oppositely charged charge carriers. A PL quenching occurring due to field assisted

dissociation of excitons signifies the photovoltaic behavior of the semiconductor junction. In simpler terms it can be said that if the total number of excitons is N_{tot} then it can be expressed as given by eq. 3.1.

$$N_{tot} = N_r + N_{nr} \tag{3.1}$$

Where N_{tot} denotes the total number of excitons at any time in the bulk of the film. Out of which N_r is the number of excitons undergoing radiative decay, and N_{nr} denote the number of excitons undergoing non radiative decay. However, N_{nr} itself is given by eq. 3.2

$$N_{nr} = N_{ph} + N_{diss} \tag{3.2}$$

Where N_{ph} denotes the number of excitons undergoing nor radiative decay via phonon coupled energy transfer, and N_{diss} on the other hand denotes the number of excitons undergoing field assisted dissociation. It is the competition between radiative and non-radiative excitonic processes in Organic light emitting diodes as well as in photovoltaic cells that govern their overall device efficiency. Generally, the luminescence lifetime τ is related to the rate constants for radiative (k_r) and nonradiative (k_{nr})decay by eq. 3.3

$$\frac{1}{\tau} = k_r + k_{nr} \tag{3.3}$$

where the radiative lifetime is $1/k_r$. The PL quantum efficiency is then given by eq. 3.4 as follows,

$$\eta_{pl} = b\left(\frac{k_r}{k_r + k_{nr}}\right) \tag{3.4}$$

where b is the fraction of absorbed photons leading to formation of excitons. As can be seen from eq. 3.4 that the balance of radiative and non radiative decay rates determines luminescence efficiency. Thus, in order to study the nature of LiF/P3HT interface qualitatively PL emission spectra from Al and LiF coated P3HT samples were compared. Figure 3.4(a) shows the effect of coating $2nm$ thick Al on top of a $97nm$ thick P3HT film. It was observed that a mere $2nm$ coating of pristine P3HT film resulted in a significant amount of PL quenching. This is mainly due to the increased value of k_{nr}, possibly due to increase in the loss of energy via phonon coupling mode although possibility of quenching caused by band bending can not be ruled out. Friend et al ref [15] also

proposed in their work that exciton quenching occurs near the metal polymer interface. They further proposed capping metal surface with high band gap materials viz. BCP, TPBI etc.[38-40] leads to reduction in the exciton recombination occurring at the metal electrode. Later a more detailed model for exciton quenching near metal electrode was developed by Blom et al [41]. Figure 3.4(b) shows the effect of coating $20nm$ thick Al on top of pristine P3HT thin films. It was found that increasing the thickness of Al electrode coated on top of P3HT leads to increased PL quenching in P3HT films. Al is well known to form a depletion layer with P3HT[17-19,21]. Thus increasing the Al thickness from $2nm$ to $20nm$ the increase in the PL quenching is mainly caused by the formation of Schottky junction near the Al/P3HT interface. The built in field near the Schottky junction is sufficiently high, and can easily cause field assisted dissociation of excitons. Although the possibility of non radiative decay of excitons via phonon coupling can not be completely ignored but the major contribution of PL quenching in the case of $20nm$ thick Al overlayers comes from the increased non radiative decay of excitons mainly due to field assisted dissociation of excitons. It can also be seen from Fig. 3.4(b) that as expected PL counts in pristine films were proportional to the thickness of these pristine films. It should also be noted that after coating $20nm$ Al on $97nm$ and $43nm$ thick P3HT film resulted in nearly identical level (80%) of quenching (defined by the ratio of PL intensity at $\lambda = 727nm$). However, it can be argued that coating $20nm$ Al on the P3HT films resulted in nearly identical thickness of depletion layer, thus the percentage PL quenching for the two films can not be the same. Here we would like to mention that this simple analogy would have been true only if the PL quenching entirely resulted due to the depletion layer formation. However, as is known that phonon coupled non radiative decay is also present, besides, there is quenching of excitons in the near vicinity of metal surface [41]. Thus, a direct comparison between the PL quenching of thick and thin film due to thick Al overlayers can not be made. Further, the fact that reflection of light may also occur can not be completely ignored, and such a phenomena would be more prominent in thin films. Thus, leading to lower level of PL quenching in these films [29].

Figure 3.5 shows the PL spectra of thick ($d = 97nm$) and thin ($d = 43nm$) P3HT

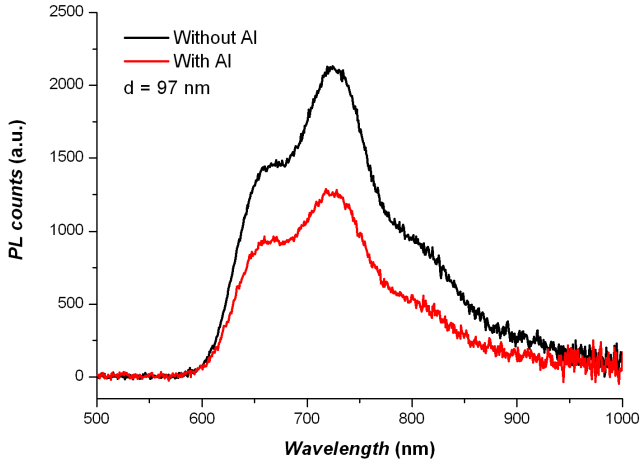

(a) Shows the PL quenching caused by the deposition of 2 nm Al on top of pristine P3HT film

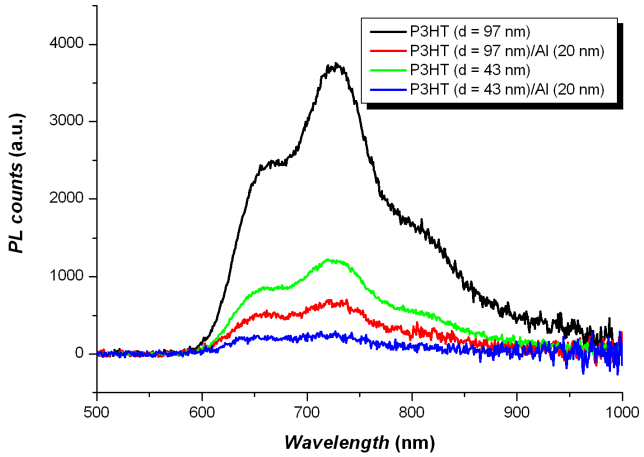

(b) Shows the effect of coating 20 nm thick Al over thick (97 nm) and thin (43 nm) P3HT films

Figure 3.4: PL spectra of various Al coated films

films coated with $20nm$ thick LiF on the top. A relatively small quenching of 5.8% was observed in thick P3HT film due to LiF coating, on the other hand in the case of thin film the quenching was found to increase upto 56.5%. Thus unlike the Al coated films the LiF coated films showed no correlation, this has been attributed to the lack of any reflection and subsequent double excitation of the bulk of the P3HT films. Here it should be noted that LiF molecules are optically transparent to the entire visible spectrum of light. A higher level of quenching for the $43nm$ film in Fig. 3.5 can be attributed to the relatively higher diffusion length of LiF molecules into the polymer matrix. Although, PL quenching was observed in both Al and LiF $20nm$ thick overlayers. A relatively higher quenching occurred in Al coated samples possibly due to the formation of depletion layer. However, it must be noted here that PL data alone does not clarify whether LiF forms a depletion layer with P3HT or not. In order to verify

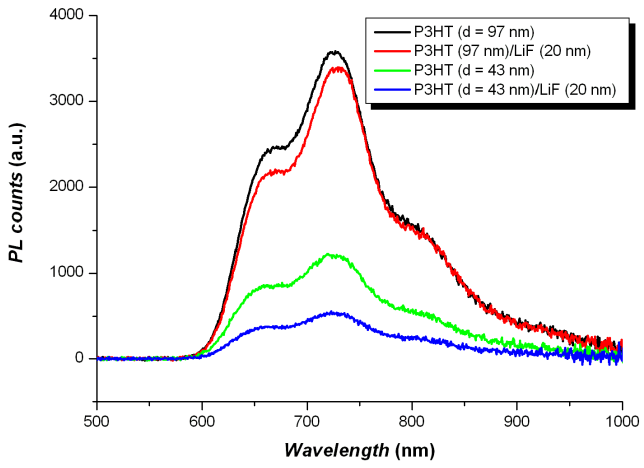

Figure 3.5: Shows the effect of coating 20 nm thick LiF over thick (97 nm) and thin (43 nm) P3HT films

the interface of LiF/P3HT interface PIMDs were fabricated using $2nm$ thick Al and LiF separately.

3.4 Photo Induced Memory Devices (PIMDs)

We fabricated two terminal photo induced memory devices (PIMDs) following the identical procedures as were first demonstrated by Ujimoto et al [20]. Here we will give a brief account of the working principle of PIMD, although the detailed mechanism can be found elsewhere[20]. A thin layer of Al ($< 2nm$) above the P3HT film leads to the formation of depletion layer near the Al/P3HT interface. It is commonly believed that electron transfer from Al to P3HT, results in loss of conductivity and thus formation of depletion layer. There exists a built in field in the depletion region. Upon illumination of light on these PIMDs, excitons generated in the bulk of P3HT film. Some of these excitons which are able to diffuse to the depletion layer dissociate into oppositely charged carriers (Usually such a dissociation of exciton is termed as *Field assisted dissociation of excitons* as was also described in the previous section). Under the applied field the holes contribute to the external current in the circuit. However, when the light is switched off, the electrons trapped on Al particles lead to prolonged memory current even after removing the light illumination.

Figure 3.6(a & b) show the bias dependent memory current in $2nm$ thin Al coated PIMDs for both $43nm$ and $97nm$ thick P3HT films. As has also been demonstrated by Ujimoto et al[20], with increasing V_{DS} the memory currents were found to increase in both thick and thin film PIMDs. Also, It is to be noted that $97nm$ thick PIMDs showed higher memory currents as compared to the $43nm$ thin PIMDs.

It was only after PIMDs fabricated using $2nm$ LiF over layer were measured that we confirmed the lack of depletion layer near the LiF/P3HT interface, as can be clearly seen from Fig. 3.7. Figure 3.7 shows the various PIMDs fabricated using LiF and Al over layers at a constant $V_{DS} = 50V$. While the memory currents were observed both in thin and thick film PIMDs coated with $2nm$ Al, However, no memory current was observed in any of the thin and thick film PIMDs that were coated with $2nm$ of LiF. This is a clear indication of lack of formation of depletion layer near the LiF/P3HT interface. Besides providing evidence we also demonstrate the effectiveness of PIMDs for probing the nature of the interface electrically. Thus, it was concluded that LiF does

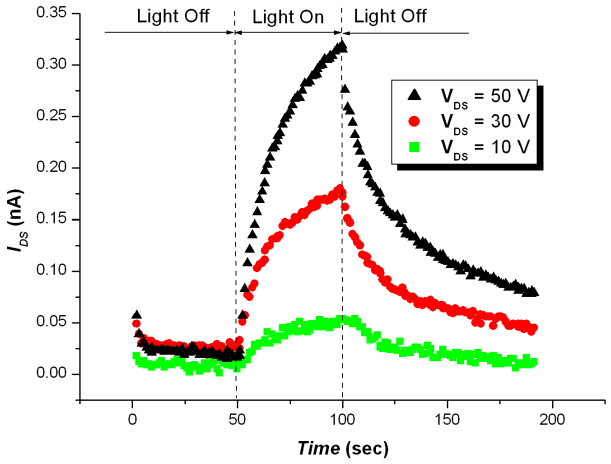

(a) $43nm$ thin film

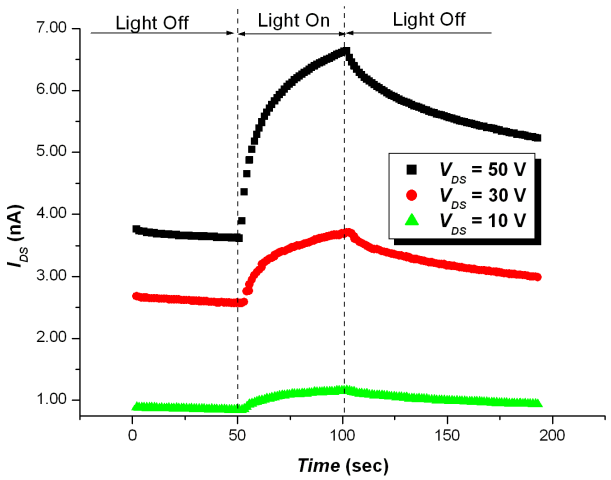

(b) $97nm$ thick film

Figure 3.6: Photo induced memory currents against increasing values of V_{DS}

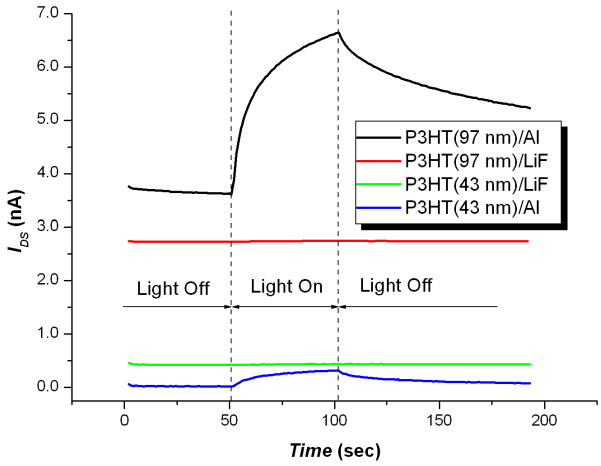

Figure 3.7: Shows memory currents in LiF and Al coated PIMDs

not dissociate into ions[29], and hence no depletion layer formation was observed near the LiF/P3HT interface. However, the PL quenching in P3HT films due to LiF over layer can be explained by the transfer of exciton energy non radiatively via additional phonon coupled vibration modes, introduced due to the presence of LiF near the interface. This is also clear from the band diagram in the two cases, as is also shown in Fig. 3.8.

3.5 P3HT based OFETs using LiF

OFETs fabricated using P3HT were found to have poor IV characteristics and poor on/off ratio as can also be seen from Fig. 3.9(a). Although charge carrier mobility were also very low of the order of $(10^{-4}cm^2V^{-1}s^{-1})$. While the charge carrier mobility is a bulk property of material and may depend on the purity of P3HT and degree of crystalline domains in the P3HT film. The on/off ratio was on the other hand limited by the large leakage current in the normally off state of the OFET. This large leakage can be due to large bulk thickness of the film [12]. In order to reduce these leakage currents and to improve the on/off ratio we decided to reduce the bulk thickness of the film. Further, In some interesting reports [26,27] researchers have pointed out that the actual channel induced by the application of gate bias V_{GS} in the OFETs may be only few nm

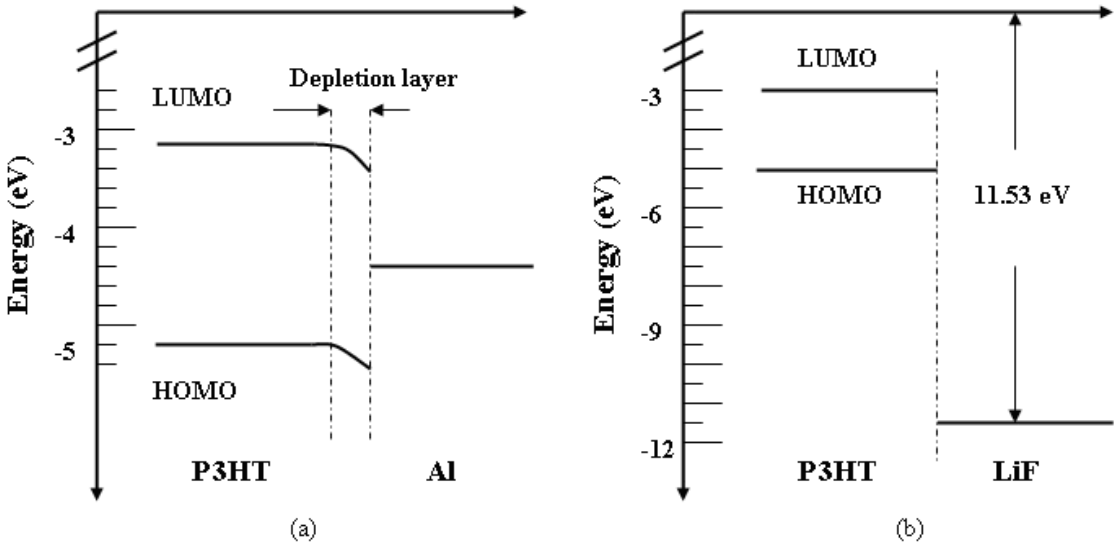

Figure 3.8: Band diagram showing the interface of (a) P3HT and Al, also showing the formation of depletion layer, (b) P3HT and LiF, no band bending shows lack of formation of depletion layer.

thick. Thus in order to further study the effect of gate induced channel in these OFETs we decided to cut- off the bulk region of the P3HT films by coating LiF on top of bottom contact type OFETs. Although, Al could also be used to achieve this. However, In the case of Al the thickness of deposited over layer is limited only up to $1 - 2nm$ above which it starts conducting [21]. LiF on the other hand is a polar, inorganic, insulating molecule. Thus, thick LiF overlayers can be deposited over the P3HT films to ensure better cut off of the bulk leakage currents.

As can be seen from Fig 3.9(a & b) that the OFET characteristics improved upon coating a ($10nm$) thick layer of LiF on top of an OFET having $85nm$ P3HT film. It is to be noted that while the IV characteristics of the transistor improved. The absolute level of currents both in the on and the off state decreased. However, the on current decreased a little while the off current decreased by one or two orders of magnitude. This led to significant improvement in the on/off ratio of LiF coated OFETs.

Figure 3.10 (a & b) show the effect of coating a ($10nm$) thick LiF on to the top of a ($43nm$) thin P3HT film. As it can be seen that the effect of coating LiF on top of a $43nm$ thin film OFET was exactly identical with that of a $85nm$ thick film. In both

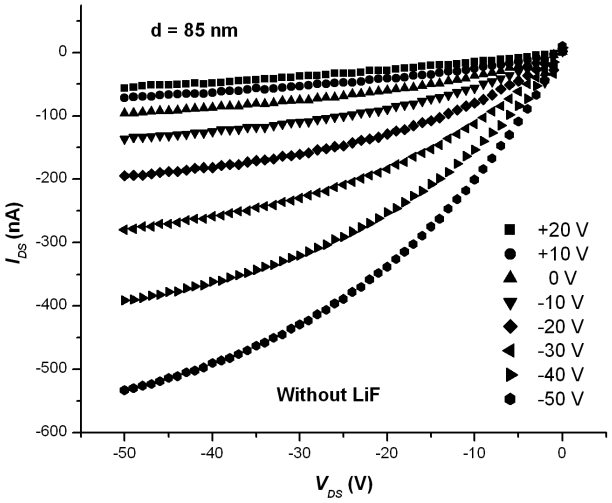

(a) without LiF coating

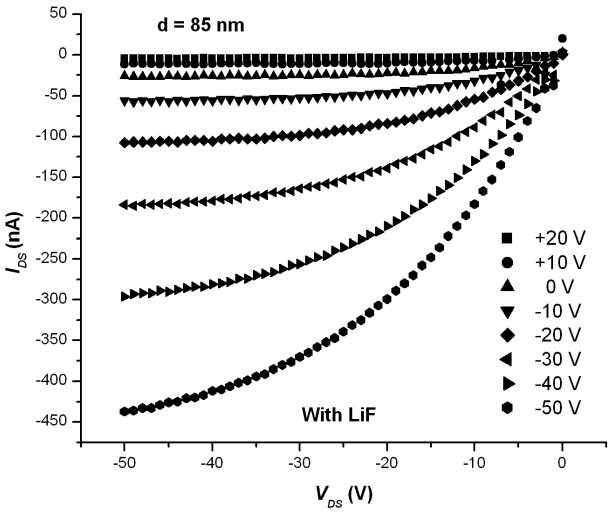

(b) with LiF coating

Figure 3.9: IV characteristics of OFET having 85 nm thick P3HT layer

the cases the IV characteristics of the OFETs improved along with their on/off ratio. It should also be noted that in general thin films are better for transistor fabrication as can also be seen by comparing Fig. 3.9(a) with Fig. 3.10(a). The on/off ratio of $43nm$ thin film OFET was higher that that of $85nm$ thick film OFET. Reducing the bulk film thickness of P3HT to $23nm$ further resulted in improved characteristics as can be easily seen from Fig. 3.11. This shows that thin films have less leakage currents and thus have better IV characteristics as well as on/off ratio of these OFETs. It also implies that the gate induced channel thickness is well below $23nm$. Similar results were also obtained by Kiguchi et al [26], where it was demonstrated that the gate induced channel in OFETs is only a few nm thick.

Figure 3.12(a) shows the plot of on and off currents in OFETs against various film thickness of P3HT films. Figure 3.12(a) shows a semi log plot of the thickness dependence of on- and off-currents at the saturation region of $V_{DS} = -50V$ and $V_{GS} = -50V$ for various OFETs. It was observed that both the on and off currents decreased for decreased film thickness and also due to LiF coating on to the top of P3HT films. However, it can be seen from Fig. 3.12(a) that the effect of coating LiF was much higher on the transistor off currents, although, slight decrease in the on currents also occurred by LiF coating. Ideally for thick film the on-current should not change due to LiF coating, since it is assumed that the field induced channel is located near the semiconductor insulator interface in the OFETs. However, small decrease of the on-current upon LiF coating particularly in the thick films can be attributed to some extent to the charge carrier distribution in the bulk of P3HT, in the direction perpendicular to the channel, as has also been pointed out by Meijer et al [42]. Figure 3.12(b) on the other hand clearly shows improvement in the on/off ratio of OFETs due to varied film thickness and also due to LiF coating. As can be seen from the Fig. 3.12(b) a significant improvement in the on/off ratio of OFET was obtained for thin film OFETs. Further it must be noted that coating LiF on these OFETs resulted in further increase in the On/Off ratio. Probably due to the cut off of the leakage current from the bulk region. However, It must also be noted that the effect of LiF coating was maximum on thick film OFETs and decreased with decreasing film thickness of the P3HT. This is because of lower film

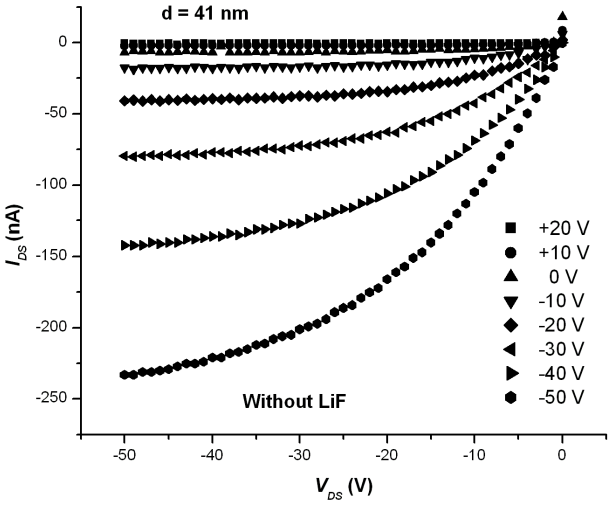

(a) without LiF coating

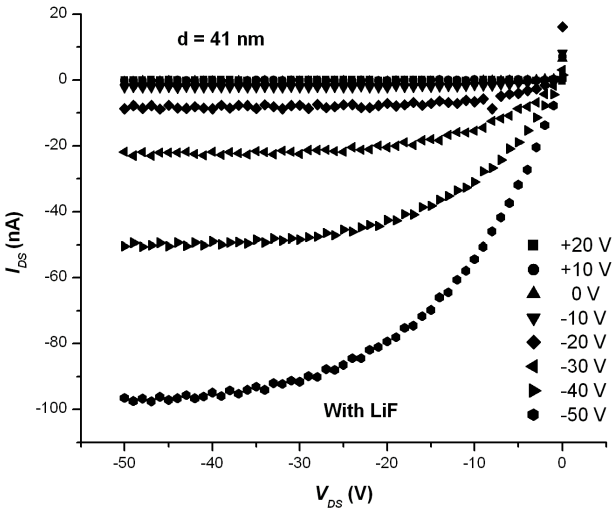

(b) with LiF coating

Figure 3.10: IV characteristics of OFET having $43nm$ thick P3HT film

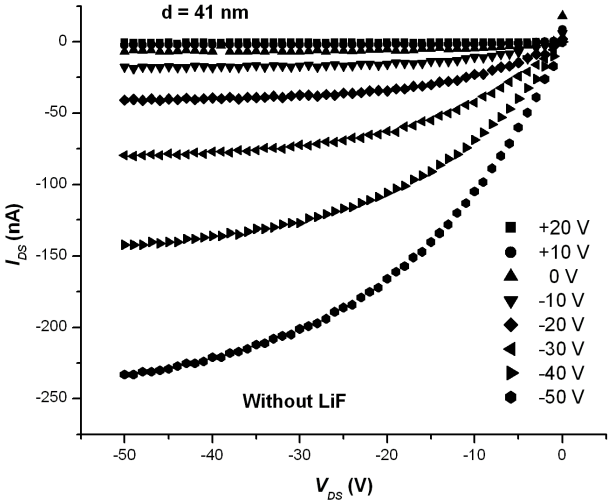

Figure 3.11: IV characteristics of OFET having $23nm$ thick P3HT film

thickness of P3HT the leakage currents are significantly lowered.

In general a resistive model of an OFET is as shown in Fig. 3.13. Where R_S and R_D denote the contact resistances at the source and drain electrodes. Also, where R_B denotes the bulk resistance of the P3HT film and R_{CH} denotes the channel resistance. It is well known that by the application of gate bias the channel resistance R_{CH} is modulated leading to the observed transistor characteristics. The observed improvement in the on/off ratio of the OFETs by LiF coating may be explained on the basis of interaction between holes and LiF dipole as has been shown schematically in the Fig. 3.14. It is known that LiF does not form a depletion layer with P3HT. LiF molecules present at the top of P3HT film may form dipole under the gradient field resulting from the application of V_{GS} on the OFET. It is these dipoles that interact with the charge carriers near the LiF/P3HT interface, and lead to trapping of the charge carriers in the vicinity of LiF/P3HT interface. This leads to cut-off of the conduction through the bulk of the film, as can be seen from the Fig. 3.12(b). In general the OFET characteristics in the saturation region are given by the eq. 3.5.

$$\sqrt{I_{DS}} = \sqrt{\frac{w\mu C_{ins}}{2L}}(V_G - V_{TH}) \tag{3.5}$$

Where Symbols have the usual meaning as described in chapter 1. Further, it must be

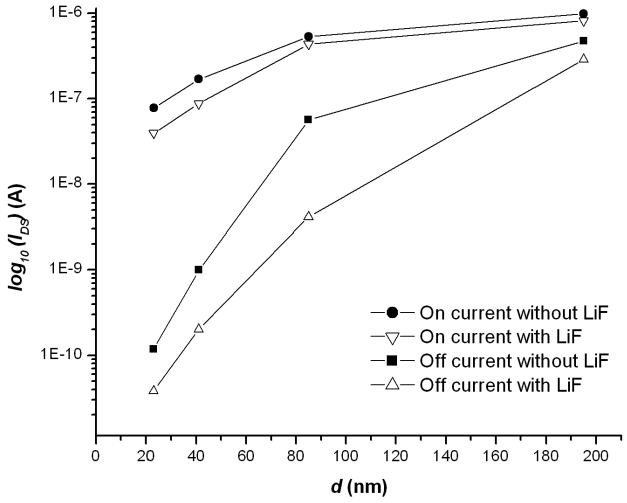

(a) I_{DS} for on and off state versus film thickness d for the devices with and without LiF

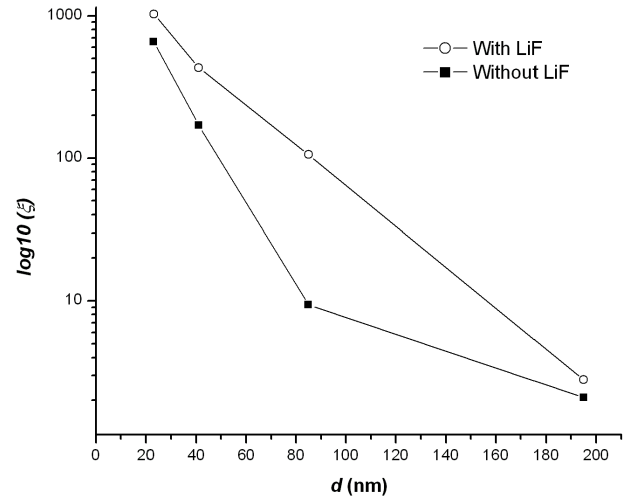

(b) On/off ratio versus film thickness d

Figure 3.12: On-off currents and the on/off ratio for various OFETs against their film thickness

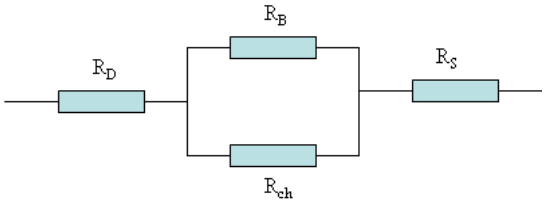

Figure 3.13: Resistive model of an OFET

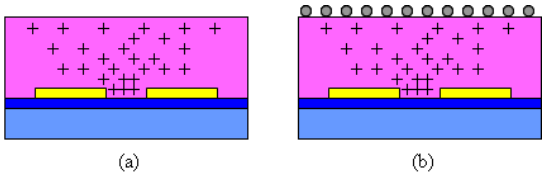

Figure 3.14: Figure showing the detailed mechanism of improvement of OFET characteristics due to LiF coating

noted that using eq. 3.5, the charge carrier mobility μ and the threshold voltage V_{TH} for these OFETs have been determined from the plot of $\sqrt{I_{DS}}$ against V_{GS} for a constant $V_{DS} = -50V$. In the Si based MOSFETs the plot of eq. 3.5 results in a linear plot. However, in the OFETs this is not the case at low gate bias voltages the plot deviates from the usual straight line curve. However, the values of charge carrier mobility μ in the case of OFETs discussed here was determined from the slope of the curve (given by eq. 3.5) in the linear region. Also, from the intercept of the line on to the Voltage axis the value of Threshold voltage V_{TH} was determined. Threshold Voltage V_{TH} represents the onset of the substantial charge accumulation in the semiconductor thin film, and is characterized by the value of gate bias V_{GS} at which I_{DS} starts increasing for a constant V_{DS}. Thus a positive V_{TH} indicates the presence of charge carrier even below $V_{GS} = 0V$. Thus under such a situation the OFET can be switched to normally off state by applying a positive gate bias well above the threshold voltage. On the other hand a negative V_{TH} signifies that the OFET is off at zero gate bias. A plot of threshold voltage V_{TH} against the film thickness d for the OFETs is shown in Fig. 3.15(a). It can be seen that V_{TH} shows a clear cut dependence on the thickness of the P3HT film. Also, the positive values of V_{TH} in conventional OFETs without LiF indicate the presence of large number of charge carriers even at zero gate bias and hence large leakage currents were observed. However, coating LiF the Threshold voltage in general showed a negative shift. Indicating the cut-off of the bulk region of the film. It should also be noted that the characteristics of OFETs shifted from depletion type to enhancement type by LiF coating on the top for the film thicknesses less than $50nm$. Commonly Under the accumulation mode model [43] of OFETs the dependence of threshold voltage V_{TH} on

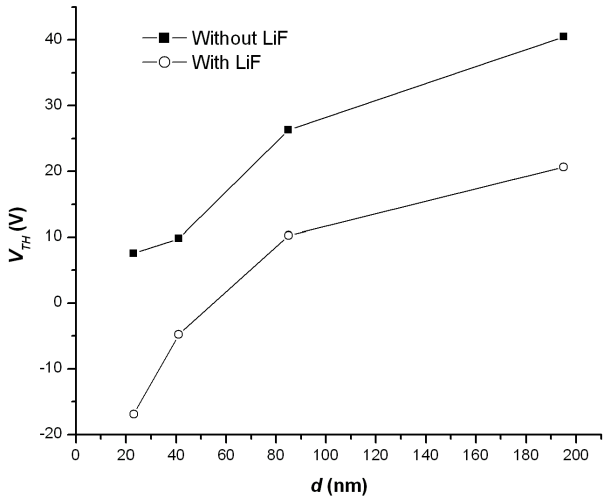

(a) Plot of V_{TH} against the film thickness d for various OFETs

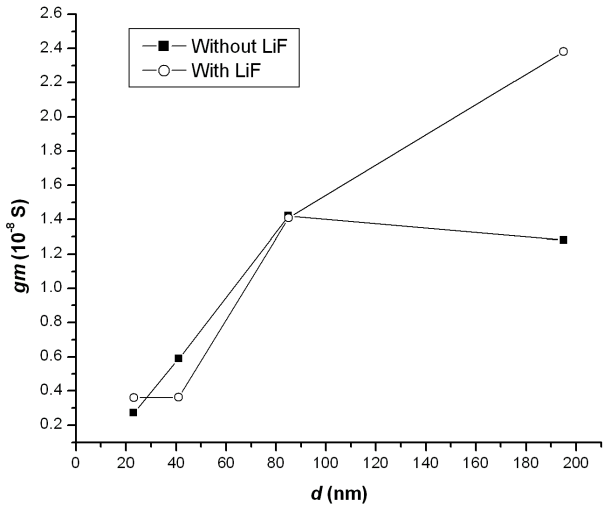

(b) Plot of trans conductance g_m against the film thickness d for various OFETs

Figure 3.15: plot of V_{TH} and g_m against film thickness d of the P3HT film

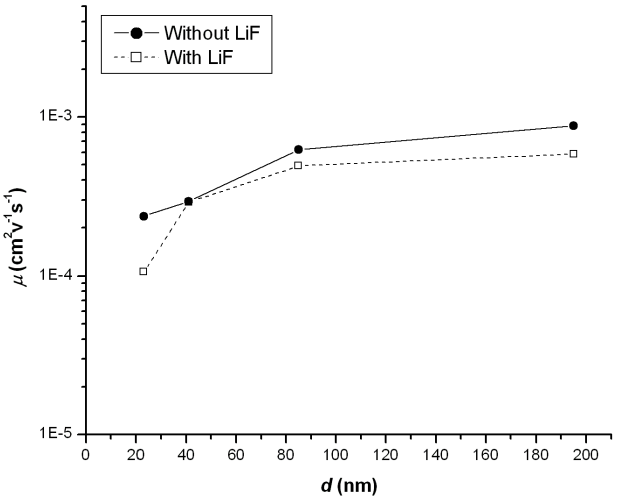

Figure 3.16: plot of μ against film thickness d of the P3HT film for various OFETs

the film thickness is given by the equation

$$V_{TH} = \frac{qN_A d}{C_{ins}} + V_{fb} \tag{3.6}$$

where, q represents the charge on the electron. N_A and d represent the charge carrier density and the thickness of the P3HT film respectively. C_{ins} denotes the capacitance of the insulator layer (in our case it was found to be $10nF/cm^2$). V_{fb} denotes the flat band potential. Eq. 3.6 has been derived under the assumption that bulk conductivity of the film is in direct contact with the channel and thus is applicable to accumulation type OFETs. Although it should be noted here that the model is different from the conventional FET of an inversion type.

The trans-conductance in the OFETs in the saturation region is given by eq. 3.7.

$$g_m = \left(\frac{\partial I_{DS}}{\partial V_{GS}}\right)_{V_{DS}=-50V} \tag{3.7}$$

Therefore from eq. 3.7 the value of g_m is given by the following equation,

$$g_m = \frac{w\mu C_{ins}(V_{GS} - V_{TH})}{L} \tag{3.8}$$

It is clear from the eq. 3.8 that g_m is directly proportional to the threshold voltage V_{TH} and which in turn depends on the thickness of the bulk of the semiconductor d as

given by eq. 3.6. Thus, it explains the almost linear increase of the values of g_m against increasing film thickness d. Although the deviation in very thick film is not completely understood at the moment. Another important point is that for film thicknesses below $100nm$ almost no change in the trans-conductance g_m has been observed after coating LiF on top of OFETs. Implying that the channel resistance doesn't get affected by the cut-off of the conduction through the bulk region. Since coating LiF only increases the bulk resistance R_b of the film, causing the observed cut-off. This effect was further confirmed by plotting the mobility in these OFETs against their film thickness. Almost same order of mobility was obtained in various OFETs despite the change in their film thickness as can be seen from Fig. 3.16.

Bibliography

[1] P. Pneumans, A. Yakimov, and S. R. Forrest: J. Appl. Phys. 93 (2003) 3693.

[2] H. E. Katz and Z. Bao: J. Phys. Chem. B. 104 (2000) 671.

[3] S. Fujimoto, K. Nakayama, and M. Yokoyama: Appl. Phys. Lett. 87 (2005) 133503.

[4] L. Ma and Y. Yang: Appl. Phys. Lett. 85 (2004) 5084.

[5] J. C. Scott: J. Vac. Sci. Technol. A 21 (2003) 521.

[6] W. R. Siliveira and J. A. Marohn: Phys. Rev. Lett. 93 (2003) 116104.

[7] W. Osikowicz, M. P. de Jong, S. Braun, C. Tengstedt, M. Fahlman, and W. R. Salaneck: Appl. Phys. Lett. 88 (2006) 193504.

[8] Y. D. Jin, X. B. Ding, J. Reynaert, V. I. Arkhipov, G. Borghs, P. L. Heremans, and M. Van der Auweraer: Org. Electron. 5 (2004) 271.

[9] T. Yokoyama, H. Ishii, and Y. Ouchi: Surf. Rev. Lett. 9 (2002), 425.

[10] M. A. Baldo and S. R. Forrest: Phys. Rev. B 64 (2001) 085201.

[11] C. J. Brabec, S. E. Shaheen, C. Winder, N. S. Sariciftci, and P. Denk: Appl. Phys. Lett. 80 (2002) 1288.

[12] V. Singh, M. Yano, W. Takashima, and K. Kaneto: Jpn. J. Appl. Phys. 45 (2006) 534.

[13] T. W. Lee, J. Zaumseil, Z. Bao, J. W. P. Hsu, and J. A. Rogers: Proc. Natl. Acad. Sci. U.S.A. 101 (2004) 429.

[14] S. Natarajan and S. H. Kim: Chem. Commun. (2006) 729.

[15] H. Becker, S. E. Burns, and R. H. Friend: Phys. Rev. B 56 (1997) 1893.

[16] A. K. Thakur, A. K. Mukherjee, D. M. G. Preethichandra, W. Takashima, and K. Kaneto: to be published in J. Appl. Phys.

[17] K. Kaneto, S. S. Pandey, and W. Takashima: Jpn. J. Appl. Phys. 40 (2001) 4933.

[18] S. S. Pandey, W. Takashima, K. Rikitake, T. Endo, M. Rikukawa, and K. Kaneto: Jpn. J. Appl. Phys. 40 (2001) 5350.

[19] S. S. Pandey, S. Nagamatsu, W. Takashima, and K. Kaneto: Jpn. J. Appl. Phys. 39 (2000) 6309.

[20] M. Ujimoto, W. Takashima, and K. Kaneto: Thin Solid Films. 499 (2006) 313.

[21] K. Rikitake, D. Tanimura, W. Takashima, and K. Kaneto: Synth. Met. 137 (2003) 1421.

[22] W.Fix, A. Ullmann, J. Ficker, W. Clemens: Appl. Phys. Lett. 81 (9) (2002) 1735.

[23] H sirringhaus, N.Tessler, R.H. Friend: Synth. Met. 102 (1999) 857.

[24] Z. Bao, Ananth Dodabalapur, and Andrew. J. Lovinger: Appl. Phys. Lett. 69 (26) (1996) 4108.

[25] G. Wang, J. Swensen, Daniel Moses and Alan J. Heeger: J. Appl Phy, 93, Number 10, (2003) 6137.

[26] M. Kiguchi, M. Nakayama, K. Fujiwara, K. Ueno, T. Shimada and K. Saiki: Jpn. J. Appl. Phys. 42 (2003) L1408-L1410.

[27] Y. Yuan, D. Grozea, S. Han and Z. H. Lu: Appl. Phy. Lett. 85 (2004) 4959.

[28] Semiconducting Polymers, chemistry, Physics and Engineering. Edited by: G. Hadziioannou and P.F.van Hutten.

[29] V.Singh, A. K. Thakur, S. S. Pandey, W. Takashima and K. Kaneto: Jpn. J. Appl. Phys. 47 No. 2B (2008) 1251.

[30] C. W. Tang and S. A. van Slyke: Appl. Phys. Lett. 51 (1987) 913.

[31] M. Koehler, I. Biaggio and M. G. E. da Luz: Phys. Rev. B. 78 (2008) 153312.

[32] A. Takshi, M. Mohammadi and J. D. Madden: Sol. Stat. Elec. 52 (2008) 1717.

[33] E. Katsia, G. Tallarida, B. K. Kotowska, S. Ferrari, E. Bundgaard, R. Sondergaard and F. C. Krebs: Org. Electron. 9 (2008) 1044.

[34] P. Kumar, S. C. Jain, V. Kumar, A. Misra, S. Chand and M. N. Kamalasanan: Synth. Met. 157 (2007) 905.

[35] I. D. Parker: J. Appl. Phys. 75 (1994) 1656.

[36] P. W. Anderson: Phys. Rev. 109 (1958) 1492.

[37] H. Bassler: Phys. Stat. Sol 120 (1993) 15.

[38] V.Tripathi, D. Datta, G. S. Samal, A. Awasthi and S. Kumar: J. Non. Crys. Sol. 354 (2008) 2901.

[39] P. Peumans, V. Bulovic and S. R. Forrest: Appl. Phys. Lett. 76 (2000) 2650.

[40] M. Vogel, S. Doka, C. Breyer, L. Steiner and K. Fostiropoulos: Appl. Phys. Lett. 89 (2006) 163501.

[41] D. E. Markov and P. W. M. Blom: Phys. Rev. B. 72 (2005) 161401(R).

[42] C. Tanase, E. J. Meijer, P. W. M. Blom and D. M. de Leeuw: Organic Electron. 4 (2003) 33.

[43] *Semiconducting Polymers, Chemistry, Physics and Engineering*, ed. G. Hadziioannou and P. F. van Hutten (Wiley-VCH, Weinheim, 2000).

Chapter 4

Optoelectronic modeling of Al/P3HT interface and its application

Summary

In the first part of this chapter we discuss the effect of coating thick Al ($30nm$) on pristine P3HT film. It was found that coating Al using the thermal evaporation technique leads to conformational disorder on the chains in these films, leading to a relative increase in the PL emission intensity of the peak corresponding to the intrachain excitons. In the second part of this chapter we propose a simple optoelectronic model to study various interface and other related effects. Based on this model the experimentally observed bias dependent Photoluminescence quenching was then used to probe the depletion layer width against applied electrical bias. The results indicate the inherent non uniform charge distribution in the bulk of P3HT film. This model was further extended to study comparatively the depletion layer formed in ITO/P3HT/Al and ITO/P3HT/LiF:Al type Schottky cells. Thus, by using Optoelectronic[1] model the true role of LiF particularly towards the efficiency improvement of the OSCs was established.

[1]Optoelectronics is the study and application of electronic devices that source, detect and control light, usually considered a sub-field of photonics.

4.1 Introduction

In the recent past conjugated polymer based electronic devices viz. polymeric solar cells (PSCs) [1,2], polymeric light emitting diodes (PLEDs) [3,4] and polymeric field effect transistors (PFETs) [5] have gained special interest due to their excellent transport properties as well as their potential application for the development of cheap and flexible electronic devices [6,7]. It has been observed that the interface between various polymeric layers and also between polymer and metal is very crucial for the high performance and development of these devices [8,9]. Treatment of bare SiO2 surface by a silanizing agent like 1,1,1,3,3,3- Hexamethyldisilazane (HMDS) is one such example of the significant role played by the nature of interface in governing the functionality of these devices [10,11].There are various techniques to study the interface of any two given dissimilar materials viz. Ultraviolet photoelectron spectroscopy (UPS), Photoluminescence (PL), X-ray Diffraction (XRD) etc.

PL emission spectrum refers to the spontaneous emission of light from a material under optical excitation and could be used to characterize a variety of material parameters. Features of PL spectra can be used to identify surfaces, interfaces, impurity levels and interface roughness [12, 13]. A simple study to ascertain the nature of interface using PL spectroscopy was done in the last chapter. In this chapter we study the PL emission spectra of thick Al coated P3HT films. It was observed that Al deposition using thermal evaporation technique led to the conformational disorder on the polymer chains in these films. It was also found that this conformational change further led to increased PL emission due to the intrachain excitons causing a relative increase of the high energy peak of the PL spectrum.

On one hand, the transient PL intensity yields the lifetime of non-equilibrium interface and bulk states, while on the other hand PL intensity variation under an applied field gives an estimate of the built in field near the interface as discussed in detail in the introduction chapter. In addition, thermally activated processes can also cause changes in PL intensity. A bias dependent PL can be used to study the different competing mechanisms of exciton generation, diffusion and dissociation [14, 15]. Thus, a bias de-

pendent PL spectrum is of critical importance as it gives information regarding the electro-luminescence (EL), photoconduction and photovoltaic effects. EL efficiency is a determining factor for the performance of PLEDs and is directly related to PL efficiency [16], as both originate from the same intermediate species, i.e. excitons [17,47-50]. In this chapter we present an optoelectronic model that relates the PL quenching to the depletion layer width. Using this model the bias dependence of depletion layer thickness was determined by experimentally observed bias dependent PL quenching and hence a new approach to study the depletion layer thickness was proposed and demonstrated. Although, in the previous chapter using the optical and electrical characterization it was established that LiF does not form a depletion layer with P3HT. However, the other underlying mechanisms for the PSCs efficiency improvement by LiF inclusion has not yet been discussed in much detail[18-22]. In this chapter we present a new approach to ascertain the role of LiF in PSCs.

4.2 Experimental Procedures

Six different types of samples namely A, B, C, D, E and F, have been fabricated as shown in Fig. 4.1 (a, b, c, d, e and f) for the purpose of PL measurements. Prior to sample fabrication, glass substrates (for samples A, B, C and D) and ITO coated glass substrates (for samples E and F) were cleaned using NH_3 and H_2O_2 followed by sonication in chloroform and iso propanol solution. Samples A and B were spin coated at 1500 (30s), 3000 (10s) rpm with a thin film of regioregular (rr) P3HT (Merck Lisicon SP001, having a average Molecular weight of 44000, and 96% regioregularity) from its chloroform solution on to the cleaned glass substrate, followed by annealing at 100℃(under vacuum for 2 hours). Samples A were divided into two lots. First lot was coated with $2.5nm$ Al (under vacuum, $P = 2.0X10^{-6}$. The second lot was coated with $1nm$ LiF prior to coating $2.5nm$ Al under identical conditions. Similarly Sample B was divided into two lots, first lot was coated with $30nm$ Al while the second lot was coated with $1nm$ LiF followed by $30nm$ Al. Sample C was divided into three lots, while first lot was spin coated with regioregular (rr) P3HT (as obtained from Merck) at $1500(30s), 3000(10s)rpm$, the sec-

ond lot was spin coated with non-regio controlled (nrc) P3HT (synthesized, using $FeCl_3$ method[31,38], having a regioregularity of 88%) at $1500(30s), 3000(10s)rpm$ [38,39] and the third lot was spin coated at $1500(30s), 3000(10s)rpm$ with regiorandom (rrnd) P3HT (used as obtained from Aldrich, having 1 : 1 HT:HH coupling). While sample C was half coated $30nm$ thick Al on to the top of the film, However, sample D was coated with $30nm$ thick Al prior to spin coating at $1500(30s), 3000(10s)rpm$ the rr P3HT film, as is also clear from Fig. 4.1 (c and d). On one hand all the lots of Sample C were used to study the effect of intrachain disorder on the absorption and emission spectra. The first lot of Sample C coated with rr P3HT was also used to compare with Sample D for the effect of coating Al on top and bottom of the film as will be discussed in detail in the next section. Figure 4.1(e and f) show the schematic diagram of the sample fabricated for the bias dependent PL spectra of the schottky cell. It should be noted that the Cells E and F were fabricated in ITO/P3HT/Al and ITO/P3HT/LiF:Al type device configurations, as is also shown in Fig. 4.1(e and f) respectively. Both LiF and Al were deposited by thermal evaporation. For the fabrication of ITO based sandwich cells, ITO coated glass substrates were patterned by etching in dilute HCl solution with Zinc powder to fabricate the ITO bottom electrodes as described in Chapter 2, which were subsequently spin coated at $1500(30s), 3000(10s)rpm$ with chloroform solution of rr P3HT. The Thickness of these films was later determined to be $200nm$. All the film Thicknesses were measured using Dektak Surface Profiler. Thicknesses of sample A and B were determined to be 79 and $55nm$ respectively, while both samples C and D were of identical thickness of $60nm$.

PL measurement was done under ambient conditions using photonic multi channel analyzer, (Hamamatsu PMA-11), kept at a distance of $70cm$ from the sample. A He-Cd Laser ($300mW$, CW, $442nm$, Kimmon IK4121R) was used as a light-pumping source. The intensity of photons incident on the sample was later calculated to be $0.15W/cm^2$ incident at an inclination of about 30^o to the normal. In-situ electrical bias was applied on the cells using Keithley 6517 A electrometer as is shown in Fig. 4.2. ITO was biased as a cathode under the reverse bias direction, as is shown in Fig. 4.3(a). Care was also taken to avoid over exposure of the sample to the laser beam. It should also be noted

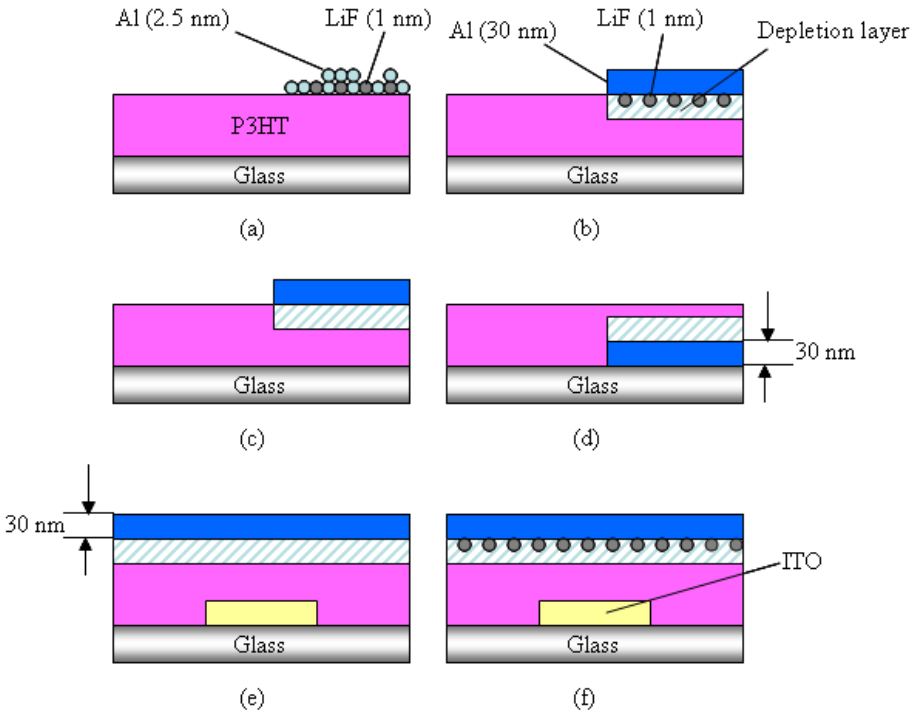

Figure 4.1: Shows the Schematic diagram of (a) (Sample A) Island deposition of LiF ($1nm$) followed by Al ($2.5nm$) on a P3HT coated glass substrate (b) (Sample B) Island deposition of LiF ($1nm$) followed by Al ($30nm$) on a P3HT coated glass substrate (c) (Sample C) Half coated with Al ($30nm$) on the top (the hashed portion shows the depletion layer formed at the Al/P3HT interface) (d) (Sample D) Half coated with Bottom Al ($30nm$) electrode (e) (Sample E) a diode cell having ITO/P3HT/Al configuration (f) (Sample F) a diode cell having ITO/P3HT/LiF:Al configuration.

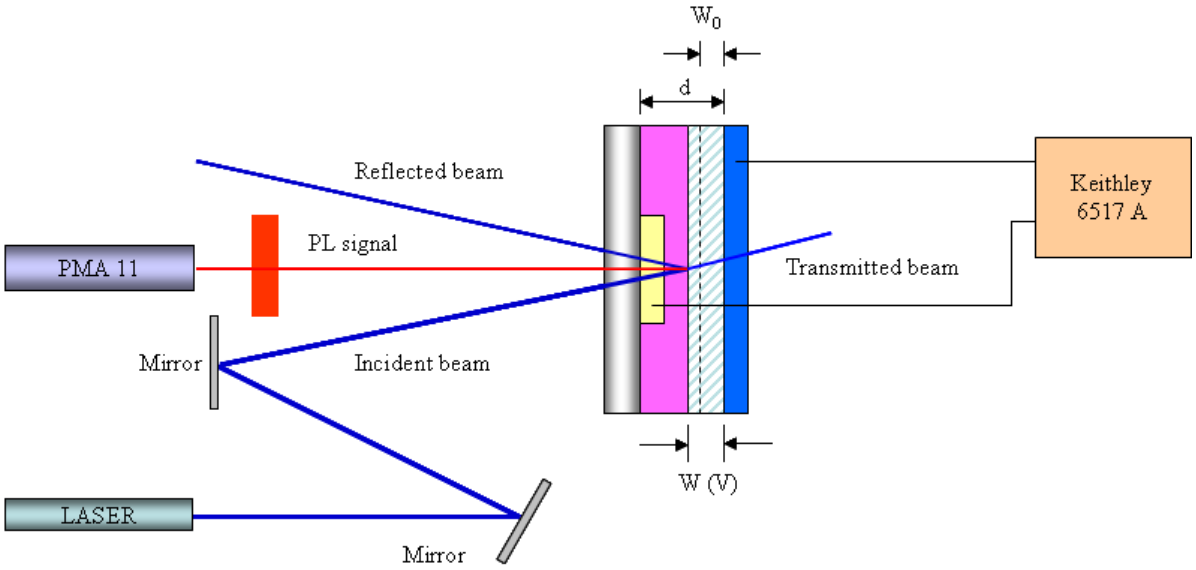

Figure 4.2: Shows the experimental set-up for measurement of bias dependent Photoluminescence spectra

that all the samples except sample D were illuminated from the glass side. However, Sample D was illuminated from the film side. The details of which will be discussed in the next section.

4.3 Effect of Al coating on P3HT

It was observed that coating Al($2nm$) [24] leads to PL quenching due to dissociation of excitons near the Al/P3HT interface due to high built in field of the depletion layer. However, Fig. 4.4. shows that increasing the thickness of Al to ($30nm$) led to an increased PL intensity. Apart from the increased PL intensity, a relative increase in the high energy peak was also observed[47]. Another significant point is the blue shift shown by the peak PL emission ($E = 1.702eV$) spectra due to Al coating on the top of P3HT film. In order to fully ascertain the exact origin of this behavior another experiment was performed in which both top and bottom Al coated samples, namely samples C and D were fabricated. While sample C was illuminated by laser light from the glass facing side contrary to the sample D which was illuminated from the film facing side. This was done primarily because the bottom Al layer (sample D) would screen the intensity of the laser excitation light and would also largely block the PL emissions from the underlying

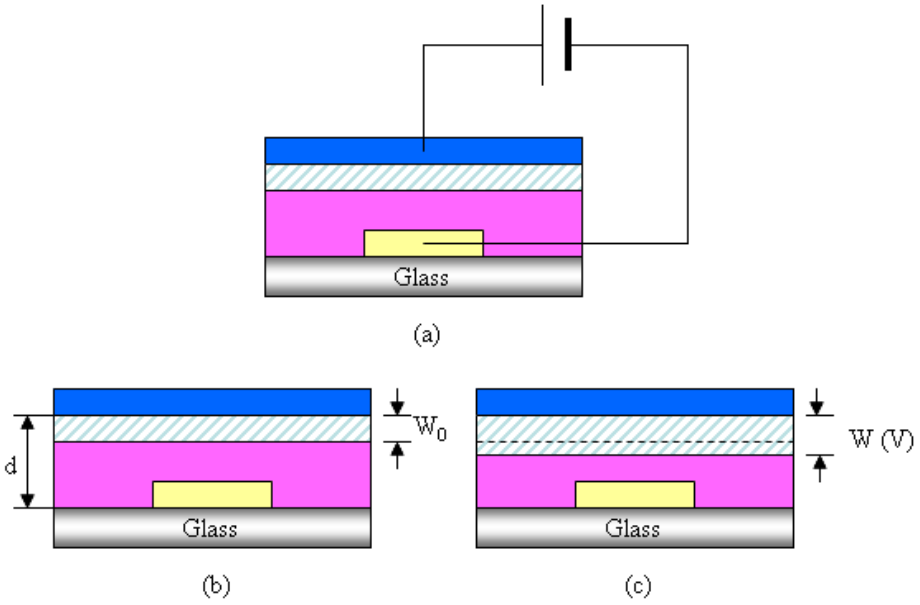

Figure 4.3: Shows the (a) typical biasing arrangement for cells E and F (b) depletion layer thickness at zero bias ($V = 0V$) (c) depletion layer thickness at negative bias ($V < 0V$)

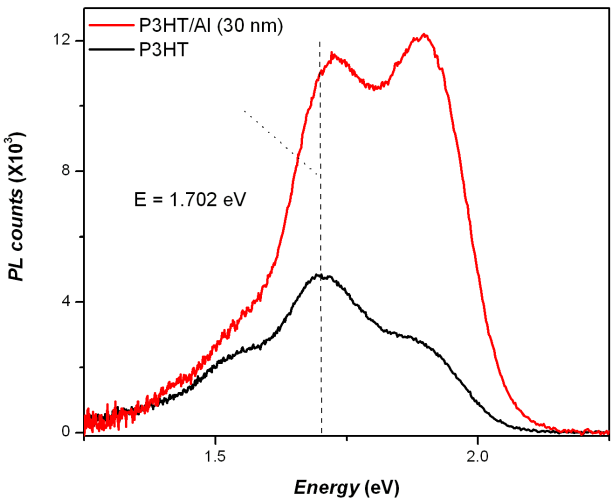

Figure 4.4: Shows the effect of coating ($30nm$) thick Al on a pristine P3HT film

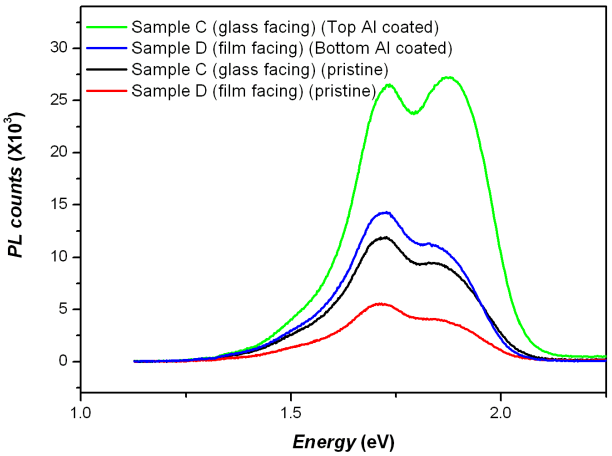

Figure 4.5: Effect of top and bottom coating of Al (30 nm) on the PL spectra of P3HT films taken from glass side (glass facing) or from film side (film facing).

P3HT bulk layer, if illuminated from the glass side. It is a general observation that intensity of PL signal is also correlated with the degree of roughness near the interface[51,52]. As can be clearly seen from Fig. 4.5, the PL counts for pristine P3HT film was higher in the case of sample C compared to that of sample D. It should be noted that both sample C and D showed an increase in the PL intensity, a clear cut evidence of dual excitation of the bulk in the two cases. However, unlike sample C, sample D did not show any increase in the high energy shoulder peak, clearly indicating that such an effect is taking place due to the thermal deposition of Al over the pristine P3HT films. The results were similar to the one observed by Thakur et al. [37], although, in their case they studied the effect of coating gold (Au) on Pristine P3HT film. They also pointed out to the difference in the level of PL quenching due to top and bottom deposition of Au electrode. Also it should be noted that the extent of PL quenching were much higher in their case, which may be due to the sputtering of metal rather than thermal evaporation. It is known that sputtering leads to very rough coating of metal. Even the Energy carried by metal atoms during sputtering is much higher compared to thermal evaporation procedure. In another similar report Brown et al. [30] also observed that the high energy peak in the PL emission occurs due to the intrachain excitons [33,34] and that the intrachain excitons are highly affected by the intrachain disorder contrary

to the interchain excitons. Thus, it can be concluded that coating Al on to the top of a film results in an increase in the intrachain disorder due to the thermal energy transfer from the hot Al atoms coated on P3HT film during the thermal evaporation process. It is known that the spin coated P3HT films are composed of microcrystalline domains embedded in an amorphous matrix. Inside these domains the polymers -stack in one direction and form lamella of interlocking chains in the other direction. Usually the side alkyl chains try to orient themselves in a least strained position (energetically). Although this type of rearrangement is less pronounced in spin coated P3HT films as compared to dip coated or casted P3HT films [35-36]. However, as a result of this energy transfer between Al and immediate P3HT, polymer chains tend to have a more strained structure of the hexyl group attached to the polymer backbone, resulting in an increase in the intrachain disorder. Also, since some of these chains may be part of a micro crystalline domain, thus an intrachain disorder may result in a decrease of degree of -stacking of these microcrystalline domains and hence of the films at the macro level, resulting in the blue shift of the PL emission peak occurring at 1.702 eV, as shown in Fig. 4.4. In order to have detailed insight about the intrachain disorder effects on PL, we further fabricated four types of films, first was spin coated with rr-P3HT, the second one was spin coated with non-regio controlled (nrc) P3HT, the third was spin coated with rrnd P3HT (as obtained from Aldrich) and the fourth one was spin coated with MDMO-PPV. Figure 4.6 shows the normalized absorption and emission spectra of rr P3HT film. The normalized absorption and emission spectra of MDMO-PPV is also shown in Fig. 4.7. It should be noted that intensity of high energy emission peak appears to have increased in MDMO-PPV as compared to rr P3HT film. This is mainly due to the fact that while rr P3HT is symmetric in terms of Alkyl substitution. However, MDMO-PPV has asymmetric alkoxy substituent attached to the main chain. This asymmetric substitution is needed to make MDMO-PPV soluble in various organic solvents. However, it is this asymmetry of the attached side groups that leads to increased amorphous nature of MDMO-PPV films compared to rr P3HT films. As can also be seen by comparing the absorption spectra of P3HT with that of MDMO-PPV, a clear appearance of shoulder peaks in the absorption spectra of P3HT suggests a good degree of stacking of chains

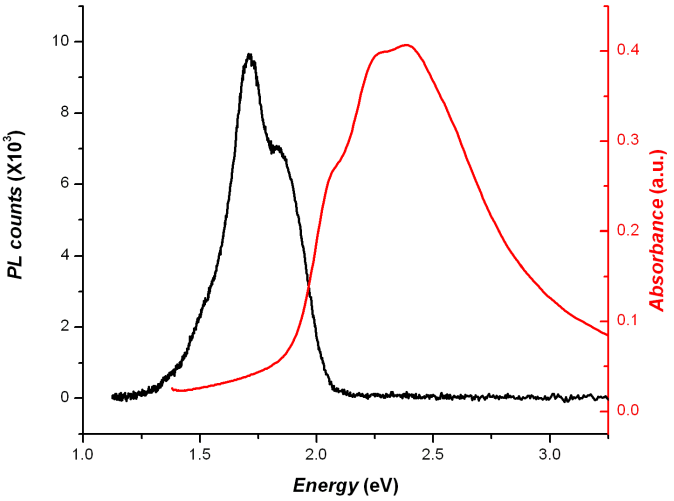

Figure 4.6: Normalized absorption and emission spectra of rr P3HT film

in these films. On the contrary the absorption spectra of MDMO-PPV shows only one peak, lack of shoulder peaks indicate poorly stacked structures of these films. Moreover, the absorption band edge of MDMO-PPV is blue shifted with respect to P3HT. These results of the absorption and emission spectra explain the observed lower mobilities in MDMO-PPV compared to rr P3HT[53]. The two conjugated polymers rr P3HT and MDMO-PPV differ in their structures as well as nature of their substituent groups. While in the case of P3HT an alkyl group is present as a substituent, however, in the case of MDMO-PPV alkoxy groups are present as a substituent on the main polymer chain. Thus, a more detailed investigation between the structure and optical properties is required to clearly understand the difference in the optical properties of these materials. In order to further confirm the role of structure in the optical (in particular the emission) properties of the conducting polymers the absorption and emission spectra of various grades of P3HT have been studied by changing the regio-regularity of P3HT. Figure 4.8 shows the absorption and emission spectra of rr P3HT, nrc P3HT and rrnd P3HT respectively. It is clearly evident from Fig. 4.8. that the transition band of the films was blue shifted [31] in the increasing order of their regio randomness, suggesting that higher degree of regioregularity leads to decrease in the band gap. This effect is

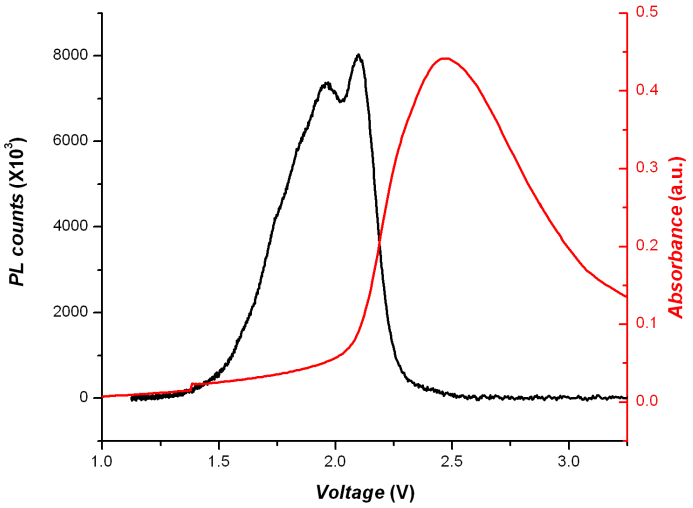

Figure 4.7: Normalized absorption and emission spectra of MDMO-PPV film

attributed to the lesser degree of effective π-conjugation [50] on the parent chain in rrnd P3HT. Even the band edge appears to be blue shifted in the increasing order of regio randomness of these P3HT films. Another striking feature is that the absorption of rr P3HT has three distinct peaks occurring at (E = 2.06, 2.26 and 2.38 eV) respectively. Pandey et al [31] have demonstrated that the lowest energy peak in the absorption spectra (at 2.06 eV) corresponds to 0-0 transition and is related to the conformational order in the chains, while the peak at 2.26 eV corresponds to 0-1 transition and is related to the interchain ordering or the stacking of the various chains. While the main peak near 2.38 eV corresponds to the 0-2 transition. Compared to the rr-P3HT these peaks were less pronounced in nrc P3HT and nearly vanished in rrnd P3HT film. In particular a clear blue shift in the absorption spectra was obtained for rrnd P3HT. However, only a little blue shift was obtained in nrc P3HT. This is probably due to high degree of regio regularity in these samples despite of being synthesized by $FeCl_3$ method [31,38]. Further if we look at the PL emission spectra of these films, we find that there is almost no shift in the emission spectra of rr-P3HT and nrc P3HT, on the contrary, a large blue shift is obtained in the emission spectra of rrnd P3HT as compared to that of rr- P3HT. It must also be noted that the 0-0, 0-1 and 0-2 transitions for the emission spectra of

rr-P3HT and nrc P3HT occur at E = 1.89, 1.7 and 1.5 eV, respectively. However, the corresponding 0-0, 0-1 and 0-2 transitions for rrnd P3HT occur at E = 2.07, 1.98 and 1.74 eV respectively. As can also be seen from Fig. 4.8 that the intensity of shoulder peaks at 1.5 eV and 1.89 eV increase in the case of nrc P3HT compared to the rr-P3HT. Brown et al. [30] have emphasized that the high energy peak at E = 1.89 eV is highly affected by the intrachain disorder, i.e. the degree of conformational order of the polymer chain. It is commonly believed that highly regioregular structure leads to high degree of effective π-conjugation in these structures. Contrary to this with the increase in regio-randomness, the structure of polymer chain becomes more strained due to high amount of steric hindrance within various substituent groups. Leading to a significant decrease in the effective π-conjugation. Thus, a relative increase of the high energy peak as can be seen from the normalized PL spectra of the two films from Fig. 4.8. confirms the lower degree of regio regularity on polymer chains present in nrc P3HT film. However, Brown et al [30] also pointed out that the peak in the emission spectra corresponding to interchain excitons (at E = 1.702 eV) doesn't get affected by the local order that is the regioregularity, as clearly corroborated by the Fig. 4.8. In the case of emission spectra of rrnd P3HT the highest energy peak at E = 2.07 eV corresponding to 0-0 transition has relatively higher intensity as compared to the 0-1 transition at E = 1.98 eV. This is because the intrachain disorder is highest in rrnd P3HT and hence the 0-0 transition in rrnd P3HT has a higher intensity as compared to 0-1 transition. Kaneto et al [32] presented the PL spectra of an electrochemically synthesized polymer, which showed very low contributions from the interchain emissive state. At the same time it must be noted that the emission at E = 1.5 eV is also relatively increased in the case of nrc P3HT. This peak relates to the conformational order and as we know that the conformational order decreases in the nrc P3HT film resulting in relatively higher values of observed PL intensity (at E = 1.5 eV). In another interesting work Tanaka et al. [34] have demonstrated a clear cut change in the characteristic PL emission spectra by the fine control of the blending ratios of rr and rrnd P3HT.

Although these discussions help us understand the metal polymer interface qualitatively. A more detailed discussions regarding the nature of interface quantitatively is required

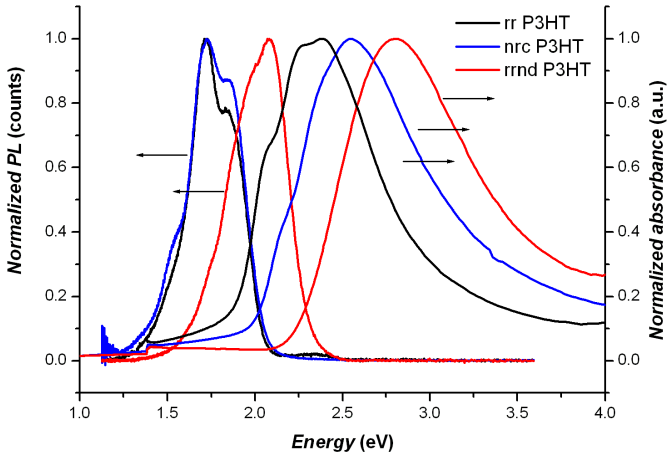

Figure 4.8: Normalized absorption and emission spectra of rr P3HT, nrc P3HT and rrnd P3HT films

to understand the various competing mechanisms at the metal polymer interface. In the next section we try to model the Al/P3HT interface using bias dependent Photoluminescence spectroscopy.

4.4 Optoelectronic modeling of Al/P3HT interface

The depletion layer formed at the interface of Al/P3HT junction, also behaves as a Schottky junction[43-46] has been utilized to give various functionalities viz. polymeric solar cells (PSCs)[1,2], polymeric light emitting diodes (PLEDs)[3,4] and the polymer based photo induced memory devices (PIMDs)[46]. In the light of these applications the dependence of depletion layer width on the applied bias voltages assumes critical significance. In uniformly doped crystalline semiconductors the bias dependence of depletion width is given by eq. 4.1. However, this is strictly not true for conjugated polymer based semiconductors, owing to the non uniform charge carrier density in these materials. Thus a bias dependence study of depletion width would be helpful in the development of more accurate model for various Schottky junction based organic devices.

$$w_V = \sqrt{\frac{2\epsilon_s(V_{bi} - V)}{qN_A}} \tag{4.1}$$

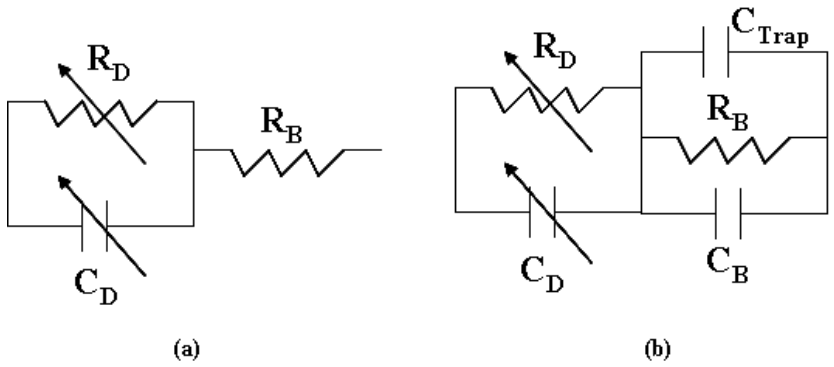

Figure 4.9: (a) Equivalent circuit model for conventional Inorganic semiconductor based Schottky diode, (b) Equivalent circuit model for Organic semiconductor based Schottky diode

At present the bias dependence of depletion layer width is experimentally studied using the standard Capacitance-Voltage (CV) measurement technique, and a Mott-Schottky plot of $1/C^2$ versus V is obtained, as is given by eq. 4.2. However, the Mott-Schottky relationship itself has been derived assuming uniform charge carrier density.

$$\frac{1}{C^2} = \frac{2(V_{bi} - V)}{A^2 q \epsilon_0 \epsilon_r N_A} \tag{4.2}$$

It should be noted here that in general the net charge carrier density in an organic semiconductor is a sum total of density of dopants and the trap density, as is given by the eq. 4.3.

$$N_{net} = N_{dopants} + N_{traps} \tag{4.3}$$

Thus, in general our determination of depletion layer profile against applied bias using CV technique is limited by the parasitic capacitances due to trapped charge carriers as well as due to space charges, that are characteristics of organic materials. The conventional equivalent circuit model particularly applicable to Si based semiconductors is as shown in Fig. 4.9(a) while a modified model with respect to organic materials is given in Fig. 4.9(b). It is these parasitic capacitances that lead to the deviation from the usual straight line Mott-Schottky plot particularly in the low bias regime in the organic materials.

In the optoelectronic model discussed here we derive a relationship between the PL quenching Q_{pl} and the depletion layer width $w(V)$, under suitable assumptions.It is

known that the depletion layer width increases with increasing reverse bias voltage[26-28,40,42,47]. An increase in depletion width results in a decrease in the bulk active region leading to PL quenching, with increasing reverse bias. Under these assumptions a relationship between the depletion layer width $\triangle w(V)$ and the PL quenching Q_{pl} has been derived. The bias dependence of depletion layer width is finally derived by using the experimentally observed bias dependent PL quenching Q_{pl}. The main advantage of this measurement is that unlike CV measurement this technique is not limited by the trapped charge carriers. Thus, it may provide us with a more accurate voltage profile of depletion layer. Further, the depletion width at zero bias was estimated by varying the Film thickness of the P3HT film. It should be noted that there are reports on PL quenching due to charge carriers [39-41], however such an effect is negligible in our case, as here we were mainly concerned with reverse bias regime. The depletion width at zero bias was found to be 17nm [26].

The bias dependent PL Quenching Q_{pl} [25,26,39,47] , defined as

$$Q_{pl} = \frac{< I_{pl}(0) > - < I_{pl}(v) >}{< I_{pl}(0) >} \tag{4.4}$$

Where $< I_{pl}(0) >$ and $< I_{pl}(v) >$ denotes the spectrally averaged PL emission intensity at zero bias and at applied bias voltage v, respectively. The spectral average of PL intensity at any given voltage v is determined using eq. 4.5.

$$< I_{pl} >= \frac{\sum I_{pl}(\lambda_i)\lambda_i}{\sum \lambda_i} \tag{4.5}$$

Figure 4.10 shows the plot of PL quenching against applied electrical bias V. Increase in PL quenching (Q_{pl}) was observed with increasing reverse bias voltage. These observed values of Q_{pl} were then used to calculate the change in depletion width using Eq. 4.15 (derived later), and plotted against the voltage as in Fig. 4.10. The plot of depletion width calculated theoretically using the eq. 4.1 is also shown in Fig. 4.10. The parameters V_{bi} and N_A of eq. 4.1 were determined from the Mott-Schottky plot of the cell. It must be noted that experimentally determined depletion width deviates from theoretically calculated values using eq. 4.1, which is derived assuming constant charge carrier density. However, the presence of localized charge carriers and traps near

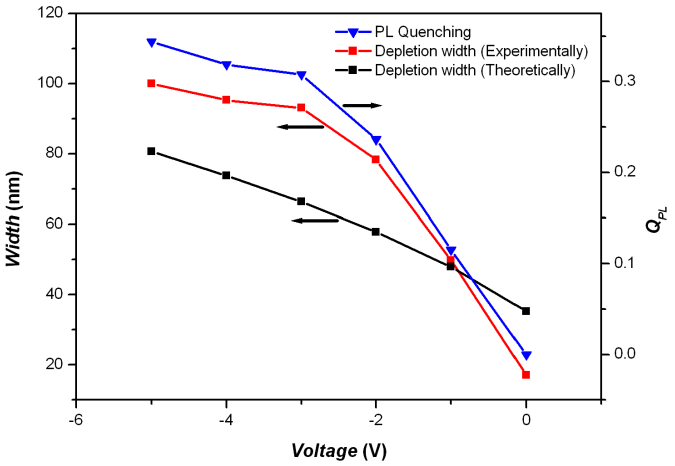

Figure 4.10: Plot of depletion width (left axis) and PL quenching Q_{pl} (right axis) against the applied bias

the Al/P3HT interface lead to non-uniform distribution of charge carriers which in turn results in the observed deviation. Similar observations were made by Takshi et al [29]. However, their method of measuring the depletion layer was based on electrical measurement. It is important to note that the voltage dependence of the depletion width calculated here is purely based on optical measurement. Also it must be noted that the difference in the built in voltage for the theoretical and the experimental curves was not substantial, although the depletion width at zero bias for experimental curve is significantly less than the depletion width at zero bias for theoretical curve. The spectrally averaged intensity of PL emission $< I_{pl}(\lambda) >$ in general is given by eq. 4.6.

$$< I_{pl}(\lambda) >= I_{abs}\eta_{pl}\eta_{d} \tag{4.6}$$

Where I_{abs}, η_{pl} and η_{d} denotes the intensity of absorbed laser light,the radiative PL efficiency and the photon capturing efficiency of the detector respectively. The PL efficiency η_{pl} in general given by eq. 4.7 [25-26].

$$\eta_{pl} = b\frac{K_r}{(K_r + K_{nr} + K_q)} \tag{4.7}$$

Where K_r, K_{nr} and K_q denote the rates of radiative, non radiative and electric field induced quenching, decay constants respectively. While, b denotes the fraction of incident photons converted into excitons in the bulk of P3HT. Usually the probability of

exciton quenching under the influence of electric field has been described by Onsager model [54-55],as was also described in Chapter 1 . However, one very important point to be noted here is that the Electric field discussed in the Onsager model imply the Field applied to the bulk of semiconductor. But, In the case of a typical Schottky diode under the reverse bias almost the entire externally applied voltage drops around the depletion layer owing to the large depletion resistance compared to the bulk resistance of P3HT film. Thus, we assume that although excitons will be generated in the bulk of the P3HT film, only those excitons which can diffuse to the depletion layer region might undergo field assisted dissociation having a probability given by the Onsager model [54-55]. It is to be noted that in general with the increasing reverse bias the PL quenching can be observed mainly because of two competing mechanisms. First mechanism is that the field in the depletion layer is increasing (as is shown by the simulated electric field in Appendix A), resulting in increased probability of exciton dissociation assisted by field itself. The second mechanism is due to the increase in the depletion layer thickness leading to decrease in the effective bulk region and thus results in observed PL quenching. It has been found that over the applied bias regime the electric field in the depletion region does not change by significant amount. Thus, it can be safely assumed that the number of excitons undergoing field assisted dissociation does not change appreciably with the increasing reverse bias application. Therefore in the present case that $K_q << (K_r + K_{nr})$. Under these conditions the PL intensity is then directly proportional to the absorbed light intensity I_{abs}.

In general the light absorbed by a P3HT film spin coated on to a glass substrate is given by the difference between the intensity of light incident on the cell to the intensity of light transmitted from the cell as given by the following equation

$$I_{abs} = I_0(1 - e^{-\alpha d}) \tag{4.8}$$

where I_0 is the incident laser intensity, α denotes the absorption coefficient of P3HT film at ($\lambda = 442nm$), and d denotes the thickness of the P3HT film. However, when these films were coated with $30nm$ thick Al it was found that double excitation of the films occurred due to strongly reflected laser light from the top Al layer. Assuming Al

top layers are having a reflection coefficient R. The intensity of absorbed light by the P3HT bulk is then given by the difference of the incident light intensity and the sum total of the transmitted and the reflected light intensity from the cell as is clear from Fig. 4.3 (b and c). The absorbed light intensity I_{abs} is given by eq. 4.9,

$$I_{abs} = I_0\chi(1-(1-R)e^{-\alpha x} - Re^{-2\alpha x}) \tag{4.9}$$

Where R denotes the reflection coefficient of Al top layer, χ is the scaling factor, which arises probably due to the interaction of laser light with the depletion layer, although the exact nature of such an interaction needs further investigation. It has been observed that ($\chi = 1.5$) [see Appendix B] yields a good agreement between the observed and simulated results for Al coated films, as shown later in Fig. 4.11. Since the origin of χ is due to the interaction of laser light with depletion layer, therefore for pristine films by definition ($\chi = 1$), due to the absence of depletion layer in these films and α is the absorption coefficient of the P3HT film at ($\lambda = 442nm$), while x denotes the thickness of the available bulk region of P3HT as measured from ITO electrode in the direction of the thickness of the film as shown in Fig. 4.3(c). Upon combining eq. 4.6 and eq. 4.9 we get eq. 4.10,

$$< I_{pl}(\lambda) >= I_0\chi\eta_{pl}\eta_d(1-(1-R)e^{-\alpha x} - Re^{-2\alpha x}) \tag{4.10}$$

From eq. 4.9 it is clear that the change in the value of I_{abs} is due to the changing values of x. At zero bias x is given by $x = (d - w_0)$, while at any applied bias V is given by $x = (d - w(V))$, (Where d is the thickness of the P3HT film) and w_0 and $w(V)$ represent the depletion width at zero bias and at any negative bias V respectively. Thus, $w(V) = w_0 + \triangle w(V)$, where $\triangle w(V)$ denotes the bias dependent change in the depletion layer width. From eq. 4.4 and eq. 4.10 we can rewrite the PL quenching Q_{pl} is given by,

$$Q_{pl} = \frac{I_0(1-(1-R)e^{-\alpha(d-w_0)} - Re^{-2\alpha(d-w_0)}) - I_0(1-(1-R)e^{-\alpha(d-w(V))} - Re^{-2\alpha(d-w(V))})}{I_0(1-(1-R)e^{-\alpha(d-w_0)} - Re^{-2\alpha(d-w_0)})} \tag{4.11}$$

which can further be simplified and then rewritten as given by eq. 4.12,

$$Q_{pl} = \frac{(1-R)e^{-\alpha(d-w_{(0)})}(e^{\alpha\triangle w(V)} - 1) + Re^{-2\alpha(d-w_0)}(e^{2\alpha\triangle w(V)} - 1)}{(1-(1-R)e^{-\alpha(d-w_0)} - Re^{-2\alpha(d-w_0)})} \tag{4.12}$$

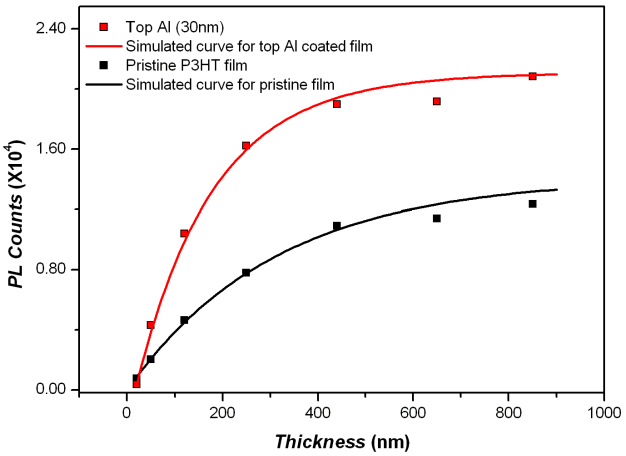

Figure 4.11: Thickness dependence of PL counts for pristine and Al coated films

upon simplifying further we get eq. 4.13

$$Q_{pl} = A(e^{\alpha \triangle w(V)} - 1) + B(e^{2\alpha \triangle w(V)} - 1) \tag{4.13}$$

Where A and B are constants given by the following relation.

$$A = \frac{(1-R)e^{-\alpha(d-w_0)}}{(1-(1-R)e^{-\alpha(d-w_0)} - Re^{-2\alpha(d-w_0)})}; B = \frac{Re^{-2\alpha(d-w_0)}}{(1-(1-R)e^{-\alpha(d-w_0)} - Re^{-2\alpha(d-w_0)})} \tag{4.14}$$

Assuming $e^{\alpha \triangle w(V)}$ to be y eq. 4.13 can be simplified as,

$$By^2 + Ay - (A + B + Q_{pl}) = 0 \tag{4.15}$$

solving for y and back substituting it we get

$$\triangle w(V) = \frac{1}{\alpha} \ln \left| \frac{\sqrt{(A+2B)^2 + 4BQ_{pl}} - A}{2B} \right| \tag{4.16}$$

The values of A and B were 0.07, 0.46 respectively and α was determined experimentally using UV-VIS spectra to be $32000 cm^{-1}$. It must be noted that eq. 4.16 describes the voltage dependent change in the depletion width. However, in order to determine the value of depletion width at zero bias the film thickness was varied from $20nm - 850nm$. The observed results are as shown in Fig. 4.11. The PL counts in the pristine films were found to be proportional to the intensity of light absorbed by the sample, which could

be obtained as given by the eq. 4.10. However, the PL counts of Al coated identical samples were found to increase rather than decreasing as observed before in Chapter 3. This observed effect was due to the strong reflection occurring from the top Al coating. Although the reflection by Al coating depends on the thickness of Al and the smoothness of P3HT film formed. Thus very thin Al coating on to the top resulted in PL quenching [24], however as thickness of Al increases its reflection coefficient is found to increase, resulting in double excitation of P3HT films by the incident laser beam. The value of the reflection coefficient R was found to be 0.92, for a $30nm$ thick Al top layer. It is also to be noted that the PL counts of $20nm$ thick P3HT film coated with Al were less than the PL counts of the pristine film as was shown in the previous chapter. This is mainly because for such a small film thickness most of the bulk is captured by the depletion layer width which does not contribute to PL emission, resulting in the observed PL quenching. The simulated curves for the thickness dependent PL, as shown in Fig. 4.11 was done using eq. 4.10. The simulated curves were found to be in good agreement with the experimental results. From these simulated curves the value of depletion width at zero bias was estimated to be about 17nm. Adding this value to the values obtained from eq. 4.16 at different bias voltages leads to the overall bias dependent depletion width variation as shown in Fig. 4.10. It can also be seen from Fig. 4.10 that the voltage profile of depletion layer using our optoelectronic model shows a clear deviation from the usual expression as given by eq. 4.1. This simply indicates the non uniform distribution of carriers in the bulk of P3HT film. Also, it must be noted that the slope of the in the low reverse bias region is higher than in the high reverse bias region. Indicating that the presence of non uniform charge distribution in P3HT, as it can be interpreted that charge carrier density is less near the Al/P3HT interface and increases gradually as we move away from the interface.

4.5 Application of Optoelectronic model

The qualitative nature of interface between LiF/P3HT has been discussed in Chapter 3. However, the discussions in chapter 3 were insufficient to clearly understand the role

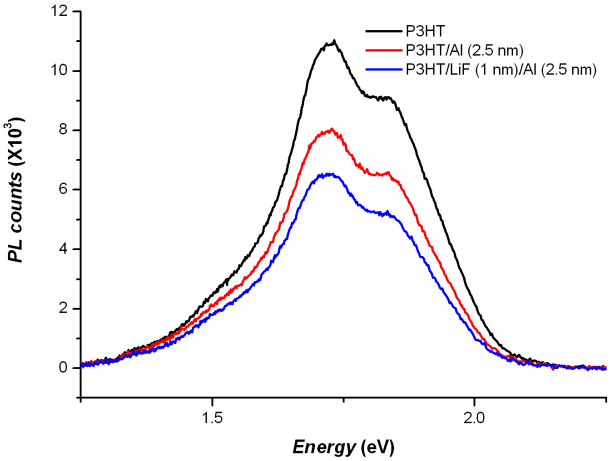

Figure 4.12: PL Quenching effect due to island deposition of Al and LiF:Al on pristine P3HT film

of LiF in a bi layered cathode structure. To further clarify the role of LiF we fabricated cells A and B as shown in Fig. 4.1 (a & b). Figure 4.12 shows the effect of coating thin layer 2.5nm of Al and 1nm LiF followed by 2.5nm Al. It was observed that coating LiF and Al both separately onto a P3HT film results in the quenching of the PL signal [24]. It should also be noted that increased impurity population near the P3HT surface, leads to increased PL quenching. The results are very similar to the ones observed in Chapter 3, and can similarly be explained by the fact that increased impurity population leads to increased values of K_{nr} due to the increase in the number of excitons undergoing relaxation via phonon coupling mode.

However, when the thickness of Al was increased from 2.5 nm to 30 nm the PL intensity increased as can be seen in Fig. 4.13. This effect has been observed due to double excitation of the film by the incident laser beam due to a strong reflection occurring from the top coated Al layer [26]. It is important to note that unlike Fig. 4.12, In Fig. 4.13 the PL counts for P3HT/LiF:Al samples were higher than that of P3HT/Al samples. Figure 4.13 also shows an increase in the high energy shoulder peak occurring due to the Al coating on to the top of pristine P3HT film. Another significant point is the blue shift shown by the peak PL emission (E = 1.702 eV) spectra due to Al coating. From the discussions from the previous section we now know that the high

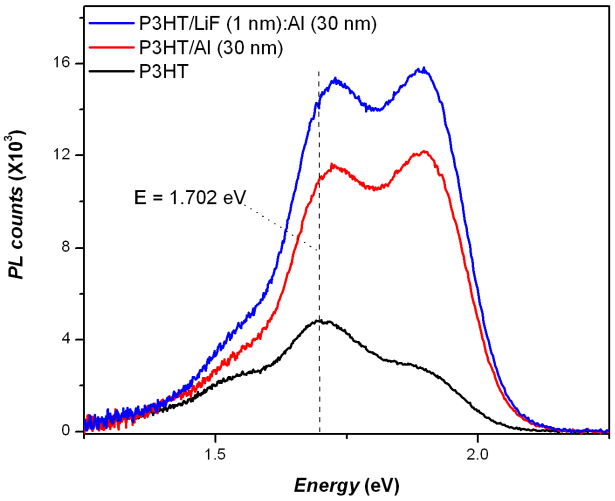

Figure 4.13: The effect of coating 30 nm thick Al on pristine and LiF (1 nm) coated P3HT films on the PL of P3HT

energy peak in the PL emission spectra relates to the intrachain disorder induced on the polymer chains in direct contact with hot Al atoms due to the energy transfer from the high energy Al atoms.

Until now we have mainly discussed the role of coating thin or thick layer of Al or LiF or both on P3HT film. However, in order to fully understand difference in the nature of interface between ITO/P3HT/Al (cell E) and ITO/P3HT/LiF:Al (cell F) cells we performed a bias dependent PL study and then analyzing the quenching patterns using the optoelectronic model discussed in the previous section. Figure 4.14 shows the IV characteristics of cells E and F. It must be noted while the IV characteristics are typical of a Schottky junction based diode. The currents were less for cell F compared to cell E under forward bias. This is in stark contrast with the current enhancement observed with LiF modified cathodes in OLEDs. It is to be noted here that the current as well as efficiency enhancement by the inclusion of a thin layer of LiF in OLEDs is actually caused by better injection of electrons from the metal to the LUMO of n-type organic material.In our study only p-type material i.e. P3HT was used, and the IV characteristics reflect the hole transport. The holes are injected from ITO into the HOMO of P3HT and from there into the Fermi level of Al. Thus, a decrease in the

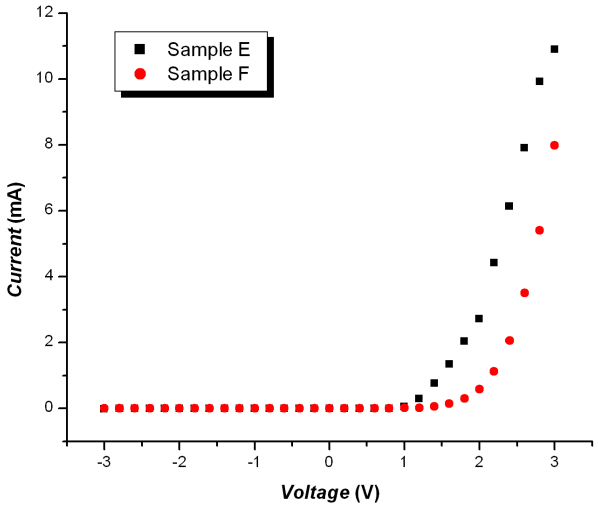

Figure 4.14: Current Voltage characteristics of cell E and F respectively

forward bias current was observed for cell F as is shown in inset of Fig. 4.14, although the built in voltage was found to increase upon the LiF coating.

Figure 4.15 shows the quenching pattern for cells E and F respectively. Cell E exhibits a relatively higher level of quenching compared to that in cell F with the increasing reverse bias voltage. Similar results have also been observed by Markov et al [49]. Although there are reports of PL quenching due to injected charge carriers [40-42] but such an effect is negligible in the present case as our discussion here concerns only with the reverse bias regime. Therefore, from eq. 4.16 it is clear that the quenching directly relates to the amount of light absorbed by the bulk of semiconductor. Using the similar analysis as was given in ref [26,56], the bias dependence of depletion width was plotted for cells E and F using the bias dependence of quenching for these cells.

Figure 4.16 shows the change in depletion layer width against applied reverse bias voltage, which has been obtained by using the eq. 4.16. The depletion layer width was more easily modulated in cell E compared to cell F. Thus it can be concluded that the presence of LiF near the interface limits the extent of modulation of the depletion layer with the applied reverse bias voltage.

Figure 4.17 on the other hand shows higher level of photocurrents in cell F as compared

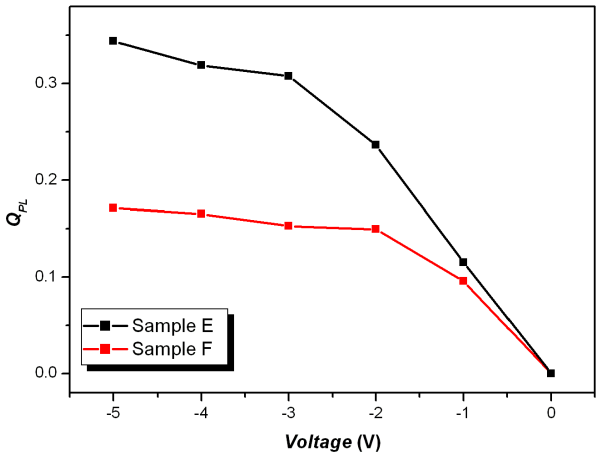

Figure 4.15: Plot of PL quenching Q_{pl} versus the reverse bias voltages for cell E and F

to that for the cell E. The photocurrents are found to increase with the increasing application of reverse bias voltage for the two cells.

Brabec et al [21] studied the effect of LiF in Bulk hetero-junction solar cells. It was observed that including a thin layer of LiF improved the solar cell efficiency of the PSCs considerably. However, in their final conclusion they attributed this effect to either the orientation of LiF or chemical reactions leading to charge transfer across the interface, thus resulting in the formation of dipole moment across the junction. However, the absence of memory currents in LiF coated photo induced memory devices as was demonstrated in the previous chapter [24] clearly rules out any such possibility. Thus, we conclude that it is the orientation of LiF near the interface that results in the dipole moment across the junction, also at the same time it is this dipole moment of LiF that leads to high localized field as is shown by the offset level in the band diagram in Fig. 4.18. The lesser values of depletion width of the cell F probably resulted due to the less steep band bending of P3HT in cell F as is shown in the Fig. 4.18. However, the high localized field near the interface in cell F resulted in higher values of photocurrents, as photocurrents are generated by the field assisted dissociation of excitons. A highly localized Field near the interface ensures effective dissociation of excitons. Thus we conclude that it is the dipole moment of the LiF molecule itself that leads to a highly

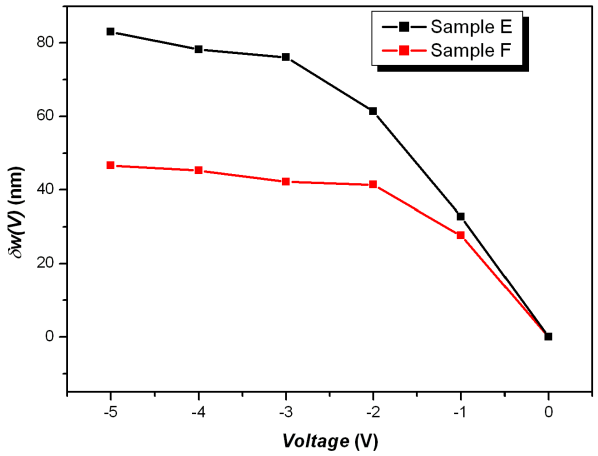

Figure 4.16: Change in depletion width $\triangle w(V)$ as a function of voltage for cell E and F

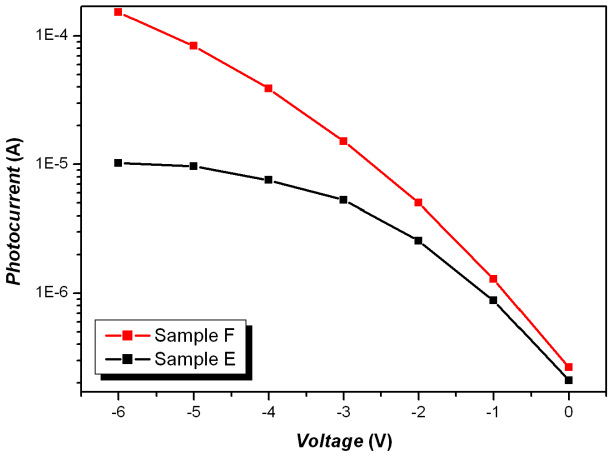

Figure 4.17: Photocurrents as a function of reverse bias voltages for cell E and F

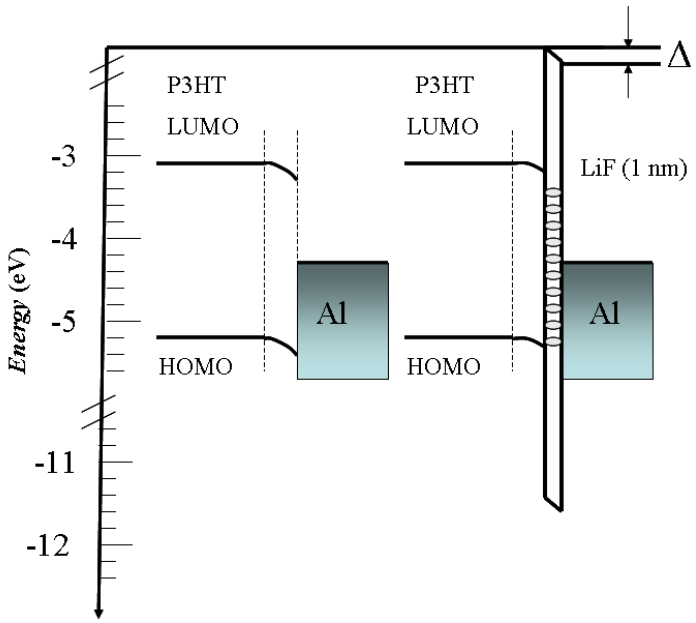

Figure 4.18: Band diagram for the cell E and F at zero bias condition

localized field, resulting in the improvement of solar cell efficiency.

Bibliography

[1] H. Spanggaard and F. C. Kerbs: Sol. Energy. Mat. Sol. Cells. 83 (2004) 125.

[2] Y. Kim, S. A. Choulis: J. Nelson, D. D. C. Bradley, S. Cook S and J. R. Durrant: J Mat. Sci. 40 (2005) 1371.

[3] T. F. Guo and Y. Yang: Appl. Phys. Lett. 80 (2002) 148.

[4] P. Pneumans, A. Yakimov and S. R. Forrest: J. Appl. Phys. 93 (2003) 3693.

[5] V. Singh, M. Yano, W. Takashima and K. Kaneto: Jpn. J. Appl. Phys. 45 No. 1B (2006) 534.

[6] D. A. Bernards, T. Biegala, Z. A. Samuels, J. D. Slinker, G. G. Malliaras, S. F. Torres, H. D. Abruna and J. A. Rogers: Appl. Phys. Lett. 84

(2004) 3675.

[7] T. W. Lee, S. Jeon, J. Maria, J. Zaumseil, J. W. P. Hsu and J. A. Rogers: Adv. Func. Mat. 15 (2005) 1435.

[8] J. C. Scott: J. Vac. Sci. Tech. A 21 (2003) 521.

[9] W. R. Siliveira and J. A. Marohn: Phys. Rev. Lett. 93 (2003) 116104.

[10] S. Grecu, M. R. Buck, A. Opitz and W. Brutting: Org. Elec. 7 (2006) 276.

[11] T. P. I. Saragi, T. F. Lieker and J. Salbeck: Synth. Met. 148 (2005) 267.

[12] B. Deveaud, A. Regreny, J. Y. Emery and A. Chomette: J. Appl. Phys. 59 (1986) 1633.

[13] B. S. Elmann, E. S. Koteles, C. Jagannath, Y. J. Chen, S. Charbonneau and M. L. W. Thewalt: Proc. SPIE 794 (1987) 44.

[14] R. Kersting, U. Lemmer, M. Deussen, H. J. Bekker, R. F. Mahrt, H. Kurz, V. I. Arkhipov, H. Bassler and E. O. Gobel: Phys. Rev. Lett. 73 (1994)

1440.

[15] G. Yu, J. Gao, J. C. Hummelen, F. Wudl and A. J. Heeger: Science 270 (1995) 1789.

[16] M. Segal, M. A. Baldo, R. J. Holmes, S. R. Forrest and Z. G. Soos: Phys. Rev. B. 68 (2003) 075211.

[17] N. S. Sariciftci, L. Smilowitz, A. J. Heeger and F. Wudl: Science 258 (1992) 1474.

[18] Y. D. Jin, X. B. Ding, J. Reynaert, V. I. Arkhipov, G. Borghs, P. L. Heremans and M. Van der Auweraer: Org. Elec. 5 (2004) 271.

[19] T. Yokoyama,H. Ishii and Y. Ouchi: Surf. Rev. Lett. 9 No. 1 (2002) 425.

[20] M. A. Baldo and S. R. Forrest: Phys. Rev. B. 64 (2001) 085201.

[21] C. J. Brabec, S. E. Shaheen, C. Winder, N. S. Sariciftci and P. Denk: Appl. Phys. Lett. 80 No. 7 (2002) 1288.

[22] S. Sohn, K. Park, D. Lee, D. Jung, H. M. Kim, U. Manna, J. Yi, J. Boo, H. Chae and H. Kim: Jpn. J. Appl. Phys. 45 No. 4B (2006) 3733.

[23] D. E. Markov and P. W. M. Blom: Phys. Rev. B. 72 (2005) 161401.

[24] V.Singh, A. K. Thakur, S. S. Pandey, W. Takashima and K. Kaneto: Jpn. J. Appl. Phys. 47 No. 2B (2008) 1251.

[25] H. Becker, S. E. Burns and R. H. Friend: Phys. Rev. B. 56 (1997) 1893.

[26] V. Singh, A. K. Thakur, S. S. Pandey, W. Takashima and K. Kaneto: Appl. Phys. Exp. 1 (2008) 021801.

[27] S. Tasch, G. Kranzelbinder, G. Leising and U. Scherf: Phys. Rev. B. 55 No. 8 (1997) 5079.

[28] M. C. J. M. Vissenberg and M. J. M. de Jong: Phys. Rev. B. 57 (1998) 2667.

[29] A. Takshi, A. Dimopoulos and J. D. Madden: Appl. Phys. Lett. 91 (2007) 083513.

[30] P. J. Brown, D. S. Thomas, A. Kohler, J. S. Wilson, J. S. Kim J S, C. M. Ramsdale, H. Sirringhaus and R. H. Friend: Phys. Rev. B. 67(2003)

064203.

[31] S. S. Pandey, W. Takashima, S. Nagamatsu, T. Endo, M. Rikukawa and K. Kaneto: Jpn. J. Appl. Phys. 39 (2000) L94.

[32] K. Kaneto, Y. Kohno and K. Yoshino: Solid State Commun. 51 (1984) 267.

[33] R. Hidayat, A. Fuji, M. Ozaki and K. Yoshino: Jpn. J. Appl. Phys. 40 (2001) 7103.

[34] H. Tanaka, Y. Yoshida, T. Nakao, N. Tsujimoto, A. Fujii and M. Ozaki: Jpn. J. Appl. Phys. 40 (2006) L1077.

[35] W. Takashima, S. S. Pandey, T. Endo, M. Rikukawa, N. Tanigaki, Y. Yoshida, K. Yase and K. Kaneto: Thin Solid Films 393 (2001) 334.

[36] G. Wang, T. Hirasa, D. Moses and A. J. Heeger: Synth. Met. 146 (2004) 127.

[37] A. K. Thakur, A. K. Mukherjee, D. M. G. Preethichandra, W. Takashima and K. Kaneto: J. Appl. Phys. 101 (2007) 104508.

[38] S. S. Pandey, W. Takashima, S. Nagamatsu, T. Endo, M. Rikukawa and K. Kaneto: Jpn. J. Appl. Phys. 39 (2000) L94.

[39] M. R. Anderson, D. Selse, M. Berggeren, H. Jarvinen, T. Hjertberg, O. Inganas, O. Wennerstrom and J. E. Osterholm: Macromolecules 27 (1994)
6503.

[40] V. Singh, A. K. Thakur, S. S. Pandey, W. Takashima and K. Kaneto: Synth. Met. 158 (2008) 283.

[41] Y. Luo, H. Aziz, G. Xu and Z. D. Popovic: Chem. Mater. 19 (2007) 2288.

[42] H. S. Majumdar, C. Botta, A. Bolognesi and A. J. Pal: Synth. Met. 148 (2005) 175.

[43] K. Rikitake, D. Tanimura, W. Takashima, and K. Kaneto: Jpn. J. Appl. Phys. 42 (2003) 5561.

[44] K. Kaneto, and W. Takashima: Curr. Appl. Phys. 1 (2001) 355.

[45] K. Kaneto, M. Nakagawa, and W. Takashima: Synth. Met. 25 (2003) 135.

[46] M. Ujimoto, W. Takashima, and K. Kaneto: Jpn. J. Appl. Phys. 39 (2001) 5350.

[47] J. L. Bredas, J. Cornil and A. J. Heeger: Adv. Mater. 8 (1996) 447.

[48] Z. G. Soos, D. S. Galvao, S. Eternad: Adv. Mater. 6 (1994) 280.

[49] D. E. Markov, J. C. Hummelen, P. W. M. Blom and A. B. Sieval: Phys. Rev. B. 72 (2005) 045216.

[50] G. D. SCholes and G. Rumbles: Nature Mat. 5 (2006) 683.

[51] S. K. Krawczyk, M. Garrigues and H. Bouredoucen: J. Appl. Phys. 60 (1986) 392.

[52] R. R. Chang, R. Iyer and D. L. Lile: J. Appl. Phys. 61 (1987) 1995.

[53] L. M. Popescu, P. V. Hof, A. B. Sieval, H. T. Jonkman and J. C. Hummelen: Appl. Phys. Lett. 89 (2006) 213507.

[54] M. Gailberger and H. Bassler: Phys. Rev. B. 44 (1991) 8644.

[55] D. F. Blossey: Phys. Rev. B. 9 (1974) 5183.

[56] V. Singh, S. S. Pandey, A. K. Thakur, W. Takashima and K. Kaneto: Organic Electron. 9 (2008) 790.

Chapter 5

Application of optoelectronic model to study the role of morphology in exciton quenching

Summary

The interface formed at Aluminum and Poly (3-Alkylthiophene) has been studied using bias dependent photoluminescence (PL) quenching in ITO (Indium Tin Oxide)/P3AT/Al sandwiched cells. Different types of bias dependent PL quenching patterns were obtained by varying the alkyl chain length and the regioregularity of the P3AT. Observed results indicate that the PL quenching and depletion layer are strongly correlated to the morphology[1] in these PAT films. Furthermore, the results also indicate the spatial charge carrier distribution in these films. Moreover, by changing the alkyl chain length a complete trend reversal was obtained between the PL quenching and the Mott-Schottky plot of these cells. These observed results have been explained on the basis of Field induced PL quenching in these films.

[1]Morphology refers to the study of interrelationship between shape, structure and arrangement of molecules in thin films.

5.1 Introduction

As we have discussed in the previous chapter that the Capacitance Voltage (CV) plot for organic Schottky junction [1-5] is limited due to inherent parasitic capacitances present due to the nature of organic materials as can often be observed in the Mott-Schottky plot [14,15] of these cells. Although the depletion layer [27-32]formed at Al/P3HT has been well utilized to give various functionalities viz. polymeric solar cells (PSCs)[6,7], polymeric light emitting diodes (PLEDs) [8,9] and the polymer based photo induced memory devices (PIMDs) [10,11]. Even the sub threshold regime in an Organic Field Effect Transistors (OFETs) [4,12,13] is also studied on the basis of depletion width in a Schottky contact. In the light of these applications the dependence of depletion layer width on the applied bias voltage assumes critical significance. Although Takshi et al [13]have presented a novel way to study the bias profile of the depletion layer electrically. They used a Schottky gated FET (MESFET) to characterize the depletion layer. Our optoelectronic model [5,19,20] as discussed in the previous chapter is also applicable to characterize the depletion layer. It was observed that the optoelectronic model presented in this work can further be used to probe the spatially distributed traps in the bulk of the semiconductors. However, besides being an alternative way to characterize depletion layer our model can also facilitate better understanding of exciton dynamics. In general an exciton lifetime consists of three stages, exciton formation, exciton diffusion and exciton recombination.

Morphology of the organic thin films depends on a variety of parameters viz. regioregularity, chain length of the substituent(especially in the case of solution processed conjugated polymers), solvent, growth conditions of the organic thin film and annealing temperature etc [21-25]. In this chapter we propose application of our previously developed optoelectronic model to study the morphologies of various organic materials and to further elucidate the role of morphology in diffusion of excitons, as can also be seen in Fig. 5.1. Moreover, the thickness dependent PL also gives us information about the relative distribution of charge carriers in the bulk of the semiconductor. The morphology of the films were changed by changing the alkyl chain length attached to

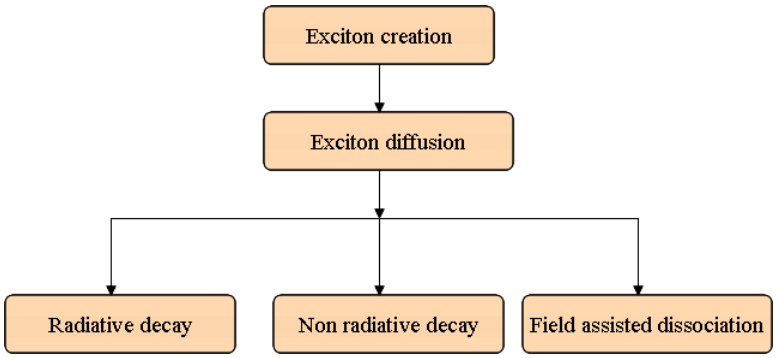

Figure 5.1: Flowchart showing the various stages during the lifetime of an exciton

the Poly(3-Alkylthiophene) as well as changing the regioregularity of the P3HT. Large PL quenching was observed in films having well stacked structures, besides this effect of coating the organic semiconductor on the absorption and emission spectra of organic materials has also been studied. Moreover the bias dependence of PL spectra has been utilized to compare the PL emission spectra of films deposited with different techniques, and thus having different thicknesses[16-20]. The results discussed in this chapter are of critical importance for the development of photovoltaic devices, besides the technique described here can be used to probe the photovoltaic properties of different materials. Moreover by changing the alkyl chain length a complete trend reversal was obtained between the PL quenching and the Mott-Schottky plot of these cells. These results have been explained on the basis of Field induced PL quenching in these films.

5.2 Experimental Procedures

In order to study the absorption and emission spectra of pristine films, Pre -cleaned glass substrate was completely spin coated with a chloroform solution of the P3AT. Prior to coating the P3AT films on these glass substrates their surface was treated with (1,1,1,3,3,3-Hexamethyldisilazane) (HMDS) to make the surface hydrophobic as was also described in the previous chapters. For the purpose of bias dependent PL spectra and the $1/C^2$ versus V plot, sandwich cells (ITO/P3AT/Al) having an active device area of $30mm^2$ were fabricated. ITO coated glass substrates were taken and etch patterned using Zinc dust and dilute HCl solution as described in Chapter 2. The surface was later

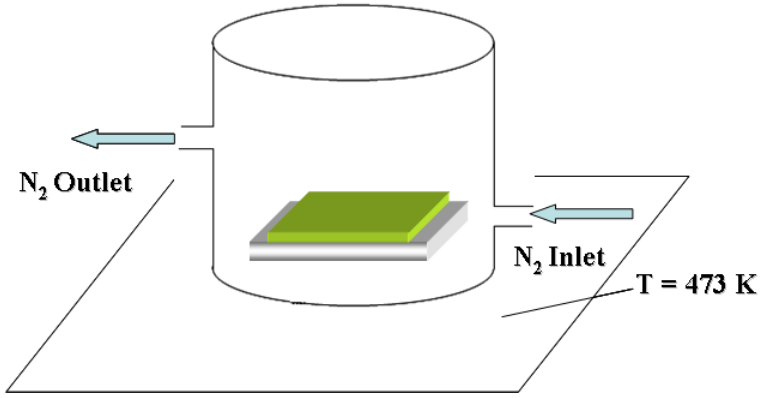

Figure 5.2: Shows the synthesis of PPV by heating at high temperature using precursor route polymerization

made hydrophobic using HMDS solution. Chloroform solution of P3AT was spin coated on top of these substrates, resulting in film thicknesses in the order of 150 210nm. Finally a 30nm thick Al electrode was thermally evaporated using shadow mask technique. The top electrode was deposited orthogonal to the bottom electrode resulting in a device as shown in Fig. 5.6(a). For the purpose of alkyl chain length variation regioregular Poly (3-butylthiophene), regioregular Poly (3-hexylthiophene) and regioregular Poly (3-dodecylthiophene) were used as obtained from Aldrich. For the sake of convenience we would refer these as rr PAT4, PAT6 and PAT12 respectively. regiorandom Poly(3-hexylthiophene) having 50% regioregularity was used to perform a comparative study about the role of regio regularity on the morphology, and hence on exciton. Also, for the sake of convenience this will be often referred to as rrnd PAT6, throughout this chapter for the sake of convenience. Besides these materials rrnd PAT12, MDMO-PPV and PPV were also used as obtained from Aldrich. While rrnd PAT 12 was used to study the effect of regioregularity on the absorption and emission spectra of P3HT films, on the other hand MDMO-PPV and PPV were used to study the effect of morphology on the absorption spectra. PPV was polymerized via precursor method [33-35], the conditions of the film growth were as shown in Fig. 5.2. The molecular structures of rr PAT and rrnd PAT films is shown in Fig. 5.3. It should be noted that for the purpose of convenience only few monomers units are shown. While the rr PAT films the only 2,5 linkage exists between the monomer unit almost throughout the polymer chain.

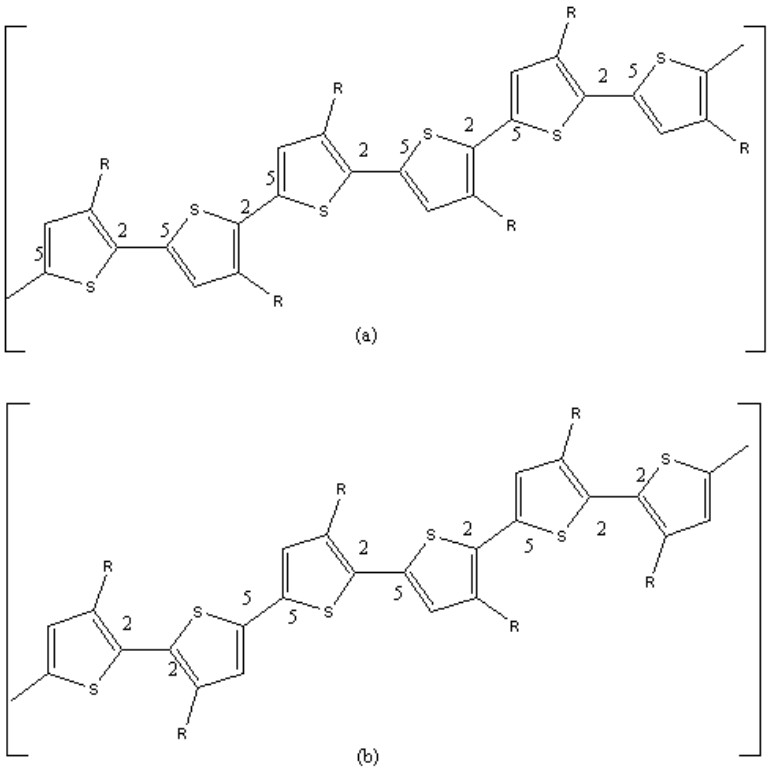

Figure 5.3: Structure of (a)rr PAT and (b) rrnd PAT

However, on the contrary rrnd PAT films have 2-2, 2-5 and 5-5, all types of linkages between the adjacent monomer units. It should be noted that both the 2-2 and 5-5 linkages are energetically unfavorable for long chain growth during the polymerization process. This limits the number of monomer units joined on a single chain in the case of random PAT films. Also, the thiophene rings tend to take out of plane geometry, due to higher steric hindrance between the side chain groups attached to 2-2 and 5-5 linked thiophene rings resulting in decreased degree of effective π-conjugation.

Figure 5.4 shows the molecular structure of MDMO-PPV. It is to be noted that the substituent group in this case is a OR (or the so called alkoxy group). Moreover, while the thiophene rings are heterocyclic in nature. On the other hand phenylene rings in MDMO-PPV are aromatic in nature. These points regarding the structural differences between these compounds must be kept in mind. The details about their difference in the characteristics of MDMO-PPV and PAT 6 will be given in the next section.

Figure 5.5 (a) shows the structure of PPV. As can be seen that PPV does not have

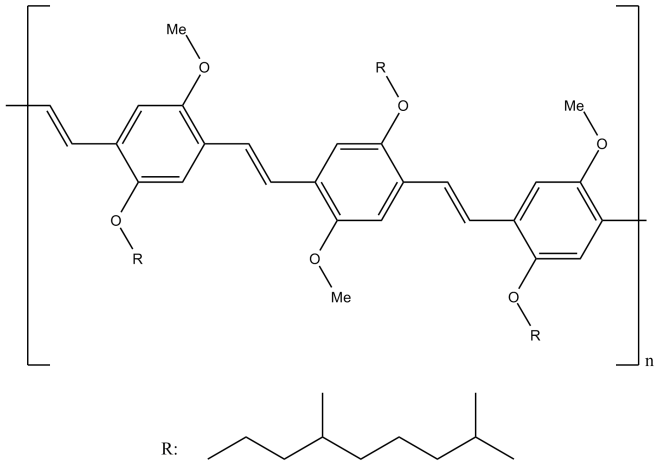

Figure 5.4: Molecular structure of MDMO-PPV

any substituent attached to the main polymer chain. This makes PPV completely insoluble in any organic solvents. Moreover, being a polymer it can also not be evaporated on to the substrate. However, a synthetic route for the polymerization using a precursor is possible. In the precursor route polymerization method [33-35], typically a soluble precursor is taken as shown in Fig. 5.5(b), and used to coat a thin film. Later by thermal, chemical or optical treatment the polymerization is done. This leads to polymerized thin film. This thin film when treated at high temperature leads to polymerization, forming a thin film of PPV. However, there is absolutely no control over the number of monomers joined in a polymer chain. usually the films formed via this technique is amorphous in nature. It is also to be noted that there are external chemical species trapped in the interstitial sites and may act as impurities. Thus obtaining a highly purified film via this method is very difficult. MDMO-PPV thin film was coated over HMDS treated glass substrate from its solution in dehydrated Toluene [36-38].

All the film thicknesses were later measured using Dektak surface profiler 6M. Figure 5.6 shows the schematic diagram of cells fabricated for the measurement of UV-Vis absorption spectra and bias dependent PL measurement. The UV-Vis spectral measurement was performed using JASCO V-570 UV/Vis/NIR spectrophotometer. PL measurements were done under ambient conditions using photonic multi channel analyzer, (Hamamatsu PMA-11), kept at a distance of $70cm$ from the sample. A He-Cd laser having a beam area $20mm^2$ ($300mW$, CW, $442nm$, Kimmon IK4121R) was used as a light source. The

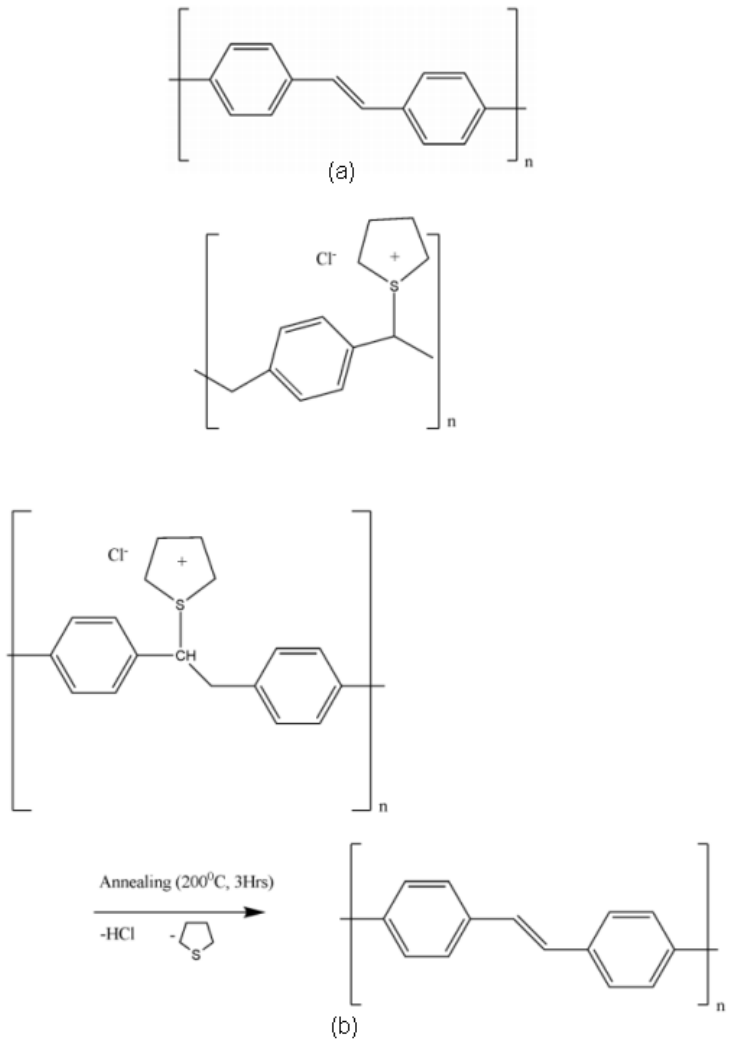

Figure 5.5: Shows the (a) structure of PPV, (b) mechanism of polymerization PPV via precursor route

intensity of light incident on the sample was later calculated to be $0.15W/cm^2$, at an inclination of about 30^o to the normal. In-situ electrical bias was applied on the cells using Keithley 6517 A electrometer. Care was also taken to avoid the over exposure of samples to the laser beam.$1/C^2$ versus V measurements were performed using HIOKI 3522-50 LCR Hi Tester. IV measurements of the diode were using Keithley 6517 A electrometer. The typical biasing arrangement of the cells was identical to as shown in the previous chapter in Fig. 4.3(a).

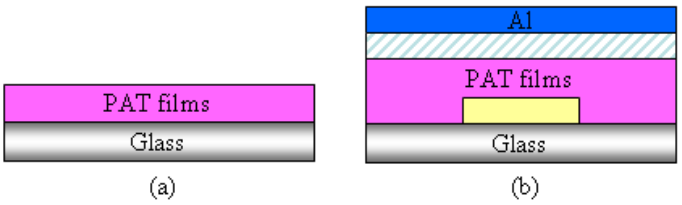

Figure 5.6: Schematic diagram of (a) sample prepared for Absorption spectrum measurement (b) sample prepared for bias dependent PL, and CV measurement

5.3 Role of morphology in absorption and emission spectra of thin films

5.3.1 Structure morphology correlation

Figure 5.7 shows the plot of absorption coefficient of rr PAT 4, 6 and 12 and rrnd PAT 6 thin films. It was observed that rr PAT 4 was having the highest absorption coefficient and with increasing chain length the value of absorption coefficient decreased. This is mainly due to the higher density of π-conjugated main chain per unit volume. As the strength of absorption coefficient directly relates to the compactness of π conjugation. The longer alkyl chain length tends to promote a well stacked structure mainly due to good interlocking of the alkyl side chains [22,23]. Although this results in good stacking in these films as can be seen from the clear appearance of shoulder peaks in rr PAT 6 and rr PAT 12 from the normalized absorption spectra shown in Fig. 5.8. However, on the contrary it is these longer alkyl chain lengths that lead to increased separation between two adjacent chains leading to decreased π-electron density per unit volume. Hence the decrease in the absorption coefficient was observed with increasing chain length. It is commonly thought that the blue shift observed in the rr PAT 4 films is mainly because in these films it is difficult to form well stacked structures due to short alkyl chain. Thus the chains in rr PAT 4 tend to take a twisted coil like shape, resulting in the observed blue shift [23]. A huge blue shift was observed in the absorption spectra of rrnd PAT 6 as compared to the rr PAT films. This is mainly owing to the high degree of regio-randomness in these chains. Large regio-randomness leads to high degree of steric hindrance between the adjacent monomer groups leads to increased gap between

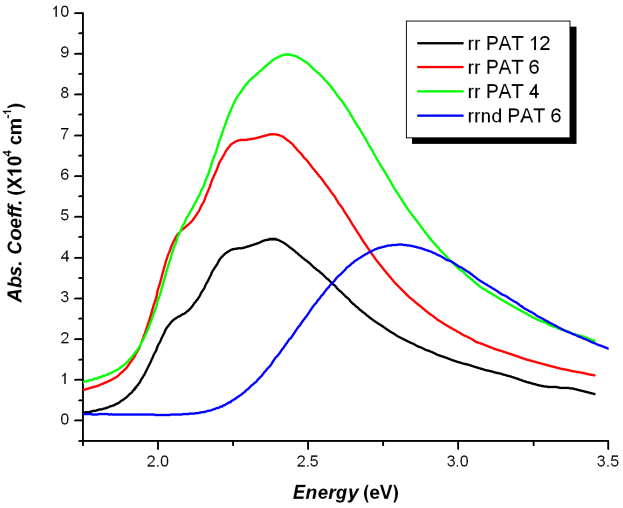

Figure 5.7: Absorption coefficient of rr PAT 4, PAT 6, PAT 12 and rrnd PAT 6

the $\pi - \pi^*$ transition leading to highly blue shifted absorption spectra of rrnd PAT 6. It must also be noted that it is also due to the highly distorted structure of these rrnd PAT 6 that leads to lesser density of pie electron per unit volume as compared to rr PAT 6, causing the significant difference between the absorption coefficients of these films. The highly amorphous nature of these films along with the lack of any stacking results in disappearance of shoulder peaks altogether as can be easily observed from Fig. 5.8.

The fact that appearance of shoulder peaks confirms the formation of stacked structures in the organic thin films was further confirmed by the absorption spectra of MDMO-PPV and PPV. It is to be noted that the absorption spectra of PPV films were highly blue shifted. However, appearance of shoulder peaks in the absorption spectra of MDMO-PPV clearly suggests that the presence of substituent groups in MDMO-PPV facilitate better stacking in these films. Once again it also demonstrates that substituent groups not only increase the solubility of the π-conjugated polymers but also help in improving the overall film morphology. Figure 5.10 shows the normalized PL spectra showing the effect of intrachain disorder [19,26] on the PL emission spectra of various PAT films. It should be noted that maximum intrachain disorder was observed in PAT

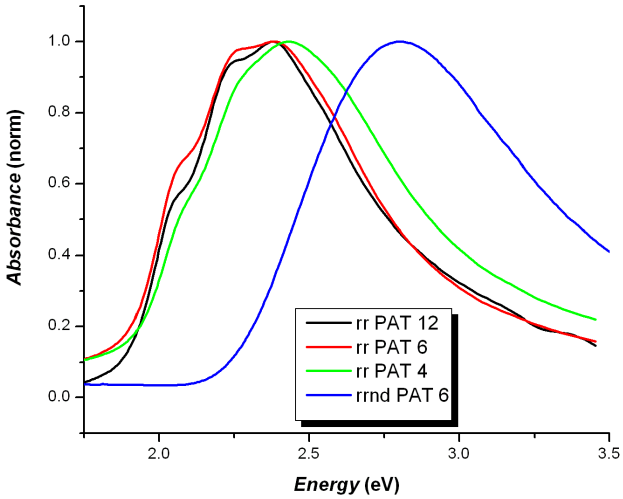

Figure 5.8: Normalized absorption coefficient of rr PAT 4, PAT 6, PAT 12 and rrnd PAT 6

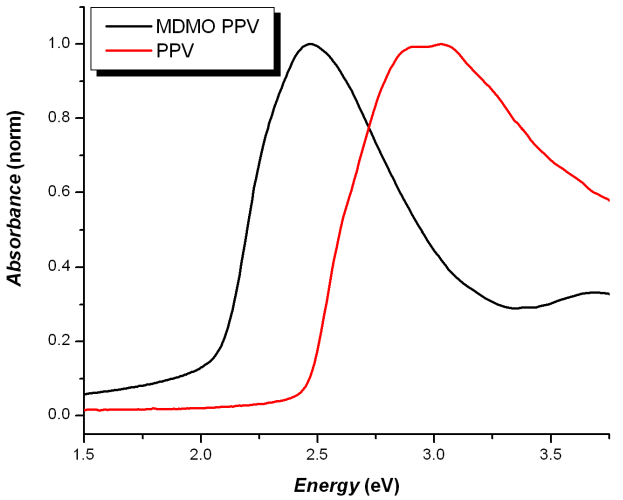

Figure 5.9: Normalized absorption spectra of PPV and MDMO-PPV thin films

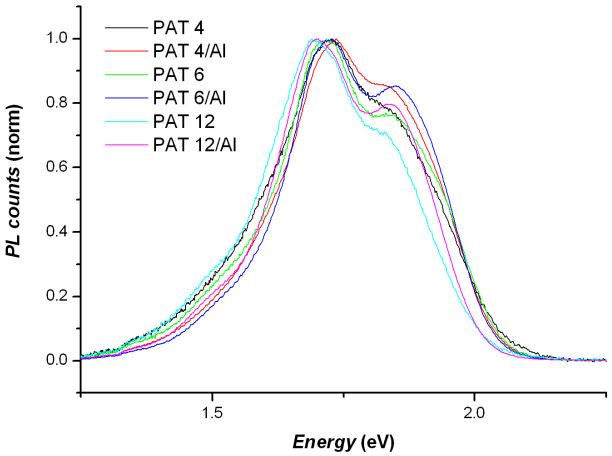

Figure 5.10: Normalized PL spectra showing the effect of intrachain disorder on the PL emission spectra of various PAT films

4 films. As the chains in these films have a highly twisted helical structure. Another important feature was the highly blue shifted emission of rrnd PAT 6. It should be noted that not much appreciable difference could be observed between the peak emission wavelengths in various rr PAT films. In our earlier work [19] we had demonstrated that the shoulder peak at ($\lambda = 681nm$) relates to the intrachain disorder[19]. As can also be seen from the Fig. 5.10 coating thick Al ($30nm$) on top of pristine PAT films resulted in increase in intrachain disorder as was also discussed in previous chapter. Thus we find that the film morphology also governs the emission spectra of the organic thin films.

5.3.2 Correlation between morphology and film growth conditions

In order to further validate the effect of thin film growth conditions on overall film morphology we fabricated three different types of film, using rr P3HT by three different methods of film deposition. While one of the film was spin coated, the other two were dip coated [40-44] and drop casted [23,40] respectively. As was mentioned in chapter 2 the growth conditions are slowest for the dip coated film, while drop casted films lies in between that of dip coated and spin coated films. And the lowest time given for the thin

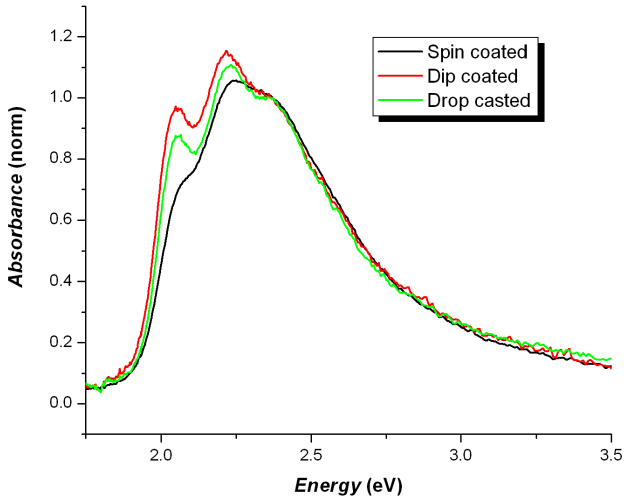

Figure 5.11: Normalized absorption spectra of dip coated, drop casted and spin coated rr PAT 6 film

film deposition was for the spin coated films. Also it was mentioned that longer time for film growth ensures better aggregation of the film. Thus, resulting in films having highly stacked structures and better morphology. As can also be seen from the Fig. 5.11, the strength of shoulder peak increases with increasing time interval for the film growth. Thus, the peak is most pronounced in the case of dip coated films and least in spin coated P3HT films. To further investigate the effect of molecular order in organic thin films on their emission spectra, four types of samples using rr PAT 12 (spin coated and casted)[23] and rrnd PAT 12 (spin coated and casted) were prepared.

Figure 5.12 shows the PL spectra of rr PAT 12 and rrnd PAT 12 thin films. It is to be noted that the emission spectrum for rrnd PAT 12 Spin coated and casted films both showed blue shift. Furthermore the emission spectra of spin coated rrnd PAT 12 film was slightly more blue shifted as compared to casted rrnd PAT 12 film. This is primarily due to the fact that spin coated films are more amorphous and hence have lesser degree of aggregation in them compared to the casted films. Figure 5.13 shows the normalized PL spectra of these films. It should be noted that degree of intra chain disorder was observed higher in spin coated rr PAT 12 film compared to the intrachain disorder in the casted rr PAT 12 film, further confirming that spin coated films have poor morphology

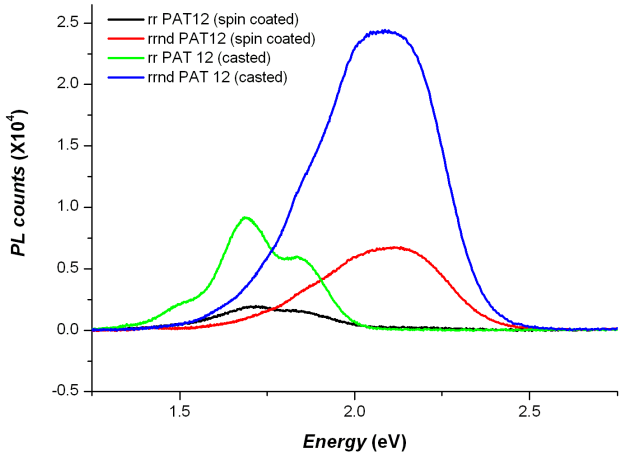

Figure 5.12: PL spectra of rr and rrnd PAT 12 films deposited via spin coating and casting methods

compared to casted films. Another significant feature of this plot shown in Fig. 5.12 is that the absolute PL intensity of spin coated films of both rr and rrnd PAT 12 were less than the their respective casted samples. However, it is known that casting of a film results in highly crystalline structures as compared to spin coated films, thus the PL intensity of the casted films are expected to be less than their spin coated films. This may be due to the large difference between the thicknesses of these films. Therefore a direct comparison between their absolute PL emission intensity is just not possible. To this effect we would further like to recall that film thickness dependence of PL intensity of spin coated films can be obtained by varying the strength of $CHCl_3$ solution of P3HT, as was done in the previous chapter.

Thus, in order to compare the absolute PL emission intensity between the spin coated and casted films, the plot of thickness dependence of PL intensity of spin coated films were used. Figure 5.14 shows the effect changing film thickness on PL intensity for rr and rrnd PAT 12 films. The PL intensity of pristine films were found to be related to the film thickness as given by eq. 5.1.

$$< I_{pl} >= \eta_d \eta_{pl} I_0 (1 - e^{-\alpha d}) \tag{5.1}$$

where symbols have their usual meaning as defined in the previous chapter. It is to be

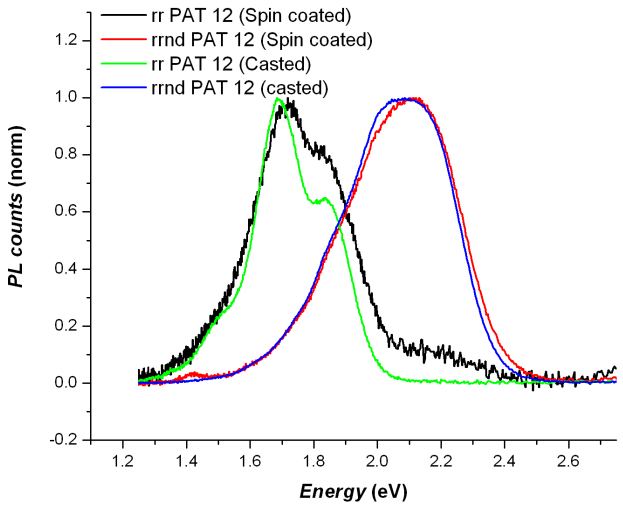

Figure 5.13: Normalized PL spectra of rr and rrnd PAT 12 films deposited via spin coating and casting methods

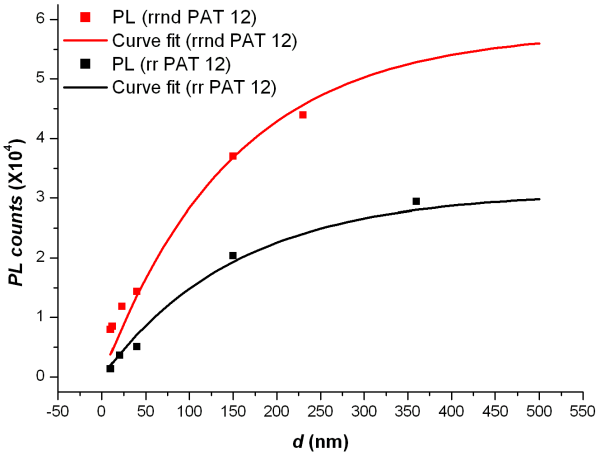

Figure 5.14: Normalized PL spectra of rr and rrnd PAT 12 films deposited via spin coating and casting methods

noted that the fitting curves plotted for both rr PAT 12 and rrnd PAT 12 were found to follow the relation given by eq. 5.1. Also it is to be noted that for a film thickness of d_0 (for the sake of convenience we call it extinction thickness) as given by the equation below

$$d_0 = \frac{5}{\alpha} \tag{5.2}$$

However, $e^{-\alpha d_0} \approx 0.0067$, this means that almost all the incident light will be absorbed by a film thickness of d_0. In the case of casted films the thickness of the films were measured to be $18 \sim 40\mu m$ thick. However, the extinction thickness were found to be $0.769\mu m$ and $1.74\mu m$ for rr PAT 12 and rrnd PAT 12 respectively. It must be noted that while the spin coated films have thicknesses well below the extinction thickness, the casted films have thicknesses much above the extinction thickness. Therefore, in order to compare the PL intensity of casted and spin coated films, we calculated the PL intensity for $0.769\mu m$ and $1.74\mu m$ thick spin coated of rrnd PAT 12 and rr PAT 12 films respectively, using the PL intensity versus the thickness fit as shown in Fig. 5.14. The spectrally averaged PL intensities of spin coated and casted rr PAT 12 and rrnd PAT 12 were then plotted against their respective extinction thicknesses as is also shown in the Fig. 5.15. As can be seen from Fig. 5.15, if PL counts are considered from identical film thicknesses, the PL counts are higher in spin coated rr and rrnd PAT 12 films, compared to their casted films respectively. This, now clearly demonstrates that increased crystallinity causes decreased PL emission. The spin coated films have a high degree of stacked chains in them, due to longer and more gradual deposition of organic layer. Another striking feature of this plot it that the ratio between the PL counts for casted and spin coated rr PAT 12 films is directly related to the ratio of their amorphicity in these films as given by the eq. 5.3.

$$\xi = \frac{< I_{pl} >_{casted}}{< I_{pl} >_{spincoated}} = \frac{(amorphicity)_{casted}}{(amorphicity)_{spincoated}} \tag{5.3}$$

Using eq. 5.3 ξ was found to be ≈ 0.3 for rr PAT 12, and ≈ 0.4 for rrnd PAT 12. These values indicate that the degree of crystallization during the casting of the films is strongly influenced by the degree of regio regularity of the polymer chains during the duration of film growth. Thus, in the above paragraph we observed that the PL is also

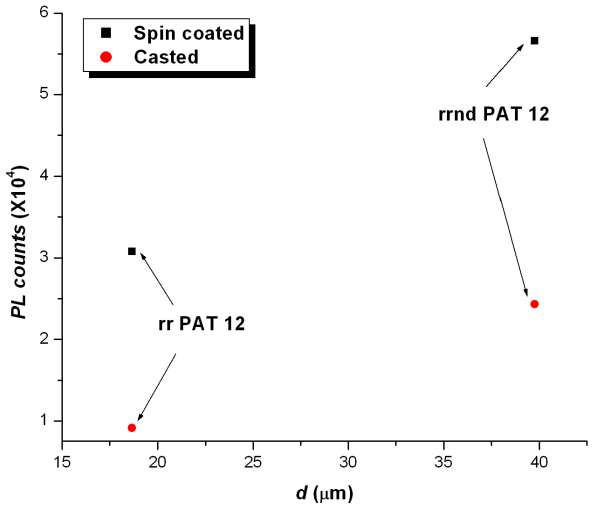

Figure 5.15: Showing the PL intensity of rr and rrnd PAT 12 prepared by casting and spin coating methods against respective film thicknesses

related to the molecular order in organic thin films. Stokes shift which is calculated from the difference between the absorption and emission maxima wavelength is indicative of the amount of energy lost by a system [45]. Figure 5.16 shows the plot of stokes shift in cm^{-1} as a function of alkyl chain length. It was observed that increasing chain length leads to lower stokes shift. Although not much appreciable difference was found to exist between the rr PAT 6 and rr PAT 12. However, a significant amount of energy was lost in rr PAT 4 film. The Stokes shift was much higher in the rrnd PAT 6 compared to any of the PAT films. Thus, the Stokes shift is also correlated to the molecular order in these films causing higher degree of stokes shift in more amorphous films. To further study the role of morphology in the PL emission and hence in the exciton quenching we performed optoelectronic study, the details will be discussed in the next section.

5.4 Application of optoelectronic model to study exciton quenching mechanism qualitatively

Another key indicator of the defects or molecular disorder present in the films is the $\ln J$ versus V plot. Figure 5.17 clearly shows a relatively higher leakage current under

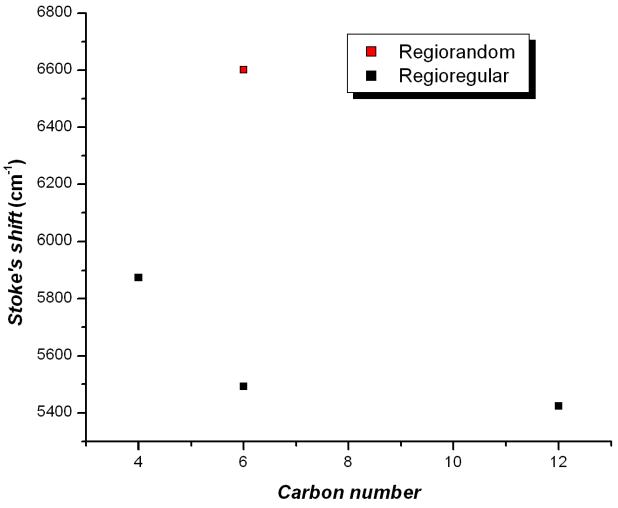

Figure 5.16: Plot of Stokes shift for various PAT films

reverse bias for rrnd PAT 6 and rr PAT 4 sandwich cells. However, on the contrary no increase in the reverse bias leakage current was observed in the rr PAT 6 and rr PAT 12 cells. It was also found that the increase in the reverse bias leakage current was higher in rrnd PAT 6 as compared to rr PAT 4, owing to the higher density of defects present in both these films.

Figure 5.18 shows the plot of $1/C^2$ versus V for rr PAT 4, rr PAT 6 and rr PAT 12. It was observed that there was a large deviation from the linearity in the low bias regime for all the cells. Decrease in the magnitude of slope in the lower bias region suggests that the depletion width in less modulated at lower bias voltages, which further means that a higher charge carrier density in the film exists near the interface and decreases as we move top to bottom from Al to ITO electrode.

However, on the contrary in a spin coated film the defects or trap density is more on the top of the film, and decreases as we move from top to down. It was found that carrier density increased with increasing alkyl chain length in rr PAT. A similar trend of charge carrier density has also been observed by Kaneto et al [21]. In their report however, the charge carrier density was determined using the empirical relation as given

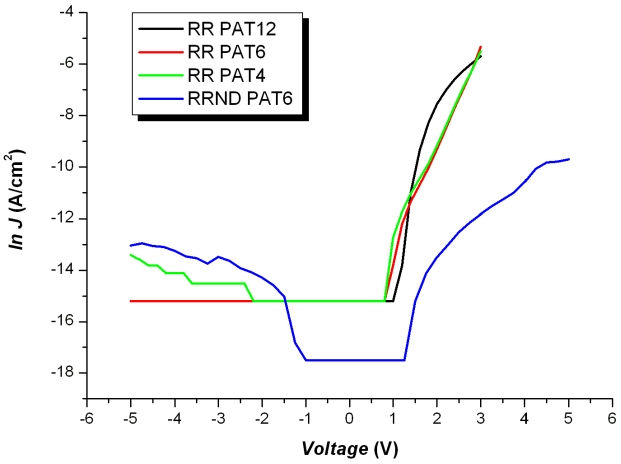

Figure 5.17: Plot of current against voltage for various ITO/PAT/Al devices

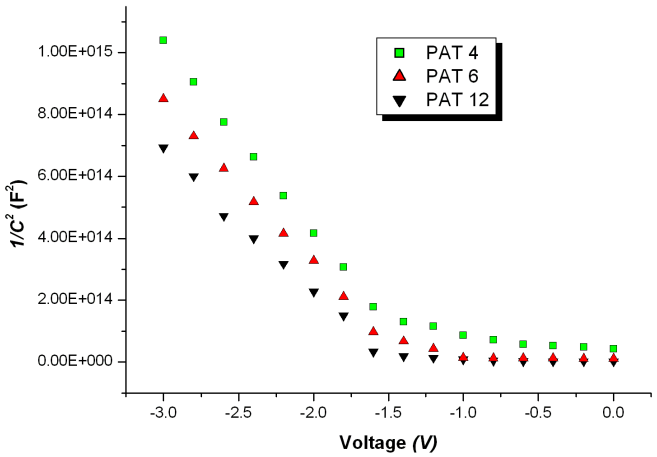

Figure 5.18: Mott-Schottky plot for rr PAT 4, rr PAT 6 and rr PAT 12 based sandwich cells

by eq. 5.4 as given below

$$\sigma = nq\mu \tag{5.4}$$

Where, σ denotes the bulk conductivity of the film, n is the charge carrier density, q is the charge on an electron and μ is the charge carrier mobility. It should be noted that while the mobility was estimated using Time of flight method [21,23] for different PAT films and the conductivity was separately estimated from the $4-probe$ conductivity measurement. It is worthwhile to note that the carrier density estimated from the linear region (or high reverse bias region) of our Mott-Schottky plot are found to be in agreement with those obtained by Kaneto et. al [21]. As discussed in the previous section that CV measurement is limited by the parasitic capacitances resulting in the observed non linearity in the Mott-Schottky plots of rr PAT films. In order to obtain a more refined spatial profile of charge carriers the bias dependent PL measurements were performed on to these cells. As reported in the previous chapter PL quenching 5,17-20) has been defined as given below

$$Q_{pl} = \frac{< I_{pl}(0) > - < I_{pl}(v) >}{< I_{pl}(0) >} \tag{5.5}$$

Where symbols have their usual meaning as defined in chapter 4. The intensity of PL emission $< I_{pl} >$ in general is given by5,19,20)

$$< I_{pl}(\lambda) >= I_{abs}\eta_{pl}\eta_{d} \tag{5.6}$$

Further it is to be noted that the PL efficiency η_{pl} is in general given by Eq. 5.7 [16-19].

$$\eta_{pl} = b\frac{K_r}{(K_r + K_{nr} + K_q)} \tag{5.7}$$

Where ,K_r, K_{nr} and K_q denote the rates of radiative, non radiative and electric field induced dissociation of excitons respectively.

Figure 5.19 shows the PL quenching against the reverse bias voltage . A relatively higher bias dependent PL quenching was observed in the rr PAT 12 cells. The extent of bias dependent PL quenching diminished with decreasing alkyl chain length. These results suggest that the PL quenching is related to the degree of molecular order in these PAT films. In our previous report we had proposed the estimation of depletion layer

width itself from the experimentally observed PL quenching for rr PAT 6 cell. However, if the PL quenching is only related to the depletion layer width under the reverse bias conditions then the PL quenching should have been maximum in the case of rr PAT 4 and minimum in rr PAT 12. Contrary to this, the obtained results are completely opposite. The relationship between the depletion layer width and the PL quenching in ref[5, 19-20] has been derived under the assumption that $K_q << (K_r + K_{nr})$. However, while comparing different materials we can not ignore the effect of field induced dissociation of excitons in different materials. As each material will have a different probability of dissociation of excitons under the same applied field. As has been argued before, that PAT 12 and PAT 6 films are well ordered having high degree of stacking between different chains in these films which probably leads to easier diffusion of excitons. Therefore greater number of excitons in these films can diffuse to the interface region of Al/PAT and under the high built in field may undergo dissociation into opposite charge carriers. Although, the relative contributions to the PL quenching by the increased depletion layer width and the electric field induced dissociation of excitons could not be clearly distinguished. A more refined and precise modeling of the process is needed. However, it is clear that the PL quenching Q_{pl} in Fig. 5.19 is not directly related to the charge carrier density in the rr PAT films. Also, under the reverse bias applications all the Electric field applied to the sandwich cells appears across the depletion layer, mainly owing to the large difference between the bulk and the depletion resistance in these devices. Figure 5.18 suggests that depletion width is less in rr PAT 12 and increases with decreasing chain length of the alkyl group. This means that under same applied reverse bias voltage, a higher electric field builds up in rr PAT 12 films than rr PAT 4. Implying that not just the diffusion of excitons is easier in PAT films with longer alkyl chain lengths but also the built in electric field near the metal semiconductor interface is stronger leading to higher level of PL quenching in these films. Another important feature of the PL quenching plot is that for rr PAT 12 and PAT 6 the slope of PL quenching is higher in the low bias region than in the high bias region. This may be due to the fact that these films are more ordered and hence the density of traps is relatively more near the top surface of these films compared to the bottom. It is this increased

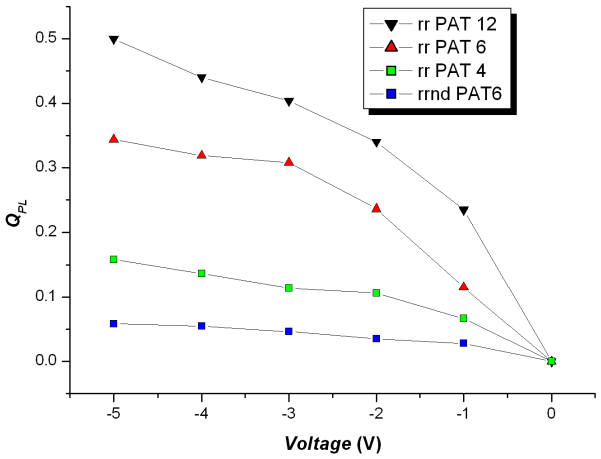

Figure 5.19: Plot of Photoluminescence quenching against the applied reverse bias voltage for rr PAT 4, rr PAT 6 and rr PAT 12 and rrnd PAT 6 based sandwich cells.

trap density near the Al/PAT interface that leads to reduced net charge density and thus increased PL quenching in the low bias regime. However, in less ordered films like rr PAT 4 and rrnd PAT 6 these traps are rather more uniformly distributed throughout the bulk of these films leading to a more uniform PL quenching profile in these devices against the reverse bias voltage. Finally we would like to conclude that the PL quenching in the PAT films is largely dependent on morphology. Highly ordered films show higher quenching mainly due to easier diffusion and higher probability of exciton dissociation near the Al/PAT interface. While the easy diffusion of excitons is directly related to the morphology of the film, the highly ordered films also have higher built in field near the interface resulting in higher probability of exciton dissociation at the interface in these films. Further more we would also like to conclude that the PL quenching Q_{pl} in ITO/PAT/Al films is also indicative of the relative spatial distribution of traps in these films.

Bibliography

[1] K. Rikitake, D. Tanimura, W. Takashima, and K. Kaneto: Jpn. J. Appl. Phys. 42 (2003) 5561.

[2] K. Kaneto, and W. Takashima: Curr. Appl. Phys. 1 (2001) 355.

[3] K. Kaneto, M. Nakagawa, and W. Takashima: Synth. Met. 25 (2003) 135.

[4] G. Horowitz: Adv. Mater. 10 (1998) 365.

[5] V. Singh, A. K. Thakur, S. S. Pandey, W. Takashima, and K. Kaneto: Appl. Phys. Exp. 1 (2008) 021801.

[6] H. Spanggaard, and F. C. Kerbs: Sol. Energy Material Sol. Cells 83 (2004) 125.

[7] Y. Kim, S. A. Choulis, J. Nelson, D. D. C. Bradley, S. Cook, and J. R. Durrant: J. Mat. Sci. 40 (2005) 1371.

[8] T. F. Guo, and Y. Yang: Appl. Phys. Lett. 80 (2002) 148.

[9] P. Pneumans, A. Yakimov, and S. R. Forrest: J. Appl. Phys. 93 (2003) 3693.

[10] V. Singh, A. K. Thakur, S. S. Pandey, W. Takashima, and K. Kaneto: Jpn. J. Appl. Phys. 47, No. 2 (2008) 1251.

[11] M. Ujimoto, W. Takashima, and K. Kaneto: Jpn. J. Appl. Phys. 39 (2001) 5350.

[12] V. Singh, M. Yano, W. Takashima, and K. Kaneto: Jpn. J. Appl. Phys. 45, No. 1B (2006) 534.

[13] A. Takshi, A. Dimopoulos, and J. D. Madden: Appl. Phys. Lett. 91 (2007) 083513.

[14] S. M. Sze, and K. N. Kwok, Physics of Semiconductor Devices, 3rd ed. (Wiley, Hoboken, NJ, 2006), Chap. 3, pp. 134-196.

[15] G. Dennler, N. S. Sariciftci, R. Schwodiauer, S. Bauer, and H. Reiss: J. Mat. Chem. 16 (2006) 1789.

[16] H. Becker, S. E. Burns, and R. H. Friend: Phys. Rev. B. 56 (1997) 1893.

[17] S. Tasch, G. Kranzelbinder, G. Leising, and U. Scherf: Phys. Rev. B. 55 (1997) 5079.

[18] M. Segal, M. A. Baldo, R. J. Holmes, S. R. Forrest, and Z. G. Soos: Phys. Rev. B. 68 (2003) 075211.

[19] V. Singh, A. K. Thakur, S. S. Pandey, W. Takashima and K. Kaneto: Organic Electron. 9 (2008) 790.

[20] V. Singh, A. K. Thakur, S. S. Pandey, W. Takashima and K. Kaneto: Synth. Met. 158 (2008) 283.

[21] K. Kaneto, W. Y. Lim, W. Takashima, T. Endo, and M. Rikukawa: Jpn. J. Appl. Phys. 39 (2000) L872.

[22] W. Takashima, S. S. Pandey, T. Endo, M. Rikukawa, and K. Kaneto: Curr. Appl. Phys. 1 (2001) 90.

[23] S. S. Pandey, W. Takashima, S. Nagamatsu, T. Endo, M. Rikukawa and K. Kaneto: Jpn. J. Appl. Phys. 39 (2000) L94.

[24] T. Minari, Y. Miyata, M. Terayama, T. Nemoto, T. Nishinaga, K. Komatsu, and Seiji Isoda: Appl. Phys. Lett. 88 (2006) 083514.

[25] Y. D. Park, D. H. Kim, Y. Jang, J. H. Cho, M. Hwang, H. S. Lee, J. A. Lim, and K. Cho: Organic Electronics 7 (2006) 514.

[26] P. J. Brown, D. S. Thomas, A. Kohler, J. S. Wilson, J. S. Kim, J. S. C. M. Ramsdale, H. Sirringhaus, and R. H. Friend: Phys. Rev. B. 67 (2003) 064203.

[27] C. W. Tang and S. A. van Slyke: Appl. Phys. Lett. 51 (1987) 913.

[28] M. Koehler, I. Biaggio and M. G. E. da Luz: Phys. Rev. B. 78 (2008) 153312.

[29] A. Takshi, M. Mohammadi and J. D. Madden: Sol. Stat. Elec. 52 (2008) 1717.

[30] E. Katsia, G. Tallarida, B. K. Kotowska, S. Ferrari, E. Bundgaard, R. Sondergaard and F. C. Krebs: Org. Electron. 9 (2008) 1044.

[31] P. Kumar, S. C. Jain, V. Kumar, A. Misra, S. Chand and M. N. Kamalasanan: Synth. Met. 157 (2007) 905.

[32] I. D. Parker: J. Appl. Phys. 75 (1994) 1656.

[33] D. D. C. Bradley: J. Phys. D. Appl. Phys. 20 (1987) 1389.

[34] J. H. Burroughes, D. D. C. Bradley, A. R. Brown, R. N. Marks, K. M. Kay, R. H. Friend, P. L. Burn and A. B. Holmes: Nature 347 (1990) 539.

[35] P. L. Burn, D. D. C. Bradley, R. H. Friend, D. A. Halliday, A. B. Holmes, R. W. Jackson and A. Kraft: J. Chem Soc. 1 (1992) 3225.

[36] S. Chambon, A. Rivalton, J. L. Gardette and M. Firorio: Sol. Energ. Mat. and Sol. Cells. 91 (2007) 394.

[37] H. Hoppe, T. Glatzel, M. Niggemann, W. Schwinger, F. Schaeffler, A. Hinsch, M. Ch. L. Steiner and N. S. Sariciftci: Thin Sol. Films 511 (2006) 587.

[38] J. Zaumseil, R. H. Friend and H. Sirringhaus: Nature 5 (2006) 69.

[39] S. R. Amrutha, M. Tayakannan: Macromolecules 40 (2007) 2380.

[40] Y. Kanemitsu, N. Shimizu, K. Suzuki, Y. Shiraishi and M. Kuroda: Phys. Rev. B. 54 (1996) 2204.

[41] G. Wang, T. Hirasa, D. Moses and A. J. Heeger: Synth. Met. 146 (2004) 127.

[42] G. Derue, D. A. Serban, Ph. Leclere, S. Melnite, P. Damman and R. Lazzaroni: Organic ELectron. 9 (2008) 821.

[43] H. F. Meng, C. C. Liu, C. J. Jiang, Y. L. Yeh, S. F. Horg and C. S. Hsu: Appl. Phys. Lett. 89 (2006) 243503.

[44] J. Ghim, K. J. Baeg, Y. Y. Noh, S. J. Kang, J. Jo and D. Y. Kim: Appl. Phys. Lett. 89 (2006) 202516.

Chapter 6

Optoelectronic evidence of exciton quenching due to injected charge carriers

Summary

Photoluminescence spectra of Poly (3-hexylthiophene-2, 5-diyl) (P3HT) has been studied in forward and reverse bias direction in a Indium Tin Oxide(ITO)/P3HT/Al schottky device. It has been observed that Photoluminescence quenching is relatively higher in forward direction and the quenching pattern gets reversed when thin insulating layer of Poly (4-vinylphenol) is coated on ITO. The observed behavior of photoluminescence quenching pattern has been explained on the basis of interaction of the injected charge carriers with the excitons generated in the bulk of P3HT together with the interaction of excitons with the applied electric field.

6.1 Introduction

Research on organic $\pi-$conjugated materials is mostly related to its device applications such as OFETs, OLEDs and photovoltaic devices [1, 2]. These applications are mainly concerned with charge transport and photo physics. The development of OLEDs basically relies on charge injection and its radiative recombination through exciton formation. Electroluminescence (EL) efficiency is a critical parameter [3, 4] for OLEDs and is directly related to Photoluminescence (PL) efficiency,[5] as both originate from the same intermediate state, i.e., excited state of excitons. While EL emission refers to the spontaneous emission of light by a material under electrical excitation, PL emission on the other hand refers to the spontaneous emission of light by a material under optical excitation. Both EL and PL spectra can be used to characterize a variety of material parameters and other optoelectronic behaviors. Since it is the exciton that forms the basis of both EL and PL, thus exciton dynamics is very much useful for the understanding of OLEDs and photo voltaic effect. A bias dependent PL spectrum thus helps in understanding the mechanism of exciton generation, diffusion and its dissociation simultaneously [6-9]. Moreover, it also provides traces of information regarding electroluminescence, photo-conduction and photovoltaic effects. Poly (3-hexylthiophene-2,5-diyl) (P3HT) is one of the preferred conjugated polymer for the purpose of Organic Field Effect Transistors (OFETs), [10] organic photo induced memory devices [11, 12] and photovoltaic devices [13-15]. It is known that Aluminum (Al) forms a schottky type contact with P3HT [28-33]. This type of contact has particularly been well exploited for photovoltaic and other related effects. Thus a detailed study of a schottky junction assumes critical importance for a clear understanding of the dynamics of exciton. In this paper P3HT based schottky cell i.e. ITO/P3HT/Al, as shown in Fig. 6.1(a) and referred to as (cell A) was studied using bias dependent PL over the entire bias range. It was found that while the depletion layer thickness caused PL quenching under reverse bias regime. However, under the forward bias regime, the PL quenching above the diode built in potential was dominated by the injected charge carriers into the bulk of P3HT film. A possible mechanism for the exciton dissociation has been proposed, further, the

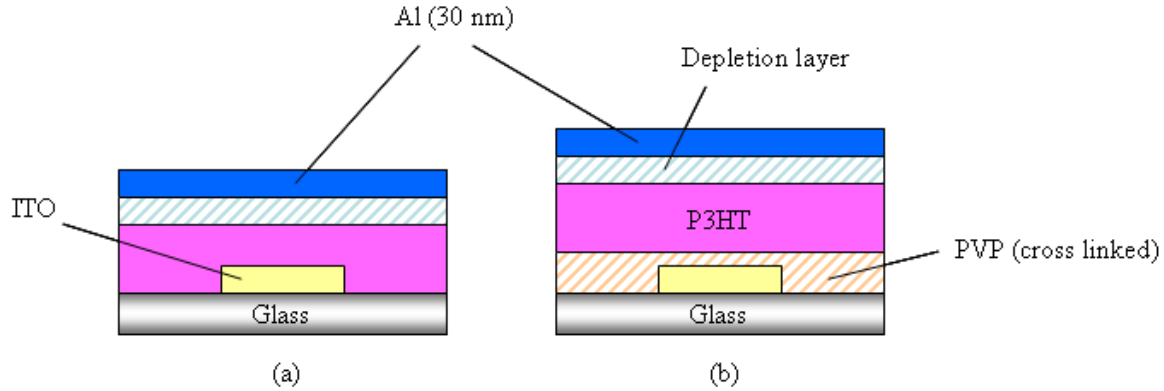

Figure 6.1: Schematic diagram of (a) cell A and (b) cell B

proposed mechanism was further verified using another type of cell ITO/PVP/P3HT/Al (cell B) as is shown in Fig. 6.1(b).

6.2 Experimental Procedures

For the purpose of Schottky cell fabrication, etch patterned ITO coated glass was taken as the substrate, which was subsequently sonicated in iso propanol and acetone solution. It was then spin coated with a chloroform solution of P3HT, which was used as obtained from Merck (Lisicon SP001). A uniform and 200 nm thick P3HT film was coated on top of these patterned ITO electrodes. Later the device was coated with $6mm$ wide and $30nm$ thick Aluminum (Al), by thermal evaporation technique, patterned perpendicular to the bottom ITO electrode. For the cell B all the other steps were identical except that in this case ITO was coated with a Poly (4-vinyl phenol) (PVP) film, followed by its cross linking [16], prior to spin coating the P3HT. The cross linking was done by heating the Polyethylene glycol monomethyl ether acetate (PGMEA) solution of PVP ($20wt\%$ in strength w/v). It is to be noted that for the purpose of cross linking a cross linking agent Poly(melamine-co-formaldehyde) butylated as obtained from Sigma Aldrich was added ($35wt\%$ in strength w/w) of PVP. The solution was stirred for about an hour a clear solution thus obtained was spin coated on top of ITO coated glass substrates @ $[1500, 30000]r.p.m.$. These films were annealed at 200^oC for 2 hours under vacuum. Thickness of PVP and P3HT were later estimated to be $500nm$ and $200nm$

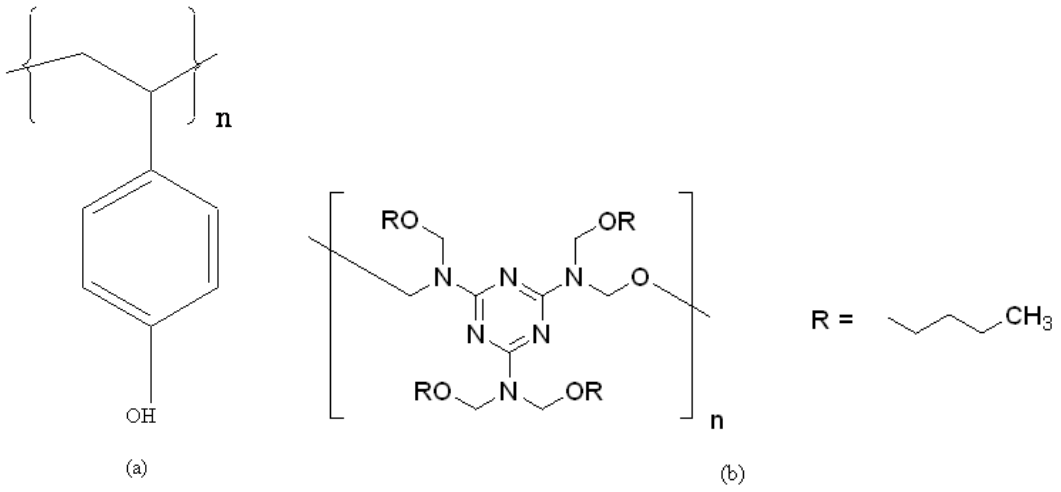

Figure 6.2: Structure of (a) Poly(vinylPhenol)(b)Poly(melamine-co-formaldehyde) butylated

respectively, as measured using Dektak surface profiler. Keithley 6517A electrometer was used for the IV measurement. PL measurement was done under ambient condition using Hamamatsu photonic multi channel analyzer; model C7473, kept at a distance of $70cm$ from the sample. A $300mW$, class III B, CW, He-Cd laser, $442nm$, model IK4121R-G by Kimmon Electric Company Limited, was used as a light pumping source. The intensity of the laser radiation falling on the sample was attenuated to be $0.15W/cm^2$.

6.3 Exciton quenching due to injected charge carriers

In Chapters 4 and 5, a PL quenching due to reverse bias application to the ITO/P3HT/Al Schottky cell has been observed. The observed PL quenching Q_{pl}[23,24] was attributed mainly to the increase in the depletion layer width due to reverse bias application. Under the assumption that the Q_{pl} due to increase in depletion layer width dominates PL quenching due to various other underlying mechanisms. Also, depletion layer can also be regarded as a dead layer for PL emission[19,27,28,29].Hence, changing the depletion layer[17,18] width results in changing the width of active bulk region of the P3HT. Since PL is basically a study of spontaneous emission from the active region of the bulk film, hence changing bulk layer thickness would result in the observable changes in the PL

signal. The radiative PL efficiency is defined as,[20, 27]. It is this depletion layer that gives ITO/P3HT/Al cell a rectifying behavior resulting in a diode like current voltage characteristics.

While the model discussed in Chapter 4 is completely applicable in this chapter as well. It is to be noted that PL quenching Q_{pl} and PL efficiency η_{pl} each given by the following relations,

$$Q_{pl} = \frac{< I_{pl}(0) > - < I_{pl}(v) >}{< I_{pl}(0) >} \tag{6.1}$$

and,

$$\eta_{pl} = b\frac{K_r}{(K_r + K_{nr} + K_q)} \tag{6.2}$$

Using the identical discussion as was done in Chapter 4, we can deduce that the change in depletion layer width $\triangle w(V)$ and PL quenching Q_{pl}, is also given by the equation

$$\triangle w(V) = \frac{1}{\alpha} \ln \left| \frac{\sqrt{(A+2B)^2 + 4BQ_{pl}} - A}{2B} \right| \tag{6.3}$$

Here it should be noted that the values of A, B and α were same as mentioned in chapter 4 for ITO/P3HT/Al type Schottky cell. Although under the reverse bias regime the PL quenching has been well attributed to the increase in the depletion layer width by our optoelectronic model. Also, this model has been further successfully applied to different to different type of Schottky cells. However, the behavior of PL under the application of forward bias to the ITO/P3HT/Al cell is worthwhile to study.

The PL Quenching for cell A along with its I-V characteristic has been shown in Fig. 6.3. Higher level of PL quenching was observed in the forward direction as compared to that observed in the reverse bias direction. Similar results were obtained by Majumdar et al [26]. It is to be noted here that the Electric Field distribution near the interface [as shown in Appendix A] of a ITO/P3HT/Al Schottky cell clearly shows that the electric field increases with increasing reverse bias, however, it decreases as the applied voltage increases above the $0V$ upto built in voltage V_{bi}. Above which the diode starts conducting and the voltage is applied to the bulk of the P3HT film and not limited to the interface. Thus the electric field drops by an order of magnitude as the applied bias increases above V_{bi}. However, despite the decrease in the magnitude of the built in field,

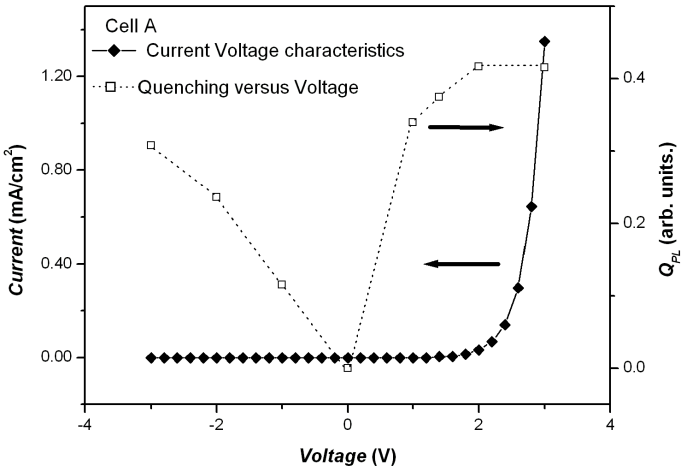

Figure 6.3: A plot of Quenching (Q) versus Voltage (V) and IV characteristics of cell A

the PL quenching continues to increase. We attribute higher level of quenching in the forward direction to the probable interaction between the excitons and injected charge carriers in the bulk of P3HT. The reverse bias quenching has been explained on the basis of the increasing thickness of the depletion layer upon the application of reverse bias. Figure 6.4 shows the plot of quenching as well as $I - V$ for the cell B which includes ITO covered by PVP. A perusal of Fig. 6.4 clearly indicates that inclusion of PVP leads to decrease in the current level in cell B and most importantly the quenching pattern of the cell B is reversed. A higher level of quenching is found to occur in cell B under the reverse bias conditions as compared to the quenching level under the forward bias condition.

In order to clearly understand the mechanism behind the PL quenching under the forward direction $\ln J$ versus $\ln V$ has been plotted for both the cells A and B as shown in Fig. 6.5. It has been found that the quenching is more pronounced in cell A under the forward bias condition, which may be due to the higher number of injected charge carrier in this cell. It can be clearly seen from the Fig. 6.5 that the injected charge carriers in cell A is almost three orders of magnitude higher than that in cell B. A clear evidence of the role of the injected charge carrier in the PL quenching. Although further investigation is needed in this regard to completely establish the relationship between

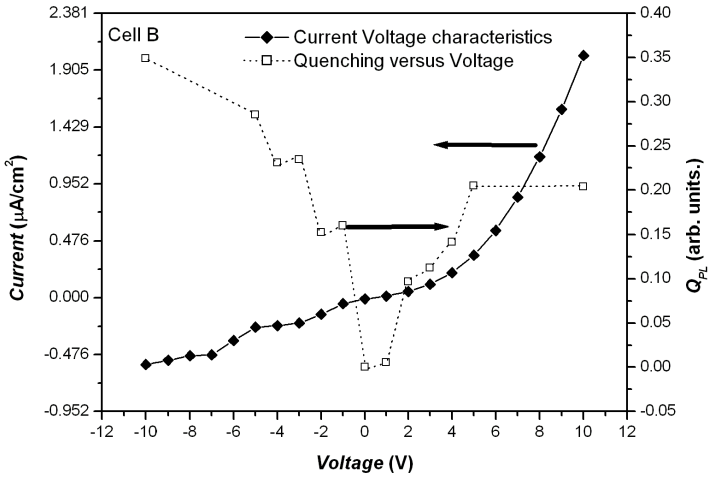

Figure 6.4: A plot of Quenching (Q) versus Voltage (V) and IV characteristics of cell B

the number of injected charge carriers and quenching in the respective cells. It must also be noted that in the case of cell B the contribution in current mostly comes from impurity and the thermally generated charge carrier as its slope is linear. In case of cell A the slope suddenly changes and the device transforms from ohmic to non-ohmic region [34], a clear signature of injection taking place in cell A and not in cell B. From these above mentioned discussions it can be concluded that the injected charge carriers interact with the excitons and hence result in PL quenching.

The values of $\triangle w(V)$ plotted against voltage V has been shown in Fig. 6.6. It exhibits that modulation of depletion width by the application of reverse bias is less pronounced in cell B as compared to that of cell A. It could probably be because of a lesser field drop across the schottky junction in cell B due to the inclusion of an insulating layer of PVP over the ITO electrode. Therefore it can be concluded that depletion layer width is directly related to the PL quenching under the reverse bias condition. However as is well known under the application of the forward bias the depletion width decreases slightly below the built in Voltage V_{bi} and above which it remains constant [25], which means an increase in the bulk active region of P3HT results in higher values of I_{abs} and thus leading to increased PL intensity in the region between $0 < V < V_{bi}$. However, it must be noted that such a behavior is characteristic of inorganic semiconductors [21,

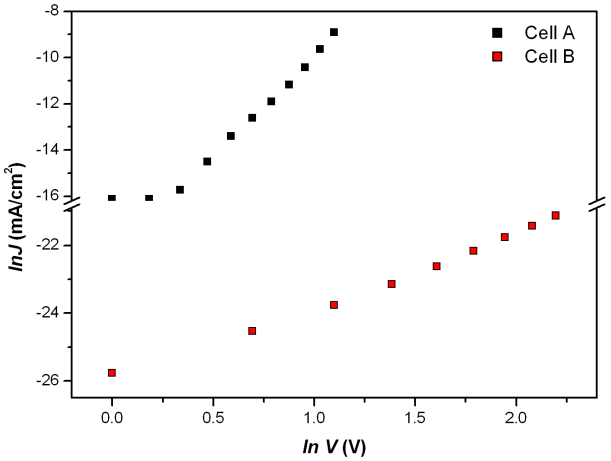

Figure 6.5: A plot of $\ln J$ vs. $\ln V$ for cell A and B

22]. In some earlier reports a PL quenching [5], Q_{pl}(decrease in the intensity of PL emission) for organic semiconductor materials was observed as electric field was applied on to the schottky cell, irrespective of the direction of applied bias. Two types of cell ITO/P3HT/Al (A) and ITO/PVP/P3HT/Al (B) have been fabricated for the purpose of bias dependent PL study. The quenching pattern obtained in the two cells was just opposite of each other. In cell A relatively higher quenching was observed under forward bias condition, however in cell B the relatively higher quenching occurred under reverse bias condition.

It was concluded that presence of charge carriers cause quenching in the forward direction, as was demonstrated by cell B. Thus in general the quenching in the forward direction of cell A has contributions from Electric field as well as bulk charge carriers; although under reverse bias the quenching is mainly due to the increasing depletion width. The results are of critical importance for the better understanding of the optoelectronic behavior of P3HT, and the possible related applications. The results presented here also demonstrate the possible current induced defects related PL quenching a characteristic of polymeric materials.

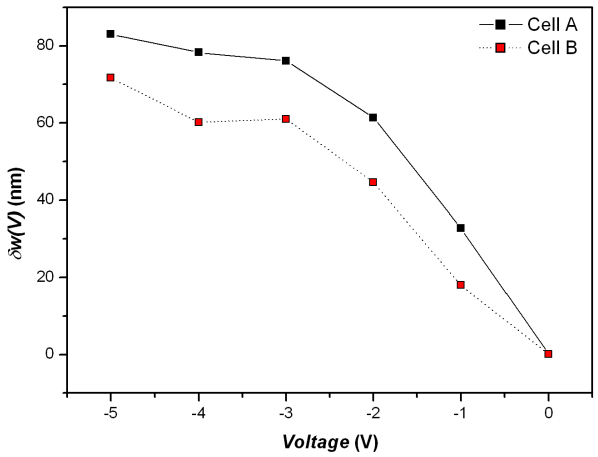

Figure 6.6: Plot of $\triangle w(V)$ versus Voltage V for cell A and B under the application of reverse bias

Bibliography

[1] P. Pneumans, A. Yakimov, S. R. Forrest: J. Appl. Phys. 93 (2003) 3693.

[2] H. E. Katz, Z. Bao: J. Phys. Chem. B. 104 (2000) 671.

[3] D. E. Markov, P. W. M. Blom: Phys. Rev. B 72 (2005) 161401.

[4] J. M. Lupton, J. Klein: Phys. Rev. B 65 (2002) 193202.

[5] M. Segal, M. A. Baldo, R. J. Holmes, S. R. Forrest, Z. G. Soos: Phys. Rev. B 68 (2003) 075211.

[6] R. Kersting, U. Lemmer, M. Deussen, H. J. Bakker, R. F. Mahrt, H. Kurz, V. I. Arkhipov, H. Bassler, E. O. Gobel: Phys. Rev. Lett. 73 (1994) 1440.

[7] U. Rauscher, H. Bassler, D. D. C. Bradley, M. Hennecke: Phys. Rev. B 42 (1990) 9830.

[8] N. S. Sariciftci, L. Smilowitz, A. J. Heeger, F. Wudl: Science 258 (1992) 1474.

[9] G. Yu, J. Gao, J. C. Hummelen, F. Wudl, A. J. Heeger: Science 270 (1995) 1789.

[10] V. Singh, M. Yano, W. Takashima, K. Kaneto: Jpn. J. Appl. Phys. 45 No. 1B (2006) 534.

[11] M. Ujimoto, W. Takashima, K. Kaneto: Thin Solid Films 499 (2006) 313.

[12] V. Singh, A. K. Thakur, Shyam. S. Pandey, W. Takashima, K. Kaneto: Jpn. J. Appl. Phys. 47, No. 2B (article in press).

[13] T. Umeda, H. Noda, T. Shibata, A. Fujii, K. Yoshino, M. Ozaki: Jpn. J. Appl. Phys. 45, No. 6A (2006) 5241.

[14] M. Kaneko, K. Takayama, S. S. Pandey, W. Takashima, T. Endo, M. Rikukawa, K. Kaneto: Synth. Met. 121 (2001) 1537.

[15] S. S. Pandey, K. Rikitake, W. Takashima, K. Kaneto: Curr. Appl. Phys. 3 (2003) 107.

[16] H. Klauk, M. Halik, U. Zschieschang, Gunter Schmid, W. Radlik: J. Appl. Phys. 92, No.9 (2002) 5259.

[17] K. Rikitake, D. Tanimura, W. Takashima, K. Kaneto: Jpn. J. Appl. Phys. 42 (2003) 5561.

[18] K. Kaneto, W. Takashima: Curr. Appl. Phys. 1 (2001) 355.

[19] R. R. Chang, R. Iyer, D. L. Lile: J. Appl. Phys. 61 (1987) 1995.

[20] H. Becker, S. E. Burns, R. H. Friend: Phys. Rev. B 56 (1997) 1893.

[21] N. N. Winogradoff: Phys. Rev. 138, No.5A (1965) A1562.

[22] D. Shvydka, V. G. Karpov, A. D. Compaan: Appl. Phys. Lett. 80 (2002) 3114.

[23] S. Tasch, G. Kranzelbinder, G Leising, U. Scherf: Phys. Rev. B 55, No.8 (1997) 5079.

[24] M. C. J. M. Vissenberg, M. J. M. de Jong: Phys. Rev. B 57, No.5 (1998) 2667.

[25] K. Kaneto, M. Nakagawa, W. Takashima: Synth. Met. 135 (2003) 25.

[26] H. S. Majumdar, C. Botta, A. Bolognesi, A. J. Pal: Synth. Met. 148 (2005) 175.

[27] V. Singh, A. K. Thakur, S. S. Pandey, W. Takashima, K. Kaneto: Appl. Phys. Exp. 1 (2008) 021801.

[28] C. W. Tang and S. A. van Slyke: Appl. Phys. Lett. 51 (1987) 913.

[29] M. Koehler, I. Biaggio and M. G. E. da Luz: Phys. Rev. B. 78 (2008) 153312.

[30] A. Takshi, M. Mohammadi and J. D. Madden: Sol. Stat. Elec. 52 (2008) 1717.

[31] E. Katsia, G. Tallarida, B. K. Kotowska, S. Ferrari, E. Bundgaard, R. Sondergaard and F. C. Krebs: Org. Electron. 9 (2008) 1044.

[32] P. Kumar, S. C. Jain, V. Kumar, A. Misra, S. Chand and M. N. Kamalasanan: Synth. Met. 157 (2007) 905.

[33] I. D. Parker: J. Appl. Phys. 75 (1994) 1656.

[34] Z. Chiguvare, J. Parisi and V. Dyakonov: J. Appl. Phys. 94 (2003) 2440.

Chapter 7

Conclusion

7.1 General conclusions

In this work Photoluminescence spectra was used as a tool to study metal/polymer interface and its related effects. The results discussed are of critical importance to clearly understand various principles governing the behavior of excitons. It is these excitons that govern the performance of various Optoelectronic devices. Besides, the results offer a new insight to probe interface itself. One of the critical issues is that of inclusion of thin layer of LiF for improvement of the efficiency of OLEDs and OSCs. Much of the effort was devoted to understand the LiF/Alq3 interface. However, very few reports are available on LiF/P3HT interface. A clear understanding of LiF/P3HT interface would throw some light on the improvement in the efficiency of OSCs by inclusion of LiF. In this thesis we studied the nature of LiF/P3HT using photoluminescence spectroscopy. While LiF coating of pristine P3HT films led to PL quenching due to increased number of excitons undergoing non radiative decay via phonon coupled vibrations. However it was the absence of memory currents in the photo induced memory devices that clearly indicated that LiF does not form a depletion layer with P3HT. One of the possible mechanisms suggested for the inclusion of LiF in OLEDs and OSCs is that it leads to the formation of a depletion layer. However, no such effect was observed in the case of LiF/P3HT interface. However, this property of LiF to form a dead layer when coated on top was P3HT layer was then successfully utilized to improve the IV characteristics of OFETs. It was observed that coating LiF on top of a bottom contact OFET led to

the formation a dead layer near the top of the film. This led to cut-off of the bulk region of P3HT leading to cut off in the transistor off currents. This, further led to a one to two order of improvement in the on/off ratio of the OFETs.

Study of depletion layer in inorganic semiconductors is usually done by studying its Capacitance voltage dependence of Schottky cell. The standard expression used in the study of depletion layer has been derived by solving Poisson's equation. It must be noted that this derivation is done under the assumption that a uniform charge carrier density exists. However, in the polymeric semiconductors this assumption is not true. As in these materials the net charge carrier density is not constant, besides these materials have parasitic capacitances present in the form of bulk capacitance and the capacitance due to trapped charge carriers. These deviations lead to a clear cut deviation in the Mott-Schottky plot. Hence a large deviation from the linear regime is often observed in these materials. In this regard Takshi et al used an entirely new approach to study the bias dependence of depletion layer. They used a MESFET structure to study the bias dependence of depletion layer. Their work forms the basis of our work as well. We also tried to determine the bias dependence of depletion layer. However, our approach was entirely based on optoelectronic model. This, besides being a novel approach could also help us establish various interface related effects that are responsible for the various competing mechanisms for excitonic decay. Studies based on P3HT based Schottky cells indicated that under reverse bias condition the increase in depletion layer was mainly responsible for the increase in the PL quenching in these cells. Based on this we proposed a model for the first time which we call for the sake of convenience as Optoelectronic model. This model directly relates the observed PL quenching under reverse bias application on a Schottky cell to the increase in its depletion layer. The novelty of this approach, in the study of depletion layer lies in it being free from the effect of any parasitic capacitances arising due to material properties. Besides this novel approach could help us uncover some of the fundamental issues related to interface in organic electronic devices.

After the successful demonstration of our optoelectronic model. It was then extended to study various different interface related issues in organic devices. Although the

LiF/P3HT interface was studied, however, its true role in a sandwich cell was not well understood. Thus, we tried to apply our optoelectronic model to study the role of LiF in efficiency improvement in a sandwich geometry based optoelectronic device. In order to study the nature of interface we fabricated two types of Schottky cells. One having the conventional geometry, however, the other included a thin layer of LiF. It was found that the inclusion of LiF in the sandwich cell led to decreased level of PL quenching in those cells compared to the conventional ones. However, the photocurrents were higher in the device fabricated using LiF. These results combined with some other characteristic data finally established that LiF performs two roles in Organic electronic devices. One is that it protects the underlying organic layer from hot Al atoms during the process of thermal deposition of Al electrode. Besides it was also found that presence of LiF near the interface leads to the built up of high electric field near the interface and hence causes easy dissociation of excitons in these cells. It is this built up that leads to lesser modulation of depletion layer in cells fabricated including thin layer of LiF. The effect of coating a thick layer of metal over polymer film was also studied in great detail. It was found that coating thick metal leads to increase in the intrachain disorder in the polymer films. Though the exact nature of the interaction responsible for these observed effects could not be established.

Later the Optoelectronic model was further extended to study the effect of molecular structure on the nature of interface formed in these Schottky cells. In order to study the effect of structure we used various derivatives of Poly(alkylthiophene). It was established that the role of alkyl chain length is to promote the formation of well stacked structures in these films, through their interlocking in one direction and thus leading to the formation of lamellar structure. Although the presence of alkyl chain ensures the solubility of the polymer derivative into the common known organic solvents, besides longer alkyl chain length helps in improving the overall film morphology but also at the same time it leads to increased separation between the polymer backbones. By performing absorption and emission spectra studies, the role of alkyl chain length and the regio regularity of the polymer chain on to their overall morphology was studied. It was found that presence of longer alkyl chain length led to improved morphology.

While PAT 12 were found to be well stacked microcrystalline domains. PAT 4 on the other hand had twisted coil shaped structures. However, it was only after combining the Optoelectronic study along with the Capacitance Voltage data of these cells that it was finally established that the charge carrier density in polymeric semiconductors are non uniformly distributed into the bulk of these materials. The bias dependent PL studies indicate the exciton diffusion is facilitated by improved morphology of the film and that easy diffusion of excitons and the higher level of interface field leads to increase in the extent of Pl quenching. Thus basically the Optoelectronic model was successfully used to establish the interrelationship between structure and morphology of polymeric thin films.

Finally using our optoelectronic model we studied the effect of PL quenching due to injected charge carriers. Increased PL quenching was observed above the diode built in voltage. It was only after capping the ITO electrode in a Schottky cell by a thick PVP (crosslinked) layer that led to significant decrease in the level of currents, that it could be said that the increased PL quenching in the conventional Schottky cell was possibly caused by exciton polaron interaction. Although the exact nature of such an interaction is still under investigation. However, if such an effect exists it provides us a whole new approach to solve some of the persisting problems in organic Optoelectronic devices.

7.2 Suggested directions

The work presented in this thesis deals with the study of interface and its related effects by using Photoluminescence spectroscopy. The novel approach of the interrelationship presented between PL quenching under the reverse bias application and the depletion layer width, is completely based on an optoelectronic model developed by combining the absorption and emission spectra in a sandwich type Schottky cells. Although later it was found that the model is not complete in the strict sense because, it does not incorporate PL quenching due to electric field assisted dissociation of excitons. Thus in order to carry out a more precise measurement of depletion layer by using the optoelectronic model presented in this thesis the field assisted dissociation of excitons needs to be

incorporated in the optoelectronic model. Besides, being a more refined method for estimation of depletion layer width. Inclusion of field assisted dissociation of excitons would also help us understand and predict the role of morphology in the PL quenching in more quantitative terms. The effect of coating metal on a pristine film was also studied using PL spectroscopy. It was found that metal coating on to the top of a pristine film, led to increase in intrachain disorder in these films. We attributed this effect to the method of deposition of metal electrodes itself, e.g. in our case it was physical vapor deposition. However, a detailed mechanism of why such an effect was observed could not be fully established. Thus the results presented in this thesis provide a groundwork to further study the effect of metal coating on to the polymer pristine film. The effect of exciton polaron interaction discussed in this thesis is a relatively new concept. Not many reports have appeared on this topic in the past. It should be noted that a signature of exciton polaron interaction occurring in organic materials has been observed in the work presented in this thesis. Although, this effect also needs further investigation before applications of this effect can be envisioned. Although the signature of exciton polaron interaction was observed in our work but the exact mechanism for such an interaction is not well understood. Further investigations in this direction could yield a wealth of new information about organic optoelectronic devices.

Appendix A

Built in Field as a function of applied bias

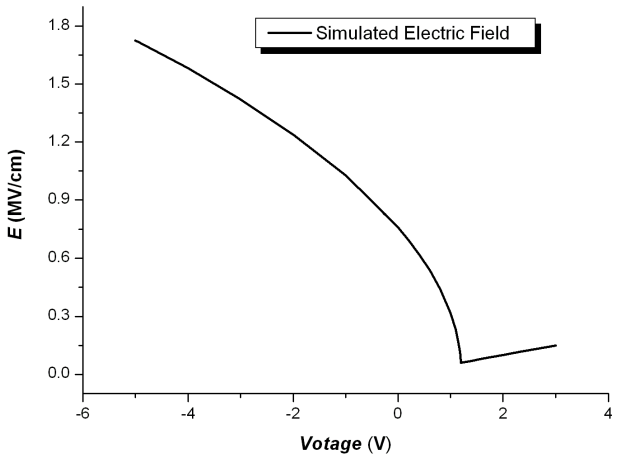

Figure A.1 Plot of Simulated Electric Field near the interface for ITO/P3HT/Al based Schottky cell.

The electric field is simulated for a $200nm$ thick P3HT film, using the standard expression of bias dependent depletion layer thickness as given by the equation,

$$w(V) = \sqrt{\frac{2\epsilon_s(V_{bi} - V)}{qN_A}} \tag{A.1}$$

This further implies that below the built in voltage the built in electric field is given by

$$E = \sqrt{\frac{qN_A(V_{bi} - V)}{2\epsilon_s}} \tag{A.2}$$

which can be rewritten as

$$E = E_0 \left(1 - \frac{V}{V_{bi}}\right) \tag{A.3}$$

where electric field E_0 is given by

$$E_0 = \sqrt{\frac{qN_A V_{bi}}{2\epsilon_s}} \tag{A.4}$$

Above the built in voltage the diode starts conducting and thus the applied voltage is applied to the bulk of the film. This further results in a drastic reduction of the field. As can be seen from Figure A.1 and further increase in the positive bias voltage above the built in field results in a linear increase in the field applied to the bulk of the P3HT film. It should be noted that while below V_{bi} particularly under the reverse bias application on the Schottky cell, the electric field is sufficient to cause field assisted dissociation of excitons. However, the decrease in the built in field particularly above the built in voltage V_{bi} is quite low of the order of $10^4 V/cm$, thus above built in voltage V_{bi} the PL quenching is essentially not caused by field assisted dissociation of excitons.

Appendix B

Different values of χ

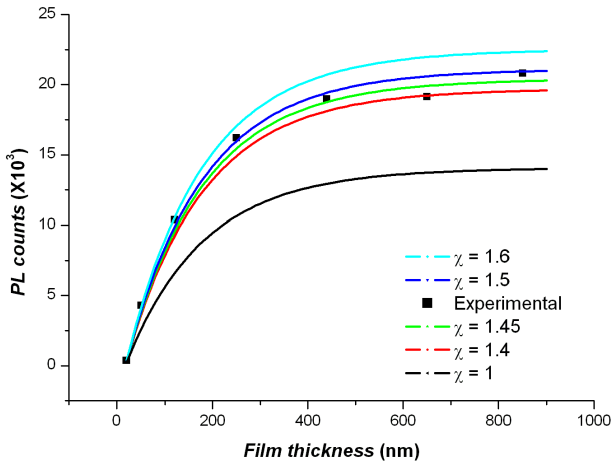

Figure B.1 Figure Shows the simulated PL counts for different values of χ.

Appendix C

Publication list

List of Publications in International Journals

1. **Vipul Singh**, Shyam S Pandey, Wataru Takashima and Keiichi Kaneto: "Role of morphology on Photoluminescence quenching and depletion width formed at the interface of Aluminum and Poly(3-Alkylthiophene)" in press (Jpn. J. Appl. Phys.).

2. **Vipul Singh**, Anil K Thakur, Shyam S Pandey, Wataru Takashima and Keiichi Kaneto: "A comparative study of Al and LiF:Al interfaces with Poly (3-Hexylthiophene) using bias dependent Photoluminescence technique" Organic Electronics 9 (2008) 790. Citation: 0

3. **Vipul Singh**, Anil K Thakur, Shyam S Pandey, Wataru Takashima and Keiichi Kaneto: "Evidence of photoluminescence quenching in Poly (3-Hexylthiophene-2,5-diyl) due to injected charge carriers" Synthetic Metals 158 issue 7 (2008) 283-286. Citation: 1

4. **Vipul Singh**, Anil K Thakur, Shyam S Pandey, Wataru Takashima and Keiichi Kaneto: "Characterization of depletion layer using Photoluminescence technique" Appl. Phys. Exp. 1 (2008) 021801. Citation: 2

5. **Vipul Singh**, Anil K Thakur, Shyam S Pandey, Wataru Takashima and Keiichi Kaneto: "Optical and Electrical Characterization of Poly (3-Hexylthiophene-2,5-diyl) interface with Al and LiF" Jpn. J. Appl. Phys. 47 No. 2 (2008) 1251-1255. Citation: 2

6. **Vipul Singh**, Makoto Yano, Wataru Takashima and Keiichi Kaneto: "Study of gate induced channel in Organic Field Effect Transistors using Poly (3-hexylthiophene) films" Jpn. J. Appl. Phys. 45 No. 1 (2006) 534-537. Citation: 3

Appendix D

List of conference attended

Poster Presentations

1. **Vipul Singh**, Anil K Thakur, Shyam S Pandey, Wataru Takashima and Keiichi Kaneto "Effect of Regioregularity and Alkyl chain length on the depletion layer width formed at the interface of Al and Poly(3-Hexylthiophene)", [Materials Research Society (Fall 2007 Meeting)], F9.3, Boston, MA, United States, (26-30 November, 2007).

2. **Vipul Singh**, Anil K Thakur, Wataru Takashima and Keiichi Kaneto "Behavior of LiF/Poly (3-hexylthiophene) interface.", [Fourth International Conference on Molecular and Bioelectronics], P-22, Tokyo, Japan, (14-16 March, 2007).

3. Naoharu Masumoto, **Vipul Singh** and Keiichi Kaneto "Frequency response of Field effect transistor using conducting polymer", [Pusan-Kyeongnam/Kyushu-Seibu Joint symposium on high polymers (12th) and fibers (10th)], Fukuoka, Japan (November 2005).

4. **Vipul Singh**, Wataru Takashima and Keiichi Kaneto "Thin Film OFETs using Poly (3-hexylthiophene)", Kitakyushu, Japan, (2nd July, 2005).

5. **Vipul Singh**, Wataru Takashima and Keiichi Kaneto "Study of gate induced channel in Organic field effect transistors using Poly (3-hexylthiophene) films." [Third international conference on molecular and bioelectronics], 4P-B30, Tokyo, Japan, (3-4 March, 2005).

Oral Presentations

1. **Vipul Singh**, Shyam S Pandey, Wataru Takashima and Keiichi Kaneto "Characterization of interface using bias dependent photoluminescence of Schottky cell",[40th Conference on Solid State Devices and Materials 2008], I-6-1, Tsukuba, Japan (23rd -26th September, 2008).

2. **Vipul Singh**, Chungpin Xu, Yuji Ishizaki, Makoto Yano, Keiichi Kaneto "Electrical properties of gate induced channel in OFETs using Poly (3-hexylthiophene) film", [International Polymer Conference], Sponsored by the Society for Polymer Science in Japan, 29A10, Fukuoka, Japan, (26-29, July 2005).